Faculdade de Engenharia da Universidade do Porto

U.PORTO

FEUP **FACULDADE DE ENGENHARIA**
UNIVERSIDADE DO PORTO

Wrist Vascular Dominance Assessment

Elsa Filipa Quadrado de Sousa

MASTER DISSERTATION

Integrated Master in Bioengineering

Supervisor: Ricardo Vardasca, PhD

Co-supervisor: António Ferreira, PhD

Co-supervisor: Joaquim Gabriel Mendes, PhD

June, 2017

Abstract

The analysis of vascular dominance of the radial and ulnar arteries is important for health professionals when preparing for a flap surgery, for example. An objective, practical and fast method to recognize the major source of vascularization to the hand can lead to a more sustained decision on which artery to sacrifice and, consequently, to a better surgery result and recovery, reducing the risk of postoperative complications, such as hand ischemia or function loss.

The aim of this dissertation was to assess wrist vascular dominance with thermal infrared imaging, which is able to measure microvascular perfusion with efficiency and accuracy. It was intended to clarify how the radial and ulnar arteries contribute to the blood perfusion to the hand.

Manual analysis of thermal images and definition of regions of interest (ROI) of hands is a tedious and time-consuming task. Towards the automatic detection of anatomical thermal ROIs, an algorithm to automatically detect fingertips and phalanges was developed, using MATLAB®. The best approach showed a hit score of 88.6%. In the future, it could be applied when physicians need to get information about the hand/fingers blood flow, or get objective measurements of the modified Allen's test, by automatically accessing the phalanges temperatures.

A mechanical stress was applied, through modified Allen test, and the resulting hand blood perfusion of 47 healthy participants was analysed, using a FLIR® E60sc thermal camera.

The main objectives of this research have been achieved. It was possible to quantify the thermal effects of the modified Allen test, objectively. Medical thermography was able to prove that, in both hands, the changes in temperature are higher in the middle area of thumb when the radial artery is released first, than in the middle phalanx of the little finger when the ulnar artery is released first. Besides, collateral reperfusion by both arteries does not cause a strong thermal manifestation.

There is not a clear conclusion on whether radial or ulnar artery play the most important role in blood perfusion to the hand, using thermal imaging information, since both collateral and non-collateral reperfusions strengths are important to clarify the vascular dominance. Therefore, future studies should address this issue in a larger sample and with complimentary methods.

Keywords: thermography; wrist vascular dominance; hand blood flow; modified Allen test.

Resumo

A análise da dominância vascular das artérias radial e ulnar é importante para os profissionais de saúde, aquando da preparação para cirurgias com retalho, por exemplo. Um método objetivo, prático e rápido de reconhecer a maior fonte de vascularização para a mão pode levar a uma decisão mais sustentada em relação à artéria a sacrificar e, consequentemente, a um melhor resultado cirúrgico e melhor recuperação, reduzindo o risco de complicações pós-operatórias, como isquemia ou perda de função da mão.

O objetivo desta dissertação foi estudar a dominância vascular do pulso usando termografia médica infravermelha, que mede a perfusão microvascular com eficiência e exatidão. Era pretendido clarificar de que forma as artérias radial e ulnar contribuem para a perfusão sanguínea da mão.

A análise manual de imagens termográficas e a definição das regiões de interesse na mão é uma tarefa entediante e demorada. Com vista a uma deteção automática de regiões de interesse anatómicas de imagens térmicas, um algoritmo foi desenvolvido para detetar automaticamente as pontas dos dedos e falanges, utilizando MATLAB®. A percentagem de acerto da melhor abordagem é de 88.6%. No futuro, poderia ser aplicado quando os médicos precisam de obter informação relativa ao fluxo sanguíneo da mão/dedos, ou obter medições objetivas do teste modificado de Allen, acedendo automaticamente às temperaturas das falanges.

Um *stress* mecânico foi aplicado, através do teste modificado de Allen, e a resultante perfusão sanguínea da mão de 47 participantes saudáveis foi analisada, usando uma câmara térmica FLIR® E60sc.

Os objetivos principais deste estudo foram alcançados. Foi possível quantificar os efeitos térmicos do teste modificado de Allen, de uma forma objetiva. A termografia médica provou que, em ambas as mãos, as mudanças de temperatura são maiores na área média do polegar quando a artéria radial é libertada primeiro, do que na falange média do dedo mindinho quando a artéria ulnar é libertada primeiro. Para além disso, a reperfusão colateral de ambas as artérias não causa uma manifestação térmica forte.

Não se pode concluir de forma clara qual das artérias, radial ou ulnar, tem um papel mais importante na perfusão sanguínea da mão, usando a informação proveniente da termografia médica, uma vez que a eficácia de ambas as reperfusões, colateral e não colateral, é importante para clarificar a dominância vascular. Assim, estudos futuros deveriam analisar esta questão, utilizando uma amostra maior e métodos complementares.

Palavras-chave: termografia; dominância vascular do pulso; fluxo sanguíneo da mão; teste modificado de Allen.

Acknowledgements

Filipa Sousa

Contents

List of figures

List of tables

Abbreviations and Symbols

List of abbreviations

AC	Alternate current
ANOVA	Analysis of Variance
AVA	Arteriovenous anastomose
BMI	Body Mass Index
BPU	Blood Perfusion Units
CT	Computed Tomography
DC	Direct current
df	Degrees of freedom
DSP	Digital Signal Processing
FPA	Focal Plane Array
Ge	Germanium
iPPG	Photoplethysmography imaging
IR	Infra-red
IT	Infra-red thermography
LDF	Laser Doppler flowmetry
LDPI	Laser Doppler perfusion imaging
MRI	Magnetic Resonance Imaging
NETD	Noise Equivalent Temperature Difference
PPG	Photoplesthysmography
PRU	Peripheral Resistance Unit
ROI	Region of interest
Si	Silicon
SkBF	Skin Blood Flow
TI	Thermal Imaging
Ti	Thermal index

List of symbols

ε	Emissivity
σ	Stefan-Boltzmann constant

Chapter 1

Introduction

Hand blood flow dynamics is a crucial information when health professionals are planning digital island-flaps or surgeries that include radial or ulnar artery removal. Hand ischemia must be prevented and postoperative hand function must be preserved. These factors might be assured as long as the blood vessel that contributes the most to the digital blood flow is not sacrificed (Dumanian, Segalman, & Buehner, 1998; Haerle, Häfner, Schaller, & Brunelli, 2002).

A flap is a mass of tissue for grafting, usually including skin, only partially removed from one part of the body so that it retains its own blood supply during transfer to another body location (Miller-Keane Encyclopedia and Dictionary of Medicine, Nursing, and Allied Health, 2003).

The radial forearm flap is a reliable fasciocutaneous flap. It is considered the ideal flap for certain facial structures reconstructions, such as floor-of-mouth reconstruction and partial glossectomy, due to its thinness and pliability. Donor-site morbidity, although not recurrent, is a source of patient dissatisfaction. Some post-surgical problems may include exposure of the flexor tendons, sensory deficits, cold intolerance, and poor aesthetic outcomes caused by scarring from skin grafts. Many of these complications are avoided with use of the ulnar artery perforator flap (Yu, Chang, Selber, & Hanasono, 2012).

The ulnar forearm flap has actually more advantages because of the less hairy skin of the ulnar forearm region, especially for intraoral and pharyngeal soft tissue replacement. Furthermore, the more conveniently located donor area results in a better camouflage (P Sieg & Bierwolf, 2001; Peter Sieg, Jacobsen, Hakim, & Hermes, 2006). Also, its thinner layer of subcutaneous tissues is favorable: in head and neck reconstructions, defects are thin in most cases, so fasciocutaneous flaps need to be as thin as possible. Sieg and co-workers (P Sieg & Bierwolf, 2001) compared the use of these two flaps for head and neck reconstruction. In 75 patients, 51 ulnar and 24 radial forearm flaps were used. Flap survival rate, respectively wound healing, in the recipient region showed no differences. However, compared with its radial equivalent, closure of the ulnar donor side by skin grafting resulted in a significantly lower donor site complication rate (Table 1) (P Sieg & Bierwolf, 2001).

Table 1 — Postoperative complications in the donor region.

	Radial forearm flap	Ulnar forearm flap
Number of flaps	24	51
Effusion after mobilization	8	---
Dehiscence	5	4
Partial loss of skin graft	2	---

However, ulnar artery–based flaps have never gained widespread popularity, mainly due to concerns over vascular dominance of the hand (Peter Sieg et al., 2006; Yu et al., 2012). Another reason is a conviction based on classic anatomy which states that the ulnar artery is the dominant artery of the human forearm and that sacrificing the radial artery is safe (Haerle, Haffner, Dietz, Schaller, & Brunelli, 2003).

In 1973 and 1983, two studies (Doscher, Viswanathan, & Stein, 1983; Little, Zylstra, West, & May, 1973) stated that the ulnar artery is the dominant source of supply in most hands. Most recently, it was found that the ulnar artery is dominant at the elbow, but after originating its collateral branches, the radial artery becomes the dominant artery in the distal forearm and, consequently, constitutes the major source of vascularization to the hand. The ulnar artery is rarely dominant at the forearm level and is physiologically less important. Therefore, in terms of hemodynamics, using the radial artery is not preferable to the use of the ulnar artery for any invasive procedures (Haerle et al., 2003; Tonks, Lawrence, & Lovie, 1995). Dumanian and co-workers (Dumanian et al., 1998) have also shown that the ulnar artery is less likely to compensate for loss of radial artery perfusion in the hand, whereas the radial artery can more often compensate for the lost ulnar blood flow.

Consequently, it is a controversial issue that needs to be clarified scientifically, so as to eliminate this uncertainty across the medical community.

1.1 - Motivation

The dominance of the radial or ulnar artery at the forearm level and their contributions to the blood circulation of the hand remain a matter of discussion across the health professionals and the scientific community (Haerle et al., 2003).

In 1946, Debakey and Simeone (DeBakey & Simeone, 1946) reported a 1.6% incidence of loss of the hand after ligation of the ulnar artery in injuries occurring in war, while the incidence for loss of the hand after radial artery ligation was significantly higher, at 5.1% (DeBakey & Simeone, 1946; Kleinert, Fleming, Abel, & Firrell, 1989).

Nevertheless, the ulnar artery has been considered to be the dominant arterial supply to the common digital arteries of the hand for a long time. For this reason, the radial artery is often ligated during ganglion excision or after trauma and is commonly catheterized during cardiac procedures. Complications with these procedures, however, have a reported incidence of between 0.2% and 10% (Kleinert et al., 1989).

Coleman and Anson (Coleman & Anson, 1961) study on the vascular supply of the hand reports that the thumb and index finger and the radial side of the middle finger derive their supply from the deep arch or radial artery. The ulnar side of the middle finger, the ring finger, and the little finger collectively are supplied almost exclusively from the superficial arch (by the ulnar artery). This means

that the hand is supplied by both arteries. Furthermore, they also reported that the superficial arch was only complete 78.5% of the time and the deep arch was complete 97% of the time (Coleman & Anson, 1961; Kleinert et al., 1989).

Anatomic dissections provide only a static representation of the potential flow to the hand, which cannot demonstrate the dynamics of the circulation, since flow is dependent on the relative pressure in the two arteries, as well as on downstream vascular resistance. Therefore, there is the need of studying the influence of the major forearm vessels in the dynamics of blood circulation to the hand, using other techniques. Kleinert and co-workers (Kleinert et al., 1989) used pulse volume recording (PVR) technique, while Haerle and co-workers (Haerle et al., 2003) used color duplex sonography and five-channel Photoplethysmography (PPG) to address this issue.

This research project proposes the use of more sophisticated techniques, such as thermal imaging (TI), laser Doppler perfusion imaging (LDPI) and PPG, with proven efficiency in measuring microvascular perfusion (Allen & Howell, 2014), to study the wrist vascular dominance.

1.2 - Aim

The aim of this study was to assess the wrist vascular dominance with thermal infrared imaging, complementing it with laser Doppler perfusion imaging and photoplesthysmography. It was intended to clarify the dominance of ulnar and radial arteries at the wrist level, as well as how they contribute to the blood perfusion to the hand, allowing a more conscious and accurate medical decision in surgical procedures. Also, the possible influence of sex on wrist vascular dominance was studied.

Obtaining accurate objective data required the definition of standard acquisition protocols. Posterior processing and analysis of this data would lead to the establishment of a recommendation to the clinical practice community, regarding which artery plays a dominant role in blood perfusion to the hand.

1.3 - Contributions

This dissertation had three major contributions:

1. Application of thermography in evaluating hand blood flow and quantifying the thermal effects of the modified Allen test, objectively;
2. A systematic review on the application of medical infrared thermal imaging in hands, that was be submitted to *Infrared Physics and Technology* (impact factor: 1.588);
3. An algorithm for automatically detecting fingertips and phalanges, using MATLAB®, approved to VipIMAGE 2017 conference.

1.4 - Structure of the Dissertation

This document is separated into six sections.

This introduction describes the problem, motivation, aim of the study and the contributions of this dissertation.

The next section, a literature review, describes the hemodynamics of blood circulation and microcirculation, factors affecting the blood flow and blood pressure, and the anatomy and physiology of the wrist. It also describes the optical imaging techniques that were intended be used in this study:

TI, LDPI and PPG. Additionally, it presents the research on vascular dominance assessment using those three techniques, as well as the variables of influence.

The third section outlines the methodologies that were used in this research project.

The results are presented in the fourth section.

The fifth section presents the automatic detection of hand fingertips and phalanges in thermal images.

The work is discussed in the sixth section.

The final part of this document is the Conclusion, where the final conclusions are established and the future work is suggested.

The dissertation outline is presented in Figure 1. The specific chapters of Literature Review that contributed the most for each step in the Methodology are signed.
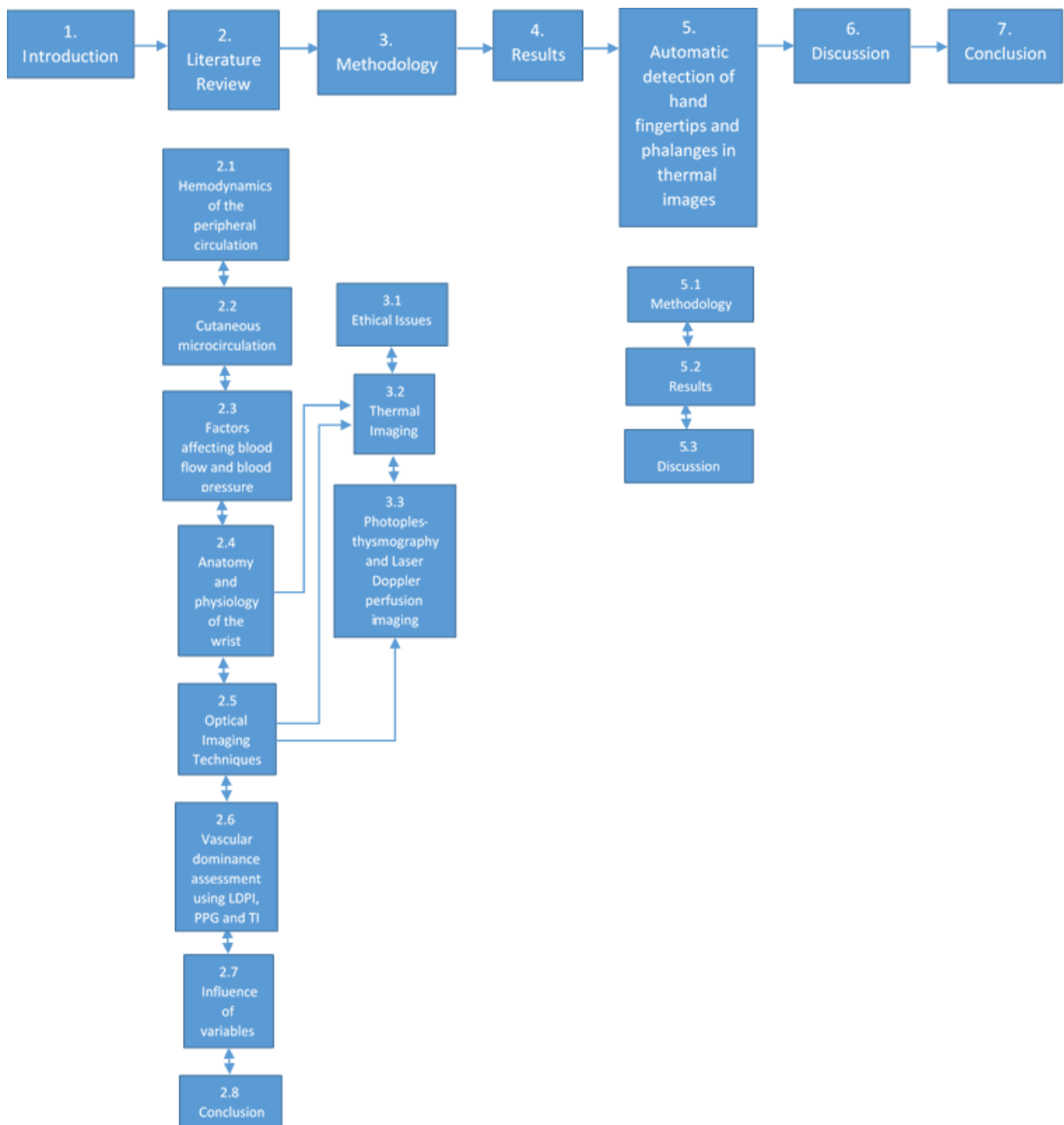
Figure 1 – Dissertation outline.

Chapter 2

Literature Review

In this chapter, hemodynamics of the peripheral circulation, factors affecting blood flow and blood pressure and the anatomy and physiology of the wrist are presented, as well as the fundamentals on medical thermal imaging, laser Doppler perfusion imaging and PPG techniques. Research on vascular assessment using these techniques in the literature is also addressed.

2.1   Hemodynamics of the peripheral circulation

The sympathetic nervous system plays an important role in body function. Movements require complex adjustments in blood flow and blood pressure, which are ultimately coordinated by sympathetic nerves in conjunction with parasympathetic modulation of heart rate (Charkoudian & Rabbitts, 2009).

The physical principles of fluid dynamics still constitute the basis of understanding of the factors regulating blood flow. The rate of flow Q of fluid through a tube is equal to the driving pressure ΔP (which, in case of the circulation, is the arterial pressure minus the venous pressure) over the resistance R, $Q = \Delta P / R$. The resistance to flow is dependent upon the anatomic dimensions of the vasculature. The previous equation contains the most important factors involved in vascular flow and corresponds to Ohm's law for the calculation of electrical resistance. The resistance opposing flow cannot be measured directly but it is calculated from simultaneous determinations on flow and pressure gradient. The simplest unit, Peripheral Resistance Unit (PRU), is the resistance requiring a pressure gradient of 1 mmHg to force 1 mL of blood per minute through a vessel, described in Equation (1) (Abramson, 1967).

$$\mathrm{PRU} = \frac{1\ \mathrm{mmHg}}{1\ \mathrm{mL.\,min^{-1}}} \tag{1}$$

Consequently, arteries and nerves are important body structures that influence the hemodynamics of peripheral circulation (see Section 2.4).

2.2   Cutaneous microcirculation

Human skin is the largest organ of the body: it accounts for approximately 5% of the total body weight, extends over about 1.8 m^2 and has an average thickness of 1-2 mm. It provides the mechanical barrier to protect the body surface and prevents water loss. It is involved in sensory perception and vitamin D metabolism, in inflammation, hemostasis and wound healing. Human thermoregulation highly depends on this organ. Consequently, blood flow to the skin goes far beyond its nutritive demands. The nutritive blood flow is estimated to represent only 20% of the skin blood flow (SkBF), whereas the rest represents the functional blood flow (Lenasi, 2011).

There is a constant competition between thermoregulatory and non-thermoregulatory challenges. Many different mechanisms, ranging from systemic to local factors, constantly try to balance these two demands. SkBF is regulated by centrally mediated neural mechanisms and peripheral sensorial perception. Neural mechanisms include sympathetic fibers that supply all skin areas and regulate vasoconstriction of skin blood vessels. In what regards the latter, factors mainly released from the vascular endothelium are able to regulate vascular tone (Lenasi, 2011).

Microcirculation comprises arterioles, capillaries and venules. The microvessels in the papillary dermis vary in diameter from 10 to 35 μm, but most range from 17 to 22 μm. The cutaneous arteries arise from the subcutaneous tissue and enter the dermis to form the cutaneous arterial plexuses (Figure 2). The arterioles and venules of the cutaneous microcirculation form two important horizontal plexuses parallel to the skin surface: an upper horizontal plexus in the papillary dermis (papillary plexus) from which the nutritive capillary loops arise and a lower horizontal plexus at the dermal-subcutaneous border (cutaneous plexus). These two plexuses communicate with each other and with arterioles and venules and represent the physiologically important areas in the skin (Lenasi, 2011).

Arteriovenous anastomoses (AVAs), shown in Figure 2, are a special feature of human skin microcirculation. These are direct connections between arterioles and venules of the deep epidermal plexus and have thick muscular and richly innervated walls. They provide a low resistance short circuit for the passage of blood from arterioles to venules at high flow rates, as in response to body heating. They are found mainly in the apical regions of the skin (hands, feet, nose, lips and ears) and are most numerous in the nail beds, tips of digits, and palmar surfaces of digits, palms and soles, but they are almost absent from the dorsum of these areas (Lenasi, 2011).
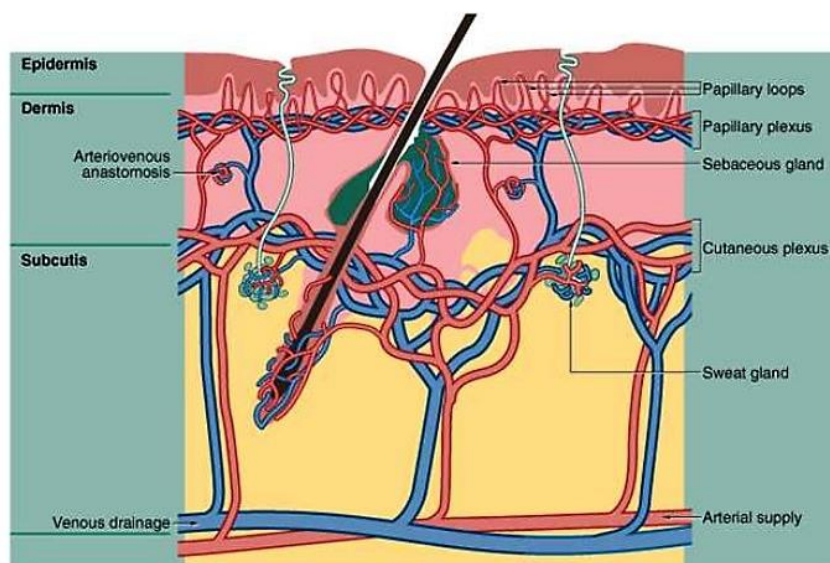
Figure 2 – Skin layers representation (Young, Woodford, & O'Dowd, 2013).

Physiological measurement of microcirculation properties is a challenge because the vessel structure is spatially inhomogeneous and perfusion can exhibit high variability over time (Allen & Howell, 2014). However, there are methods used to study the dynamics of the skin microcirculation: optical methods such as intravital dynamic capillaroscopy, photoplethysmography (PPG), venous occlusion plethysmography, laser Doppler flowmetry (LDF) and laser Doppler imaging. Alternative methods are based on thermographic assessment of blood flow, which is an indirect approach. The most recently developed methods include orthogonal polarization spectral imaging technique, sidestream dark field imaging technique, and laser speckle contrast imaging (Lenasi, 2011).

2.3 Factors affecting blood flow and blood pressure

There are variables that influence blood flow and blood pressure, such as: cardiac output, compliance, volume of the blood, viscosity of the blood, blood vessel length and diameter and emotional factors.

If the cardiac output increases, by increasing heart rate or stroke volume or both, the blood pressure will be higher and it will promote blood flow. This can happen due to sympathetic stimulation, catecholamines epinephrine and norepinephrine, thyroid hormones, and increased calcium ion levels. On the other hand, parasympathetic stimulation, elevated or decreased potassium ion levels, decreased calcium levels, anoxia, and acidosis can decrease the cardiac output, by decreasing heart rate or stroke volume or both, which will decrease arterial pressure and blood flow (OpenStax, 2016).

If an artery has a great compliance, it is more effectively able to expand to tolerate increases in blood flow without increased resistance or blood pressure. In the presence of a vascular disease that causes stiffening of arteries, compliance is reduced and resistance to blood flow is increased, which results in a reduced blood flow (OpenStax, 2016).

As blood volume increases, pressure and flow increase, and vice-versa. Under normal circumstances, blood volume variation is small. However, there are medical conditions that cause a low blood volume, called hypovolemia, or excessive fluid volume, called hypervolemia (OpenStax, 2016).

Viscosity of fluids affects their ability to flow. The blood viscosity is directly proportional to resistance and inversely proportional to flow. Any condition affecting erythropoiesis, such as polycythemia or anemia, can affect viscosity. The liver produces the majority of plasma proteins, therefore any medical condition affecting liver function can also change the viscosity and consequently the blood flow (OpenStax, 2016).

The length of a vessel is directly proportional to its resistance: the longer the vessel, the greater the resistance and the lower the blood flow. The length of blood vessels does not change in adults under normal circumstances. In opposition to length, the diameter of blood vessels changes throughout the body, according to the vessel type, and it may also change throughout the day because of neural and chemical signals that cause vasodilation and vasoconstriction. Considering the same volume of blood, an increased diameter will cause a lower resistance and, subsequently, an increase in flow, and vice-versa (OpenStax, 2016).

Also, some emotions such as embarrassment are associated with an increase in blood flow to the limbs (Holling, 1965). A very slight emotional stress or a mild environmental disturbance frequently cause a fluctuation in the sympathetic vasoconstrictor nerves activity, which reduces the blood circulation through the extremities' skin (Greenfield, 1965).

2.4   Anatomy and physiology of the wrist

The brachial artery branches at the elbow to form the ulnar artery and the radial artery, which supply blood to the forearm and hand (Figure 3) (VanPutte, Regan, & Russo, 2015).
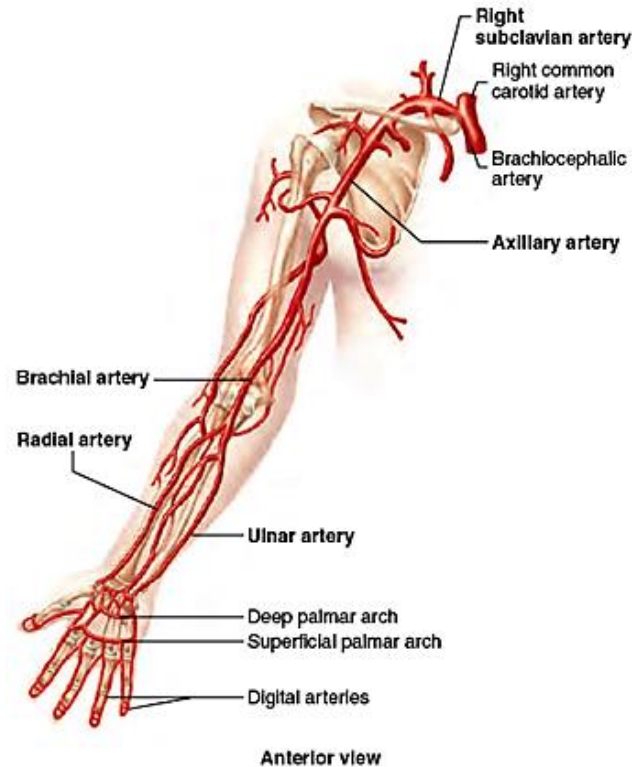
Figure 3 – Anterior view of the arteries of the right upper limb and their branches (VanPutte et al., 2015).

The radial artery contributes substantially to the supply of the thumb and the lateral side of the index finger. The remaining digits and the medial side of the index finger are supplied mainly by the ulnar artery. The radial and ulnar arteries form two interconnected vascular arches (superficial and deep) in the palm. The superficial palmar arch is formed by the ulnar artery and is completed by anastomosing with the radial artery. The deep palmar arch is formed by the radial artery and is completed by anastomosing with the ulnar artery. This arch is deep and proximal to the superficial arch. Digital arteries branch from each of the two palmar arches and unite to form single arteries on the medial and lateral sides of each digit (the fingers and the thumb) (Drake, Vogl, Wayne, & Mitchell, 2014; Seeley, R. R., VanPutte, C. L., Regan, J., & Russo, 2011). Figure 4 represents the arterial supply of the hand (Drake et al., 2014).

Figure 4 – Arterial supply of the hand. The radial artery supplies the deep palmar arch, and the ulnar artery supplies the superficial palmar arch. Both arches give rise to the digital arteries (Drake et al., 2014).

The hand is innervated by the ulnar, median and radial nerves, shown in Figure 5 (Healthwise, 2015). The three nerves contribute to cutaneous or general sensory innervation. The ulnar nerve innervates the skin over the ulnar side of the hand, two anterior forearm muscles and all intrinsic muscles of the hand except for the three thenar muscles and the two lateral lumbricals, which are innervated by the median nerve. The median nerve also innervates most of the anterior forearm muscles and the skin over the radial side of the hand. The radial nerve innervates all the muscles in the posterior arm and forearm as well as the skin over the posterior surface of the arm, forearm and hand (Drake et al., 2014; VanPutte et al., 2015).
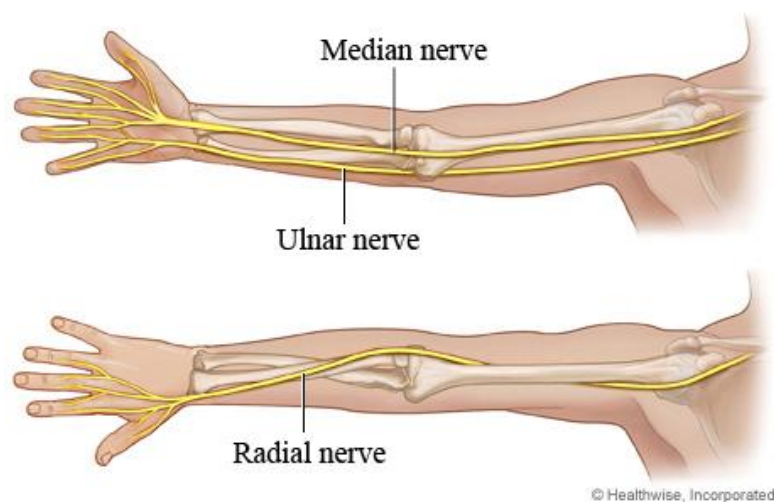
Figure 5 – Nerves of the arm (Healthwise, 2015).

2.5   Optical Imaging Techniques

Imaging methods for measuring perfusion of microvessels are experiencing important developments, since there has been a growing interest in the microvasculature. The non-invasive technologies are largely optical based, and spatial resolution is required for perfusion measurement. Comparing with standard medical imaging modalities, such as magnetic resonance imaging (MRI) and computed tomography (CT), optical based imaging techniques are generally less expensive and bulky. Portable optical imaging systems are currently being developed to improve and facilitate microvascular measurement (Allen & Howell, 2014).

2.5.1 Medical Thermal Imaging

Thermal imaging firstly became available for non-military applications in 1956. The technology has become financially more attractive with its improvements and widespread usage. Its performance is constantly improving, as well as its portability, and, consequently, it is now a recognized, useful, non-contact and non-invasive tool in clinical practice (Allen & Howell, 2014; John, Niumsawatt, Rozen, & Whitaker, 2016; Ring & Ammer, 2012). If this technique is performed under controlled standard conditions, the interpretation of the results may support objectively the diagnose of certain conditions and the monitoring of the reaction of a patient's physiology to a thermal, mechanical or chemical stress. The principle of thermography for microvascular imaging relies on the fact that changes in tissue perfusion often result in a change in tissue temperature (Allen & Howell, 2014). As ambient temperature rises above core body temperature, an increase in skin blood flow is able to keep skin temperature below 37°C (Allen & Howell, 2014; Mabuchi et al., 1995). Seifalian and co-workers (Seifalian, Stansby, Jackson, Howell, & Hamilton, 1994) described an asymptotic relationship between skin blood flow and skin temperature on hand skin. It is actually possible to convert a thermal image into an image estimating cutaneous blood flow at each pixel point. Merla and co-workers (Merla et al., 2007) developed a heat-flow model that allows to do it.

Infrared thermography is being used successfully in neurology, vascular disorders, rheumatic diseases, tissue viability, oncology, dermatological disorders, neonatal, ophthalmology, and surgery (Jones, 1998). For example, in plastic surgery, TI can be used to identify perforators in planning flap reconstruction, intraoperatively to assess perfusion and post operatively for flap monitoring (John et al., 2016).

Humans are homoeothermic beings, who are capable of generating and regulating the essential levels of temperature for survival. For example, in a situation of a temperature increase, neuronal signals are sent to activate methods of heat loss such as vasodilatation, perspiration, exhalation, and a reduction in the metabolic rate (Figure 6). This is important to maintain the homeostasis, a relatively constant environment within the body, regarding the functions and composition of fluids and tissues. Changes in the core temperature of more than a few degrees either way is an indicator of a dysfunction, and temperature variations outside this range may affect the vital biochemical processes in the body. For instance, localized increases in temperature suggest the existence of abnormalities such as fibrosis, inflammation, and infection; this causes the appearance of hot spots or asymmetrical patterns in an infrared TI output (Jones, 1998; Jones & Plassmann, 2002).

Healthcare professionals fail to detect a significant proportion of temperature disparities, according to Tse and co-workers (Tse et al., 2016). Skin temperature changes are usually assessed using tactile and visual physical examination methods, which could be improved using an objective measurement tool (Tse et al., 2016). An infrared (IR) camera detects the natural thermal radiation

released by the body and records the temperature distribution of the outer surface layer of the skin (Jones, 1998).
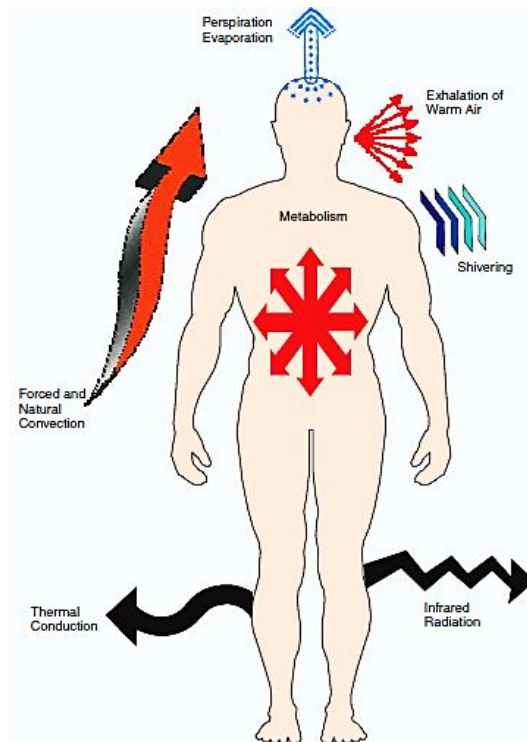
Figure 6 – Dynamic bodily heat balance (Jones & Plassmann, 2002).

2.5.1.1 Principle of Infra-red thermography

Any object whose temperature is above absolute zero, -273.15 ℃ (or 0 kelvin), emits radiant energy according to the Stefan-Boltzmann law (Ring, E. F. J., Thomas, R. A., & Howell, 2010):

$$\text{Total radiated power } Q = \sigma \varepsilon A T^4 \ [W] \tag{2}$$

It relates the radiated energy (electromagnetic radiation) emission rate Q, and the absolute temperature of the body T which is affected by the emissivity ε at the surface of area A. The constant σ is the Stefan-Boltzmann constant ($5.67 \times 10^{-8} \ W \ m^{-2} K^{-4}$). Every atom and every molecule of that object vibrates kinetically. Figure 7 shows that the transfer of radiant energy by electromagnetic waves in the thermal range occurs between 0.1 and 100 µm (Ring, E. F. J., Thomas, R. A., & Howell, 2010; Vardasca & Simoes, 2013).
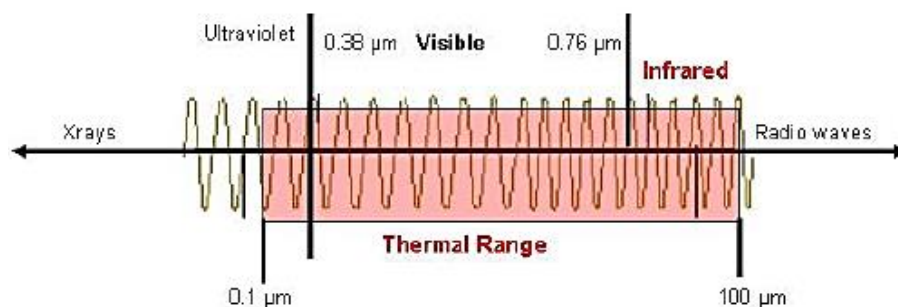
Figure 7 – Thermal range of electromagnetic radiation (Ring, E. F. J., Thomas, R. A., & Howell, 2010).

A physical object that absorbs all incident electromagnetic radiation is called a blackbody, which is also the best possible thermal radiator based on the Kirchhoff's Law. It states that a body that can absorb all radiation is equally capable of the emission of radiation. The emissivity of a body (ε_v) equals the ratio of the body's surface emissive power (E_v) to the emissive power of a blackbody (E_{bv}) at a specific temperature (Jones, 1998):

$$\varepsilon_v = E_v/E_{bv} \tag{3}$$

The emissivity ε_v quantifies the rate of emission or absorption for different surfaces and indicates how well an object emits or absorbs radiant energy. It has values between 0 and 1; a perfect blackbody has an emissivity value of 1 and is considered a perfect emitting surface, while highly reflective materials emissivity value approaches zero. The emissivity of a surface depends on the wavelength of the radiation being emitted (or absorbed). The emissivity of human skin is more or less constant at a value of 0.98 ± 0.01 between wavelengths of 2 and 14 μm. Therefore, human skin behaves as a physical blackbody in this wavelength region (Jones, 1998; Ring, E. F. J., Thomas, R. A., & Howell, 2010).

Thermal cameras include sensors that convert energy radiated by the human body into voltage, creating radiometric images where the pixel values are proportional to the perceived temperature values (Just et al., 2015).

2.5.1.2 Thermal imaging protocol standardization

A Medical Imaging Research Group in the United Kingdom conducted studies to understand the influence of the object imaged, the objects' position, the camera system, the calibration of the imager, the standard procedures for image capture, subject preparation and image analysis to the accuracy and precision of temperature measurements from thermal images. It was concluded that following a strictly standard procedure reduces errors and increases results reliability, also providing high reproducibility of recorded images and temperature readings (Ammer, 2006, 2008). Standardization of the technique reduces the influence of variables. Errors made due to the lack of using a standard image capturing methodology contributes to a loss of credibility.

Measurements are affected by environmental conditions such as temperature, relative humidity, incident luminance and air flow. A patient having medication, meals, drinks, drugs and physiotherapy before the appointment, and having ointments, jewelry and clothing over the skin during examination will influence the results of the recordings. Also, the duration and thermal conditions of the subject pre-examination acclimatization period affects the results. The quality of the measurements is reinforced by using standardized regions of interest (ROI), because a correct subject positioning and distance from the camera can be easily achieved. If all these variables are taken into account, it is possible to generate reliable results, which contribute to the modality improvement (Vardasca & Simoes, 2013).

2.5.1.3 Infra-red camera characteristics

The main components of a thermal camera are: the optics, that focus the IR energy onto the detector; the infrared detector array, which converts the infrared energy into a proportional electrical signal; the shutter system, that performs an image correction whenever the auto adjust button is depressed and the Digital Signal Processing (DSP) unit, which is the electronic component

that process the electrical signal to produce a radiometric picture and perform temperature calculations. The IR camera optics are mainly made of Silicon (Si) or Germanium (Ge). Germanium lenses are used for long-wavelength (7–14 μm) cameras and Silicon for short-wavelength (3-5 μm) cameras. The most recent system to construct the images is based on a matrix of sensor elements, called Focal Plane Array (FPA), which is capable of record the whole scene at once, being faster and producing images of better quality (Ring, E. F. J., Thomas, R. A., & Howell, 2010; Vardasca & Simoes, 2013).

There are two types of infrared detectors, the cooled and the uncooled. The cooled require cooling and normally operate at cryogenic temperatures. The need of cooling is power and time consuming, which increases the costs of their production and usage. When compared with the cooled detectors, the uncooled detectors produce images of lower quality and sensitivity to differences in the scene temperatures, but cameras using them are smaller, easy to use and have cheaper lenses (require smaller focal length) and are not limited in terms of usage time (Vardasca & Simoes, 2013).

There are parameters that should be taken into consideration when choosing a camera, such as: portability, size, weight, mode of operation, type of sensor, dynamic range, size of the sensor array, Noise Equivalent Temperature Difference (NETD), reproducibility and responsiveness. The Noise Equivalent Temperature Difference (NETD) is the temperature difference that will produce a signal-to-noise ratio of unity, which describes the system's electronic noise, for a given signal (how will it vary depending on the temperature of the object) (Ring, E. F. J., Thomas, R. A., & Howell, 2010; Vardasca & Simoes, 2013).

2.5.2 Laser Doppler Perfusion Imaging

The Doppler effect explains the change in a wave frequency when there is a relative movement between the source of the wave and an observer. Since the relative velocities of the source and the observer influence this frequency change, the Doppler effect can be employed to measure velocities. The laser was invented in 1960 and started being applied to Doppler techniques a few years after. The use of laser Doppler to assess blood flow has been investigated since the early 1970s (Briers, 2001).

The Doppler effect consists in the change in frequency that occurs when there is a relative movement between the source of a wave and a detector. It occurs because the waves emitted by the source are either compressed (if the source and detector are moving towards each other) or spread out (if they are moving away from each other) (Briers, 2001).

The Doppler effect does not only occur with sound, but also with light waves. However, their frequencies are very high and difficult to measure directly. This problem can be overcome by superimposing the Doppler-shifted wave with a reference wave of the original frequency. The resultant frequency, that is equal to the difference in frequency between the two waves, is much lower than either of the two waves and it is easily measured. It corresponds to the frequency shift produced by the Doppler effect, which is proportional to the velocity being measured. The relationship between the frequency change and the relative velocity of source and detector is given by Equation (4) (Briers, 2001):

$$f' - f = \frac{v}{c - v} f, \qquad\qquad (4)$$

where f is the original frequency of the light, f' is the shifted frequency, v is the relative velocity of the source and the detector and c is the velocity of the wave. In what concerns light waves, the velocity of light c is usually much larger than the velocities being measured and Equation (4) can be simplified to Equation (5) (Briers, 2001):

$$f' - f = \frac{v}{c}f, \tag{5}$$

Laser Doppler flowmetry (LDF) measures tissue blood flow by analyzing the Doppler frequency shift of low-power (typically in the region of 1 to 5 mW and single mode) laser light that is produced when moving red blood cells interact with the photons. The frequency-broadened light is scattered by the tissue and detected, and the resulting photocurrent is processed. Laser Doppler signals are recorded in Blood Perfusion Units (BPU), which is a relative unit scale. The red blood cell perfusion (or flow) is proportional to the blood perfusion output signal and is defined as the product of mean blood cell velocity and mean blood cell number concentration present in the small measuring volume of tissue under illumination from the probe. Probes are calibrated against a constant, known motility standard so that, for a given perfusion situation, all LDF probes will read the same value of blood perfusion expressed in BPU (Allen & Howell, 2014; Moor Instruments, 2016; Shepherd, 1990).

LDF is able to assess, non-invasively, blood flow information in the capillaries close to the skin surface as well as the underlying arterioles and venules involved in regulation of skin temperature (Figure 8), depending on the laser wavelength applied. The tissue thickness sampled by a red or IR laser system depends on probe design and tissue characteristics, but it is typically 1 mm (Allen & Howell, 2014; Moor Instruments, 2016).
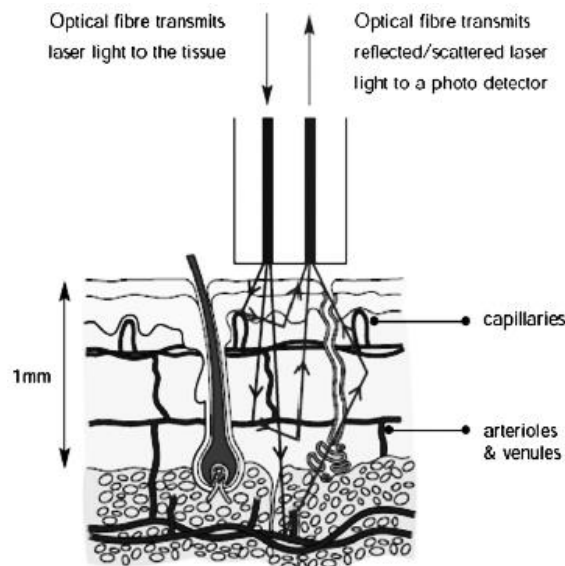
Figure 8 – Dermal layers and microcirculation probed by laser Doppler techniques (Moor Instruments, 2016).

Single point LDF measurements do not have an extended clinical utility since the spatial variability in blood flow across tissue, such as the skin, is high. Laser Doppler perfusion imaging (LDPI) technology (Figure 9(a)) overcomes this issue, since it provides a two-dimensional colour-coded representation of blood flow (Figure 9(b)). LDPI performs a systematic X-Y scanning of the laser beam and horizontal mapping of the cutaneous blood flow in a larger area of the skin. The laser beam position is controlled in the X and Y directions by a system of mirrors. A digital image composed of numerous single-point

recordings is displayed on a computer monitor and can be stored, analysed, and printed out. Figure 10 shows laser Doppler imaging applied to a free flap on the face after surgery (tissue was taken from the patient's back for the graft). As expected, flow is much lower in the flap than in the surrounding tissue. Spatial resolution can be adjusted by setting the target tissue size; a square field size in a range from a few centimetres up to 0.5 m is usually chosen (Allen & Howell, 2014; Briers, 2001; Fullerton et al., 2002).
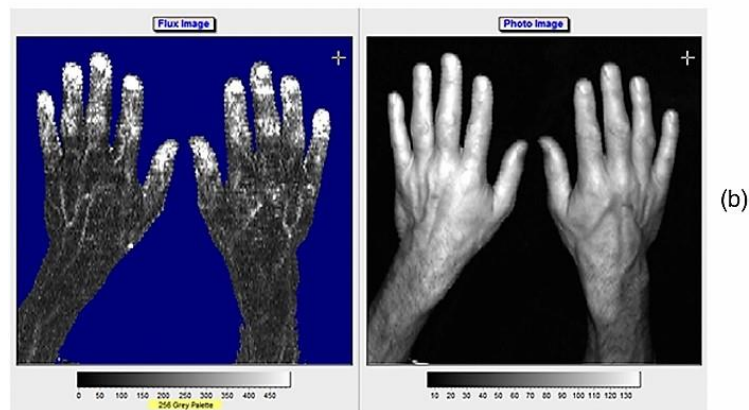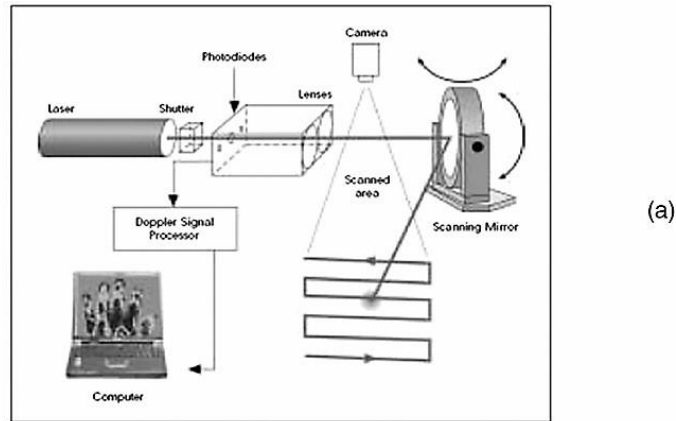
Figure 9 – (a) Schematic diagram of raster scanning based LDPI technology. (b) Example of LDPI of the hands alongside a visible light image. The increased perfusion is easily seen through the finger nails and on the edge of the thumb. The perfusion scale is also shown. (Allen & Howell, 2014).
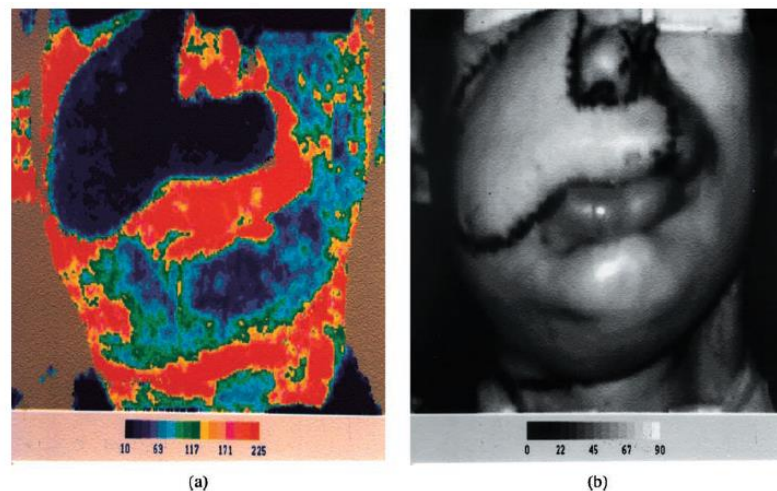
Figure 10 – (a) Laser Doppler image of a free flap on the face after surgery, showing much lower perfusion in the flap than in the surrounding tissue (b) Photograph of the same area, for reference (Briers, 2001).

LDPI is already a fully engineered instrument available commercially. Laser Doppler imagers have already proved to be a valuable tool and they have been extensively employed in clinical studies, namely regarding burn depth assessment, dermatology and plastic surgery, inflammation, wound healing, rheumatology, diabetes, pain, endothelial function assessment, cancer and angiogenesis. Further modality improvements may allow real-time operation, which will contribute for making it more attractive to the medical profession (Allen & Howell, 2014; Briers, 2001).

2.5.2.1 Comparison between LDF, LDPI and TI

TI and LDF are both non-invasive and accurate methods of measuring skin blood flow. However, they both have some practical disadvantages (Seifalian et al., 1994).

TI relies on skin temperature, that is, however, dependent on internal and external factors. Heat delivery through the blood changes the skin temperature, which also depends on the thermal conductivity of the subcutaneous tissues. In addition, heat may be lost by radiation, convection and conduction. Therefore, it is crucial to properly control and define the conditions under which skin temperature is measured. For these reasons, TI might only be able to provide accurate qualitative information on skin blood flow indirectly if a strict protocol is followed (Seifalian et al., 1994).

The major LDF setback is the cutaneous blood flow spatial heterogeneity, which is largely overcome by using LDPI. It allows an adequate statistical testing of possible differences in SkBF between selected skin areas within the same image or at comparative experimental situations. Technically, there are more advantages, including the possibility of employing image processing techniques such as spatial averaging (Fullerton et al., 2002; Seifalian et al., 1994).

Seifalian and co-workers (Seifalian et al., 1994) compared these techniques. LDPI compared well with LDF: a least-square regression analysis yielded a linear relationship with a high correlation coefficient of 0.960 (p < 0.01, n=38). However, the relationship between the TI and LDPI estimation of the skin blood flow at identical locations results in a correlation coefficient of 0.577 (p < 0.01, n=38) (Seifalian et al., 1994).

On the other hand, a more recent study (Merla et al., 2007) concluded that cutaneous blood perfusion values obtained from thermal imaging correlate to those obtained using LDPI, with the advantage of a better time resolution.

Diagnosis and monitoring of diseases related to cutaneous tissue and/or microcirculation might be complemented with the combination of the two techniques (Merla et al., 2007). However, correlation between the two methods at the hairless skin of the fingertips was not studied yet (Allen & Howell, 2014).

2.5.3 Photoplesthysmography imaging

Traditional PPG is a non-invasive contact optical method to detect the cardiovascular pulse wave, usually from the peripheral tissue, allowing to measure the blood volume changes in the microvascular structures. PPG systems are available commercially and recently, the interest in photoplesthysmographic sensor technology has been increasing. It is a low cost, easy to use technology, and the miniaturization of semiconductors components, along with the development of increasingly robust signal analysis algorithms, contribute to its evolution. PPG only requires two optoelectronic components: a light source to illuminate the tissue, such as LED, and a photodetector

to measure small variations in light intensity, which result from light interaction with the tissue (Allen & Howell, 2014; Izzati Zainal & Azami Sidek, 2016).

The reasons beyond the light intensity changes are not completely understood, although it is thought that the shifting orientation of red blood cells between systole and diastole, vessel wall movement and variations in tissue blood volume (due to blood pressure variations in the blood vessels, that occur during the cardiac cycle) might be responsible. It is generally accepted that PPG can provide valuable information about the cardiovascular system. PPG currently has clinical applications, such as the measurement of oxygen saturation (pulse oximetry), heart and respiration rates, blood pressure and cardiac output, vascular evaluation (pulse transit time, arterial compliance, endothelial dysfunction, vein evaluation, vasospastic conditions, microvascular blood flow and tissue viability), and nervous system evaluation (vasomotor function and thermoregulation, heart rate variability and orthostatic stress). The PPG waveform comprises a pulsatile, alternate current (AC) physiological waveform attributed to cardiac synchronous changes in the blood volume with each heart beat (Figure 11), and is superimposed on a slowly varying, direct current (DC) baseline with various lower frequency components attributed to respiration, sympathetic nervous system activity and thermoregulation. The recorded pulses have a direct relationship with perfusion: the greater the blood volume, the more the light source is attenuated. In practice, the PPG waveform is often inverted, as shown in Figure 11. The appearance of the pulse is defined by two phases: the anacrotic phase being the rising edge of the pulse, and the catacrotic phase being the falling edge of the pulse. The first phase is primarily concerned with systole, and the second phase with diastole (Figure 12). However, the points marked in Figure 12 might not be identified in every photoplesthysmographic signal, because the wave shape varies with factors such as age, vascular age, physical state, among others. Both the AC and DC components can be successfully extracted, using proper electronic filtering and amplification, and subsequently analysed (Allen, 2007; Chellappan, Zahedi, & Ali, 2007; Martins, 2010).
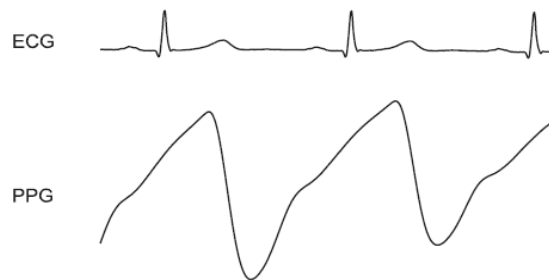
Figure 11 – The pulsatile (AC) component of the PPG signal and corresponding electrocardiogram (ECG). It represents the increased light attenuation associated with the increase in microvascular blood volume with each heartbeat. In practice, the PPG waveform is often inverted (Allen, 2007).
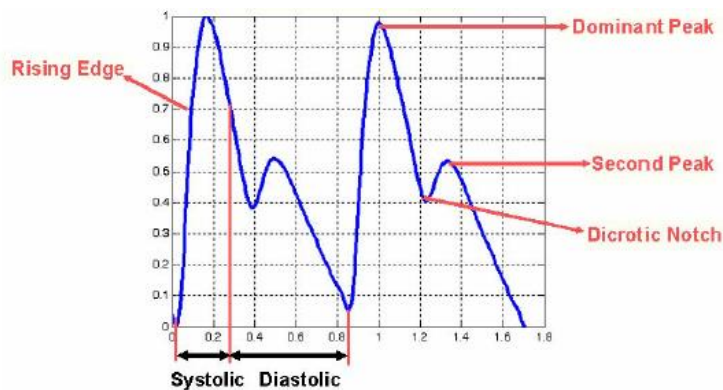
Figure 12 – Characteristic of a healthy young PPG pulses (Chellappan et al., 2007).

There are two main PPG operational configurations: transmission mode operation where the tissue sample is placed between the source and the detector, and reflection mode operation where the source and the detector are placed alongside each other. Figure 13 shows the arrangement of photodiode and the LED (light source) in the two configurations. Transmission mode PPG imposes more restrictions than the reflection mode PPG (Jayasree, 2009). A group research showed that the transmission mode failed in 17 participants whereas reflectance mode only failed in 3 participants. This suggests that reflectance mode generate better performance when compared to transmission mode (Izzati Zainal & Azami Sidek, 2016; Shafique, Kyriacou, & Pal, 2012). For these reasons, measurement systems usually operate in reflection mode in dual or triple wavelength configurations. Typically, 660 nm and/or 880 nm ring illumination sources are used for dual wavelengths (Allen & Howell, 2014).
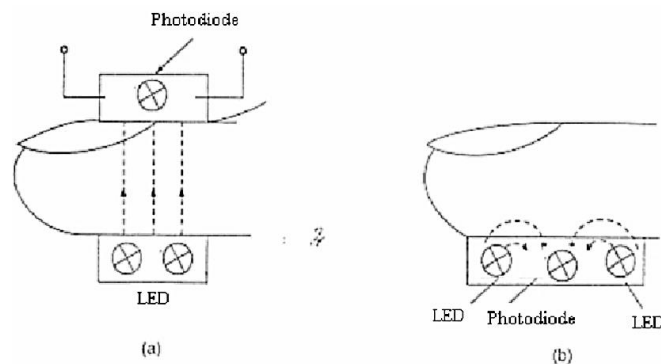
Figure 13 – Arrangement of photodiode and LED in a PPG probe (a) Transmission method (b) Reflection method (Jayasree, 2009).

In order to be able to detect the variation of volume using the information provided by the sensor, the location should have a high degree of superficial vasculature, high perfusion and few surrounding tissue layers, such as the ear lobe, finger tips and temple. Figure 14 represents a multi-bilateral site PPG pulse measurement and analysis system and example pulse recording from a healthy subject. The pulse wave signal returned by the PPG sensor is the result of the analogic and digital processing of the signal collected from the tissues (Allen, 2007; Chellappan et al., 2007; Martins, 2010).

Several studies (Rauh & Posfay, 2003; Suichies, Aarnoudse, Wouda, & Jentink, 1992; Tur, Tur, Maibach, & Guy, 1983; Ubbink, 2004) indicate that there is a significant correlation between PPG and laser Doppler flowmetry techniques.

Pulse oximeters are specially designed to allow non-invasive monitoring of oxygen saturation values by measuring the absorption of light waves as they pass through areas highly perfused by arterial blood, but most of them can also measure the heart rate and the PPG waveform of the pulse signal, which represents changes in blood volume at the sensor site that will also trigger the changes in the light transmitted through the tissues (Shamir, Eidelman, Floman, Kaplan, & Pizov, 1999). Although this technology has been available since the 1970s, the size and cost of pulse oximeters is now reduced due to science advancements and these devices are commonly used in the medical field for patient assessment, including in critical and primary care practice. Finger pulse oximeters are non-invasive, small, portable, light weighted, flexible fit and battery operated. They are able to function under a variety of blood pressures and perfusion levels and are accurate to 70% saturation (Koff, 2010).

PPG presents as disadvantages being a tissue contact technique and limited to a single or small number of measurement spots (Allen, 2007). Also, pulse oximeters have some other limitations that can affect the accuracy of the measurement. For example, a poor blood perfusion due to hypotension,

hypovolemic shock, cold environment, or cardiac failure may result in the equipment not providing a reading. Some diseases, such as anemia, as well as the presence of abnormal hemoglobins such as carboxyhemoglobin and methemoglobin, can also affect the measurement and the accuracy of the device. Nail polish, artificial nails, dirt or bright artificial lights can cause false low readings or no readings. The oximeter may not be able to identify an adequate pulse signal in the presence of motion artifacts or a shivering patient (Koff, 2010).
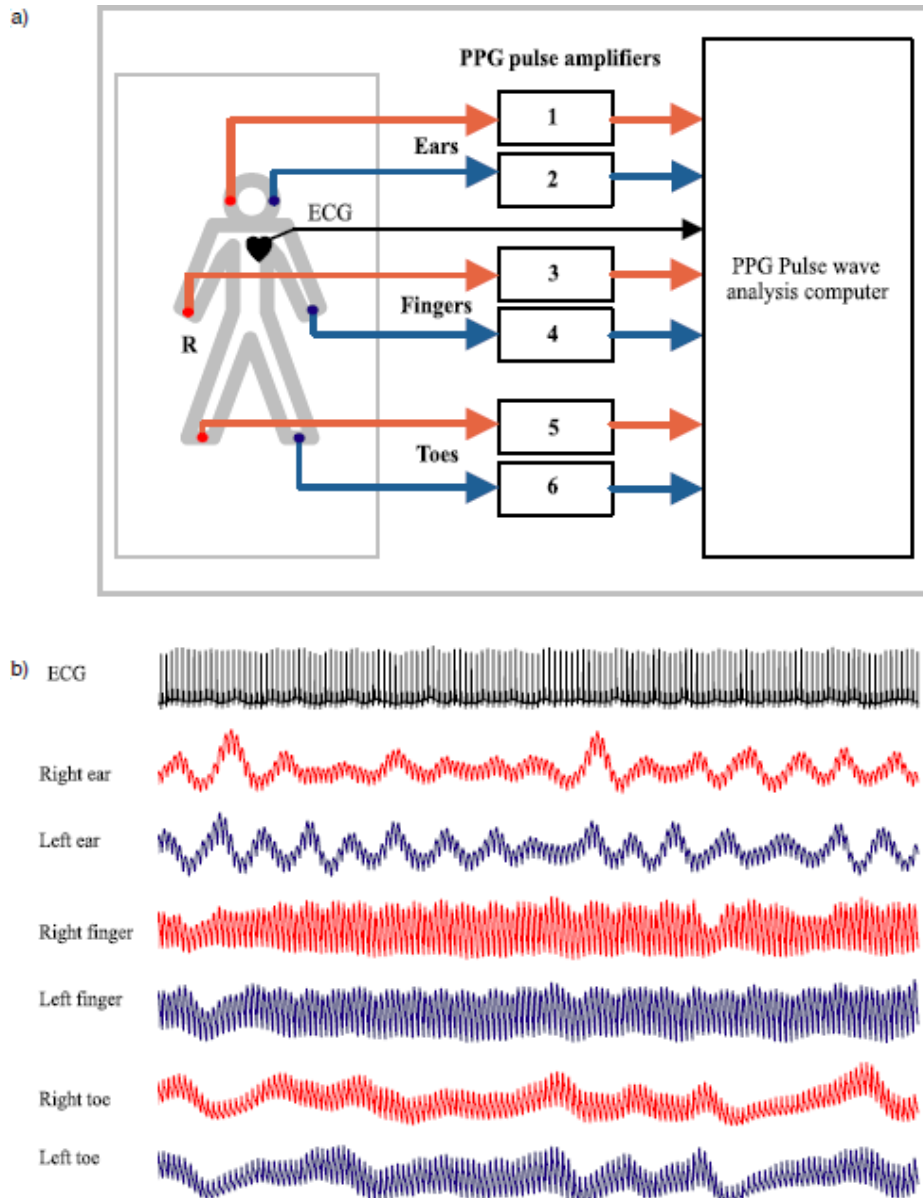
Figure 14 – Multi-bilateral site photoplethysmography. (a) An overview of a six channel PPG measurement and analysis system. (b) An example recording made from the right and left ear lobes, index fingers, and great toes of a healthy subject. There is similarity in the pulse characteristics between the right and left body sides but clear differences between the proximal and distal measurement sites (Allen, 2007).

Photoplethysmography imaging (iPPG) has been developed to give full-field and non-contact images of tissue pulsatility, which represents the regional perfusion for the superficial blood vessels, including the microcirculation. iPPG can be performed by applying single wavelength field illumination (near infrared) or dual wavelength illumination (both red and near infrared). It is able to achieve high resolutions and fast scanning speeds rates (in the range of tens of frames per second).

Nevertheless, a movement artifact can significantly influence the results. For this reason, correction algorithms play a very important role in the modality development (Allen & Howell, 2014).

Sun and co-workers studied the performance of an iPPG system by measuring the cardiac pulse from images of the hand in 12 subjects before and after five minutes of cycling exercise. The physiological parameters (heart rate and respiration rate) derived from the images captured by the iPPG system exhibited functional characteristics comparable to conventional contact PPG sensors (Sun et al., 2011).

2.6   Vascular dominance assessment using LDPI, PPG and TI

Laser Doppler perfusion imaging was already used to assess the arterial dominance in hands and vascular dynamics, in order to prevent ischemic complications to the hand after radial artery removal or cannulation (Pola et al., 1996; Ryan, Raines, Dalton, & Mathieu, 1973). Some Doppler studies' results point to an ulnar artery dominance (Little et al., 1973; Ryan et al., 1973), as described previously in Chapter 1.

PPG was also used for the same purpose: according to Winkler and co-workers (Winkler et al., 1998) results, there is a mixed dominance, while Haerle and co-workers (Haerle et al., 2003, 2002) results suggest that, as described previously in Chapter 1, the ulnar artery is rarely dominant at the forearm level.

Thermography was also a tool to address this issue, namely while studying the hemodynamic behaviour of the hand after a radial forearm flap harvesting. For example, Suominen and co-workers (Suominen & Asko-Seljavaara, 1996) evaluated circulatory changes in the donor hand of 18 patients, by performing a cold stress test and thermography of both hands, 13 months after a radial forearm flap had been harvested. It was concluded that the raising of a radial forearm flap, particularly a large one, affects the thermoregulatory system of the donor hand, results in abnormal rewarming, and can cause subjective cold intolerance, suggesting that performing this surgery is risky, since a crucial blood supplier is being sacrificed (Suominen & Asko-Seljavaara, 1996).

2.7   Variables of influence

There are variables that might influence wrist vascular dominance, such as age, sex, body mass index and handedness.

Age, body mass index and sex affect the human body thermoregulation. Normal growth provokes a high metabolic rate in young people. Due to the ageing of cells, older people present a very slow metabolic rate. Subjects having small body mass index are more affected by heat exchange with the environment than people with high body mass index. Women core temperature oscillates between 0.2 to 0.4ºC, due to their menstrual cycle (Tortora & Grabowski, 2003).

Haerle and co-workers (Haerle et al., 2003) concluded that differences found between the right and the left hands did not correlate with handedness and were probably due to variability during measurements using color duplex sonography.

Oettle and co-workers (Oettle, Niekerk, & Boon, 2006) studied the arterial supply of the hand, in left- and right-handed individuals, left and right hands and the ulnar and radial arteries, when performing the modified Allen test, using an oxygen saturation monitor. No significant differences between the modified Allen test of the left and right hands in the left and right-handed individuals were found.

However, an objective description of the influence of handedness in wrist vascular dominance, as well as other variables, such as age, sex and body mass index, using thermography as a measurement tool, is not defined in the literature yet.

2.8   Conclusion

In conclusion, this issue is not totally solved yet and is still controversial. Thermography, a highly efficient tool that is able to indirectly measure the blood flow, has only been used to reveal the changes in circulatory dynamics in the hand after harvesting forearm flaps (Iida, Numata, Shiba, & Nagata, 2002; Jaworski, Siondalski, Jarmoszewicz, & Rogowski, 2007; Suominen & Asko-Seljavaara, 1996). However, there is few research on vascular dominance at the wrist level, along with the possible influence of bilateral preference, age, sex and body mass index, using thermography.

Chapter 3

Methodology

This chapter outlines the methodology followed in this study, including the materials and protocol used in the thermal imaging data collection, information about PPG data collection and LDPI equipment, as well as the steps followed to perform an automatic detection of hand fingertips and phalanges in thermal images.

3.1 Ethical Issues

This work was conducted accordingly to the ethical principles for medical research. Ethical approval was obtained from Centro Hospitalar de S. João health ethical committee and Board of administration (Appendix A).

3.2 Thermal Imaging

Medical infrared images can be captured in several modes that are classified according to the temporal sequence of images. In the first mode, a single static image of a patient is captured at an instant in time and it is possible to identify hot and cold spots (static thermography). In the second mode, static images are captured on occasions that are separated by a substantial time interval in order to monitor the progress of a disease or treatment. In the third mode, a series of images is captured over a period of minutes to monitor the recovery of skin temperature following a provocation (dynamic thermography) such as thermal stress (cooling or heating), mechanical stress (vibration or exercise), or chemical stress (vasodilators or vasoconstrictors) (Jones & Plassmann, 2002).

In this work, the vascular dominance of the wrist was studied by applying a mechanical stress, through modified Allen test, and analysing the resulting hand blood perfusion. A modified Allen test measures arterial competency. The procedure for performing the test is represented in Figure 15. In this test, the physician compresses both arteries at the level of the wrist with the hand outstretched. The patient is then asked to open and close the hand into a fist at least ten times with both arteries still compressed. The hand is then relaxed and the radial artery is released. The entire palm and digits should fill demonstrating good collateral flow. The test is repeated, with the ulnar artery being released. Again, the entire palm and digits should fill (Oettle et al., 2006; Peterson, Khabiri,

Litzendorf, & Stawicki, 2013). This test is usually performed when planning intravascular access to the radial artery or selecting patients for radial artery harvesting, and it is also used in the diagnosis of vascular abnormalities, such as Raynaud's phenomenon. According to Kohonen and co-workers (Kohonen, Teerenhovi, Terho, Laurikka, & Tarkka, 2007), the modified Allen test is a good and valid screening test for the circulation of the hand, reaching a sensitivity of 73.2% and specificity of 97.1% when compared with more objective tests, such as upper arm Doppler ultrasonography and digital plethysmography. Being a subjective measurement, the modified Allen test contains several disadvantages. Its interpretation is based on the examiner experience, and it does not give information about the vascular anatomy of the hand, only allowing the assessment of the functional circulatory status. Furthermore, an inadequate compression of the radial artery may lead to a false-negative result, while a false-positive may be caused by the extension of the wrist (Jarvis, Jarvis, Jones, & Spyt, 2000; Kohonen et al., 2007). According to Jarvis and co-workers (Jarvis et al., 2000), the use of modified Allen's test for the preoperative assessment of the ulnar collateral blood supply of the hand in patients undergoing coronary bypass surgery is not reliable, not performing satisfactorily as a discriminatory test, and for that reason the authors suggest the use of more objective tests, such as Doppler ultrasound.
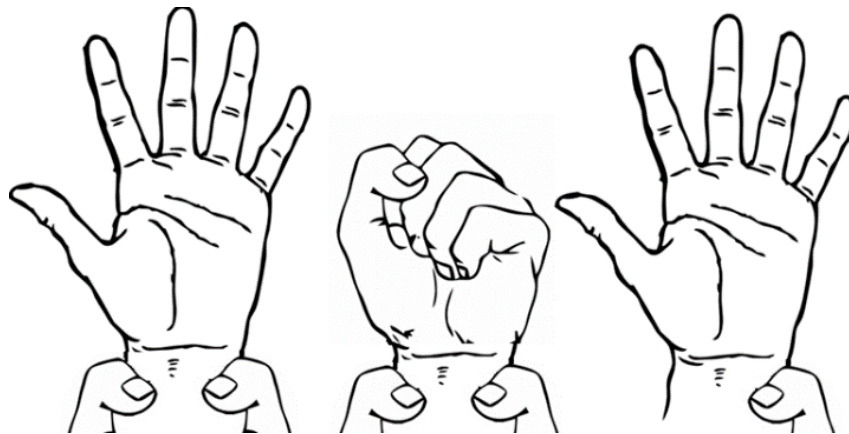
Figure 15 – Modified Allen Test (Peterson et al., 2013).

It is expected that the palmar aspect of the hand is warmer than the dorsal aspect, because of the relatively flexed position (toward a fist) that the hand often assumes, the greater amount of fatty tissue on the palmar side, and the superficial positions of the veins on the back of the hand (Oerlemans, Graff, & Dijkstra-Hekkink, 1999). However, according to Kurt Ammer review (Ammer, 2016), 75% of the articles that compared dorsal and palmar hand temperatures reported a difference less than 0.2ºC. Taking into consideration the easiness of identifying the ischemic point of the modified Allen test during the data collection process, it was decided to measure the hand volar side temperature. Also, one argument for recording the hand temperature from the non-hairy volar side over the hairy dorsal side is that the process is not influenced by the isolator effect of the hairs (Ammer, 2016).

3.2.1 Sample characterization

The thermographic study was conducted on 47 healthy participants (absent of hand blood circulation pathologies), confirmed by the questionnaire they were asked to fill (Appendix D). It was possible to get a proper sample characterization from the information obtained in this questionnaire,

including biometric parameters such as: sex (if feminine, days from last menstruation), age, height, weight, handedness, smoking habits, general health problems, upper limb traumas, medication and cholesterol level. Body mass index (BMI) was calculated using Equation (2) (Keys, Fidanza, Karvonen, & Kimura, 1972).

$$BMI = \frac{Weight\ (kg)}{Height^2\ (m^2)} \tag{2}$$

The total sample is composed by 26 female and 21 male individuals. The average age is 23±4 years. The average BMI is 22.7±3.6 kg/m². Five participants have left handedness, while 42 have right handedness. Five participants were smokers, while 42 are not. Thirty seven participants have no health problem, while 10 reported one. Two participants reported having an upper limb trauma in the past. Fourteen participants take some sort of medication, but it does not affect hand blood circulation. Two participants have a borderline high cholesterol level (200-239 mg/dL), five participants have a desirable cholesterol level (less than 200 mg/dL) (NHLBI, 2005) and 40 do not have the knowledge about their cholesterol level.

The participants were previously informed about the conducted procedure (Appendix C) and asked to sign an informed consent (Appendix E). All subjects were treated equally and were able to withdraw at any moment, without further implications. Their confidentiality was always preserved and their names and personal details are not used in any files. No harm or stress was caused to the participants.

3.2.2 Data collection

For the thermographic captures, a FLIR® E60sc thermal camera operated with FLIR® Researcher Pro 2.10 software (a Windows-based infrared software package for capturing, recording, and analyzing thermal images) was used. This thermal camera has a focal plane array size of 320x240, and it has sensors that measure temperatures ranging from -20˚C to +120˚C. Its NETD is of < 50mK and it has an measurement traceability of ± 2% of the overall reading. A sensor Testo 175 H1 (accuracy of ± 5% of the overall reading) was also needed for measuring the temperature and humidity of the room, which were maintained at 23.8±1.4˚C and 49.2±8.3%, respectively.

Appendix B contains the protocol reporting the procedures that were followed, including patient, equipment and examination room preparation. This protocol follows the guidelines of the "Glamorgan Protocol", which states the standard procedures for recording and evaluating thermal images for medical applications (Ammer, 2008). Appendix C, D and E contain the proper documents with the information to the participants about the study, to assess their biometric data and the informed consent.

The capture of thermal images was done while the modified Allen test is performed by a physician on the healthy participant, following the steps described in Figure 16.

Figure 16 – Scheme representing the imaging capture procedure while the modified Allen test is being performed by the physician.

The sequence described in Figure 16 was repeated to the other arm and the other artery. Firstly, the right hand was tested, with the occlusion of the radial artery, followed by the left hand test. This sequence was repeated, with the occlusion of the ulnar artery. The basal thermogram is taken after a 10 minutes acclimatization period. The thermogram corresponding to the second step of this sequence is taken immediately after the participant opens and closes the hand into a fist several times, with both arteries occlusion. In what regards the third and fourth steps, there is no agreement on the cut-off point (seconds usually necessary to achieve a correct capillary filling of the fingers of an healthy subject, after an artery release) which may vary between 3 and 10 seconds (Kohonen et al., 2007). Therefore, following the physician advice and experience, the capture was performed 7 seconds after each artery release, in a standard position: the forearm is supported in a surface, while the physician is performing the modified Allen test. The camera was placed in a tripod to keep the camera stable at a distance of 50 cm from the subject, on average, in order to capture the entire hand, allowing a more stable positioning of the target. The participant was asked to fully open his/her fingers, so that a good ROIs marking is possible. This methodology was performed on 22 participants.

A second methodology was performed on 25 participants. Regarding the second step of the sequence, thermograms were also captured 15 and 30 seconds after opening and closing the hands, with both arteries occluded. In what concerns the third and fourth steps, it was decided to capture thermograms 15 and 30 seconds after the arteries release, besides the 7 seconds cut-off thermogram.

3.2.3 Image Analysis

Image analysis was performed using FLIR® Researcher Pro 2.10 software, that allowed the manual setting of the ROIs, retrieving the mean temperature of each defined ROI as an output. The four regions of interest, in this particular case, are shown in Figure 17. They were defined in the middle area of the thumb (AR01) and the middle phalanx of the little finger (AR02), being, in this way, as distant as possible, so as to assure that AR01 is mainly supplied by the radial artery, while AR02 is mainly supplied by the ulnar artery (see Section 2.4). The distal phalanges were not considered because the blood takes more time to reach these peripheral areas, which can affect the recording of the reperfusion. Also, the ROIs were defined in the radial and ulnar arteries exits (AR03 and AR04, respectively). These four locations were defined in order to avoid interference of the two interconnected vascular arches (superficial and deep) in the palm (see Section 2.4).
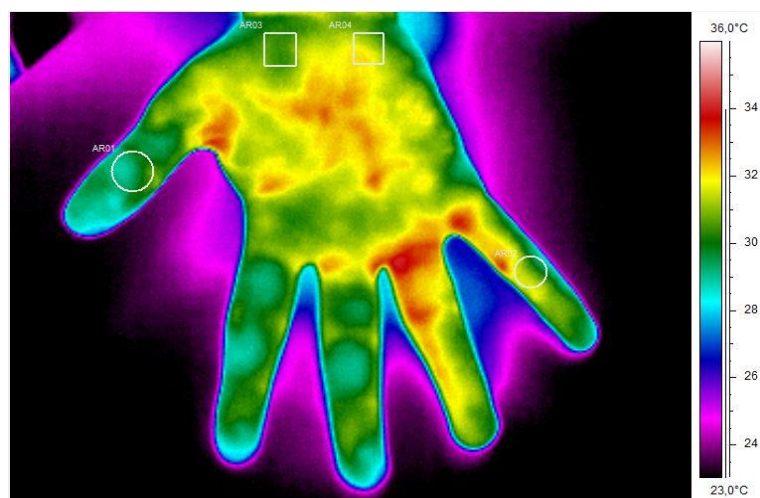
Figure 17 – Defined regions of interest, AR01 and AR02 (circles) in the thumb middle area and the little finger middle phalanx, respectively, and AR03 and AR04 (squares) in the radial and ulnar arteries exits, respectively.

3.2.4 Statistical Analysis

The IBM® SPSS® v24.0.0.1 (Statistical Package for the Social Sciences) software was used for the statistical analysis.

The statistical analysis of the collected data included a Shapiro-Wilk test, an inferential test used to verify if it follows a specific distribution (typically, the normal distribution). Shapiro-Wilk test is usually calculated for samples with less than 50 observations. If the Shapiro-Wilk test results are not statistically significant, there is not enough evidence to reject the null hypothesis that there is no difference between the tested distribution and a theoretical normal distribution, and a parametric test was used in data analysis (Repeated Measures ANOVA). On the other hand, if the test results are statistically significant ($p <= 0.05$), there is a departure from normality and nonparametric tests should be used in data analysis (Kim, 2013).

Another method of assessing normality using skewness and kurtosis of the distribution was also used. Skewness measures the asymmetry of a variable distribution. Kurtosis is a measure of the 'peakedness' of the probability distribution of a random variable. A z-test is applied to test normality of the variable distribution using these two measures, and it is obtained by dividing the skew values or excess kurtosis by their standard errors. For small samples ($n < 50$), if absolute z-scores for either skewness or kurtosis are larger than 1.96, the null hypothesis should be rejected and it can be concluded that the distribution of the sample is non-normal (Kim, 2013).

When both methods suggest that data shows a departure from normality, data transformation may be used and the distribution of the transformed variables is assessed. If, even after this transformation, the sample is not normally distributed, nonparametric methods must be used (Kim, 2013).

The statistical analysis for the first methodology showed that the data distribution is normal, after Shapiro-Wilk and z-score tests, therefore repeated measures ANOVA was used. On the other hand, the statistical analysis for the second methodology showed that the data distribution is not normal, even after a logarithmic transformation, therefore nonparametric methods were used (Friedman's two-way analysis of variance and Mann-Whitney U test).

Repeated measures ANOVA is the equivalent of the one-way ANOVA, but for related, not independent groups test. Repeated measures ANOVA is a test to detect any overall differences between related means. It is advisable for studies that investigate either changes in mean scores over three or more time points, or differences in mean scores under three or more different conditions, which is the case of this study. The within-subjects factors included in this test are: compression order (if the ulnar or radial artery is released first), hand (right or left) and time (basal, immediately after both arteries occlusion, 7 seconds after one artery release and 7 seconds after the other artery release situations). The possible effect of sex (between-subjects factor) was also studied. The null hypothesis states that the related population means are equal ($\mu_1 = \mu_2 = \mu_3 = \dots = \mu_k$, where μ is population mean and k is number of related groups). The alternative hypothesis states that the related population means are not equal (at least one is different to another). To detect which specific means significantly differ, pairwise multiple comparisons were performed by the Bonferroni post hoc test (IBM Knowledge Center, 2015; Laerd Statistics, 2013c).

ANOVAs with repeated measures are vulnerable to the violation of sphericity. Sphericity is the condition where the variances of the differences between all combinations of related groups are equal. The violation of sphericity causes the increase in the Type I error rate (incorrect rejection of a true null hypothesis). A formal test called Mauchly's Test of Sphericity is usually used for testing the assumption of sphericity. if Mauchly's Test of Sphericity is statistically significant ($p <= 0.05$), the null

hypothesis can be rejected: the variances of the differences are not equal and violation of sphericity has occurred. If there is a violation of sphericity, it is possible to apply corrections to the F-distribution so that a more valid F-value is obtained, the Greenhouse-Geisser or the Huynd-Feldt corrections. The degree to which sphericity is present, or not, is represented by epsilon (ϵ). It is recommended to use the Greenhouse-Geisser correction, if estimated epsilon (ϵ) is less than 0.75, and the Huynd-Feldt correction if estimated epsilon (ϵ) is greater than 0.75 (Laerd Statistics, 2013d).

The Friedman test is the non-parametric alternative to the ANOVA with repeated measures, also giving information about the statistic significance of the difference between the mean scores of the related groups. It can be used when the requirements to run the ANOVA with repeated measures are not met (for instance, data that does not follow a normal distribution). Pairwise comparisons are retrieved by the test (Laerd Statistics, 2013a). The Mann-Whitney U test is used to compare differences between two independent groups when the dependent variable is either ordinal or continuous, but not normally distributed. In this case, the Mann-Whitney U test was used to understand whether the variables differ based on sex (Laerd Statistics, 2013b).

3.3   Photoplesthysmography and Laser Doppler perfusion imaging

In order to validate and complement the thermal infrared imaging results, LDPI and PPG data was intended to be recorded and analysed, so as to enable the development of a more complete evaluation, since these techniques also allow the measurement of the microvascular perfusion with proven efficiency (see Sections 2.5.2 and 2.5.3).

In what concerns the laser Doppler perfusion imaging, the unavailability of an appropriate equipment in Hospital de São João prevented the use of this technique. The available equipment was only suitable for large calibre blood vessels, such as the legs', so it was impossible to record data from the hands.

Regarding the PPG, the data collection was supposed to be performed using an oximeter, after thermal imaging recording, however some technical issues prevented the success of the acquisition.

It was ensured that the participant was healthy, not wearing false fingernails and that the nails were free from nail polish. The environment had no bright artificial lights, which could interfere with the measurement (see Chapter 2.5.3). The thumb and little fingers were selected, so two fingertip pulse oximeters were used at the same time: GT-300C203 Geratherm® and CMS50D+ Contec™ models.

The transducer probes were placed over the participant fingers so that light beams and sensors oppose each other (Lippincott Williams & Wilkins., 2007).

The PPG data recording was supposed to happen while the physician is performing the modified Allen test, in a procedure similar to the sequence described in Figure 16, so that PPG and TI data could be compared. However, this methodology was not a successful approach, because the pulse oximeters are sensitive to excessive motion artifacts (see Chapter 2.5.3). Since the modified Allen test requires opening and closing the hand into a fist several times with both arteries compressed (which was impossible to do in a proper way, due to the volume of the equipments attached to the fingers), so that the blood leaves the hand blood vessels (Figure 15), the oximeters' readings were not reliable. Despite the arteries occlusion, the value of oxygen saturation remained in the healthy range, with little to no variation. Also, the resolution of this variable (1%) in both oximeters was not enough to detect smaller variations.

Chapter 4

Results

In this chapter, the results obtained from the methodologies described in Chapter 3 are presented. Firstly, the results obtained following the first methodology will be addressed.

Figure 18 shows the thermograms related to participant 3 over time, where the ROIs are the middle area of the thumb (radial zone), the middle phalanx of the little finger (ulnar zone), used in most of the metrics described below, and the radial and ulnar arteries exits (only used for the metric described in Figures 23, 24, 32 and 33).
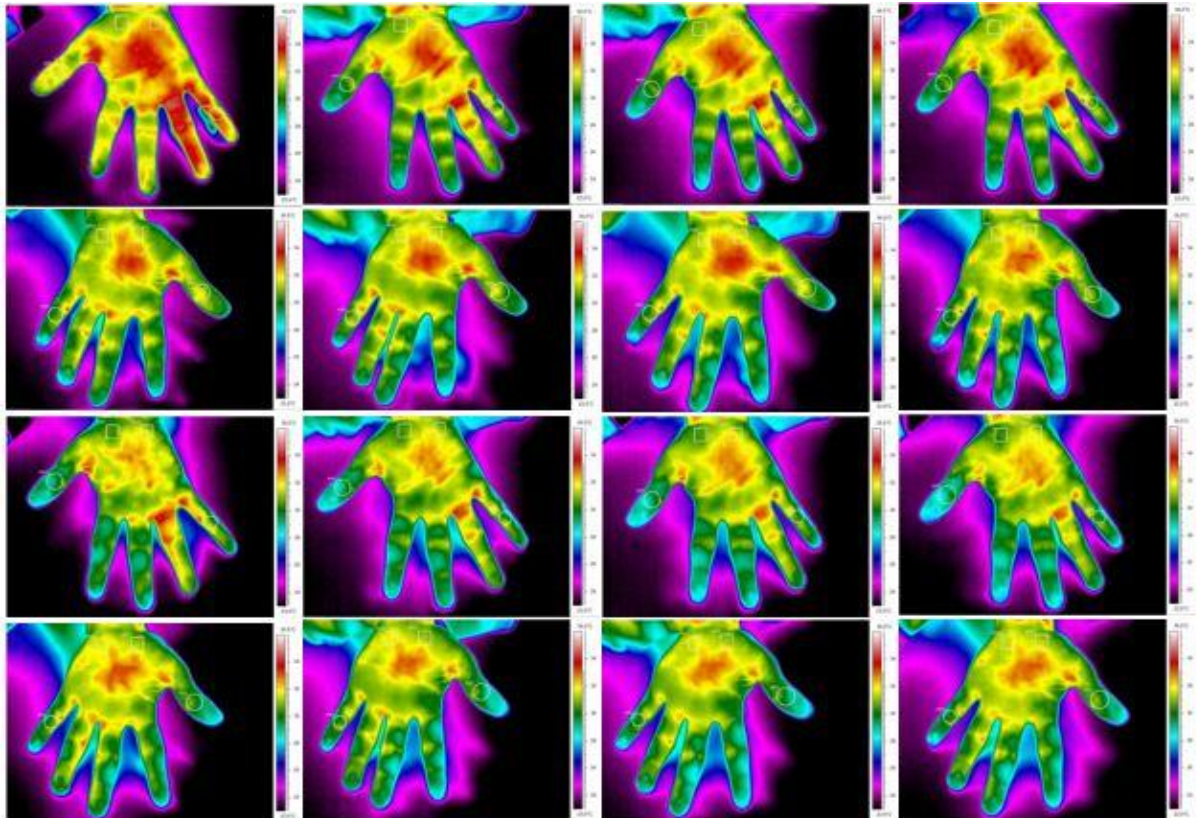
Figure 18 – Thermograms related to participant 3 over time, where the ROIs are the middle area of the thumb and the middle phalanx of little finger (circles), as well as the radial and ulnar arteries exits (squares).

In Figure 18, the first and second rows of thermograms are related to the right and left hands, respectively, where the ulnar artery is released first. The third and fourth rows of thermograms are related to the right and left hands, respectively, where the radial artery is released first.

Situation 0 refers to the basal situation (first column of thermograms in Figure 18). Situation 1 refers to the situation where both arteries are occluded (second column of thermograms in Figure 18). Situation 2 refers to the situation where one artery was released (third column of thermograms in Figure 18). Situation 3 refers to the situation where the other artery was also released (fourth column of thermograms in Figure 18). Pairwise comparisons p-values will be complementing the results presentation, telling which metric results are statistically significant.

Figure 19 presents the average of the temperature difference between situation 1 and situation 0, for both hands, representing the thermic manifestation that happens in each ROI when the blood leaves the hand, in response to the occlusion of both arteries, when the ulnar artery is released first and when the radial artery is released first. The differences are statistically significant ($p=0.000$).

Figure 19 – Average of the temperature difference between the situation 1 and the situation 0, for the left (at left) and right (at right) hands, when the ulnar artery is released first (top) and when the radial artery is released first (bottom).

Figure 20 shows the average of the temperature difference between situation 2 and situation 1, for the left and right hands, representing the thermic manifestation that happens in the blood reperfusion of the zone correspondent to the released artery (non-collateral reperfusion), i.e., the ulnar zone reperfusion when the ulnar artery is released and the radial zone reperfusion when the radial artery is released. The values are statistically not significant ($p=1.000$).
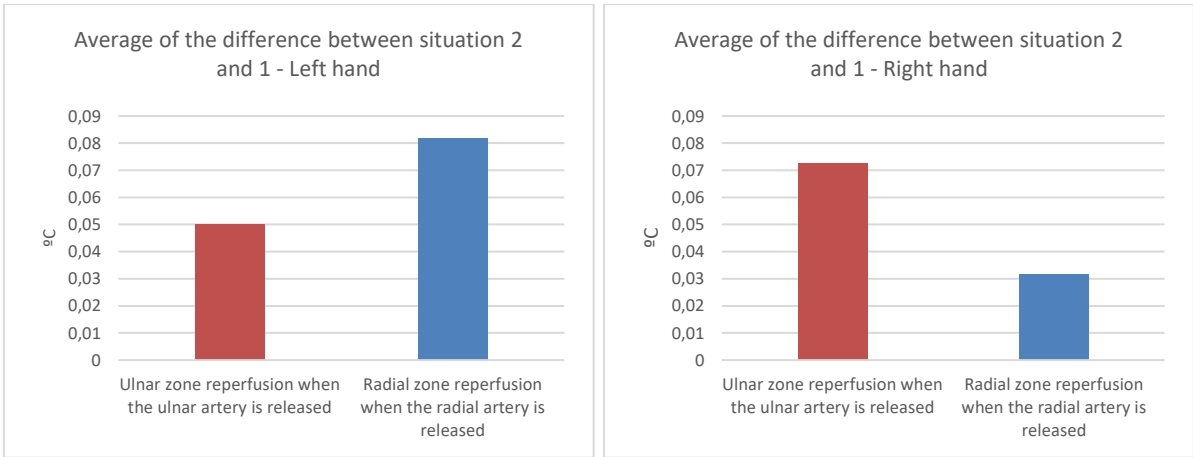
Figure 20 – Average of the temperature difference between situation 2 and situation 1, for the left (at left) and right (at right) hands (reperfusion of the zone correspondent to released artery).

Figure 21 shows the average of the temperature difference between situation 2 and situation 1, for the left and right hands, representing the thermic manifestation that happens in the blood reperfusion of the opposite zone to the released artery (collateral reperfusion), i.e., the radial zone reperfusion when the ulnar artery is released and the ulnar zone reperfusion when the radial artery is released. Statistically, the values are not significant (p=1.000).

Figure 21 – Average of the temperature difference between situation 2 and situation 1, for the left (at left) and right (at right) hands (reperfusion of the opposite zone to the released artery).

The temperature differences from each situation (both arteries compressed, one artery released and both arteries released) to the basal situation were calculated. Figure 22 shows the thermal indexes (gradients) Ti1, Ti2 and Ti3 that represent the differences between the ROIs corresponding to the artery released firstly and the artery released later, regarding the differences of situations 1, 2 and 3, respectively, to the basal situation. The difference between Ti2 and Ti1 is not significant (p=0.135), while the difference between Ti3 and Ti2 is statistically significant (p=0.046).

Figures 23 and 24 show the temperature differences between the phalanges and the corresponding artery exit (for example, the middle phalanx of the little finger and the ulnar artery exit, which are the ulnar ROIs), over time, for both hands, when the ulnar artery is released first and when the radial artery is released first, respectively. The gradient decrease in all graphics is generally significant (p=0.002), but the gradient increase is not statistically significant from moment 2 to 3 (p=0.101), neither from moment 3 to 4 (p=1.000).
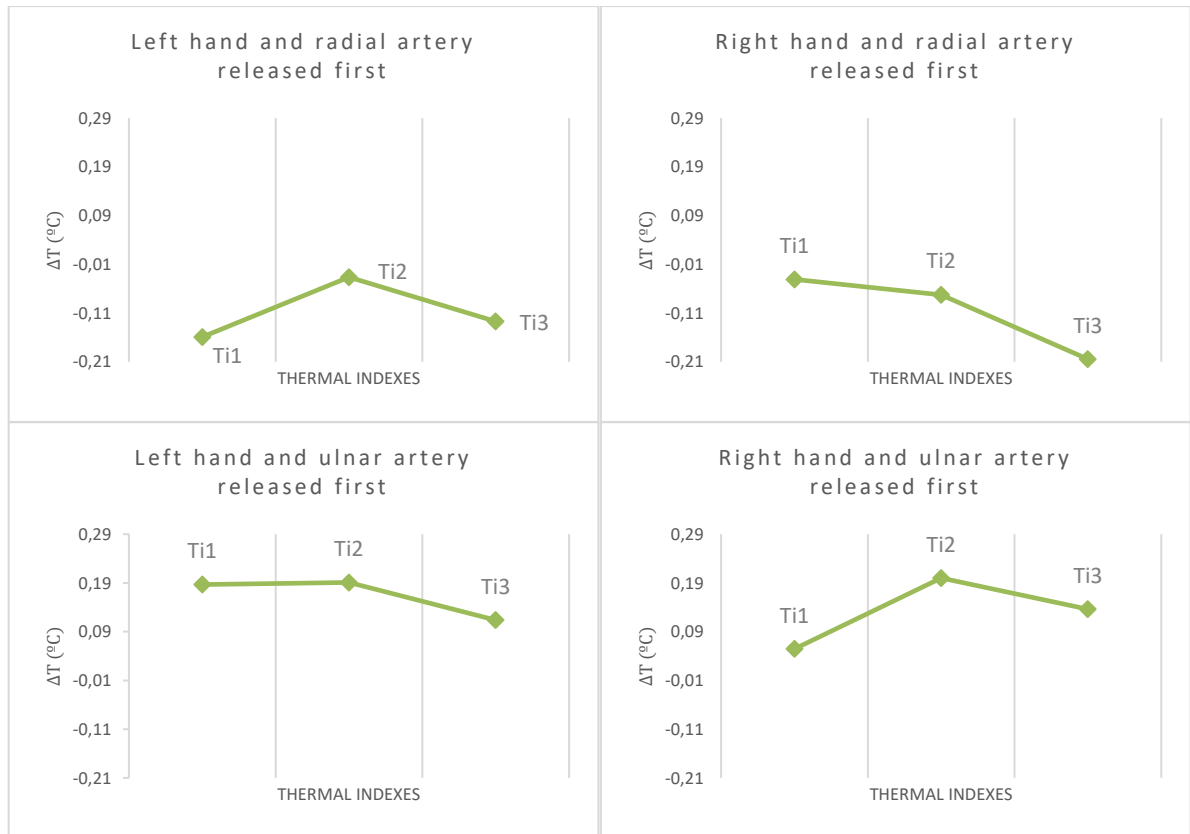
Figure 22 – Graphics representing the thermal indexes Ti1, Ti2 and Ti3, for both hands, when the ulnar artery is released first and when the radial artery is released first.
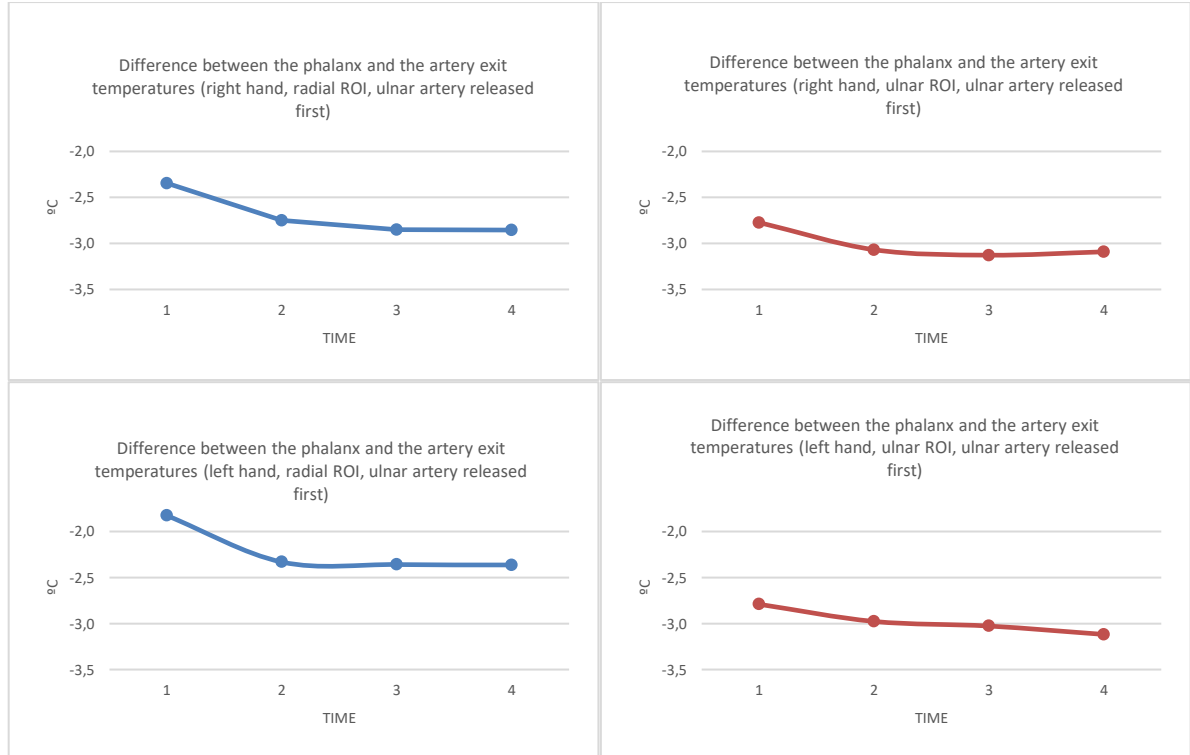
Figure 23 – Graphics representing the differences between the phalanges and the corresponding artery exit, over time (times 1, 2, 3 and 4 correspond to the situations 0, 1, 2 and 3, respectively), for both hands, when the ulnar artery is released first.
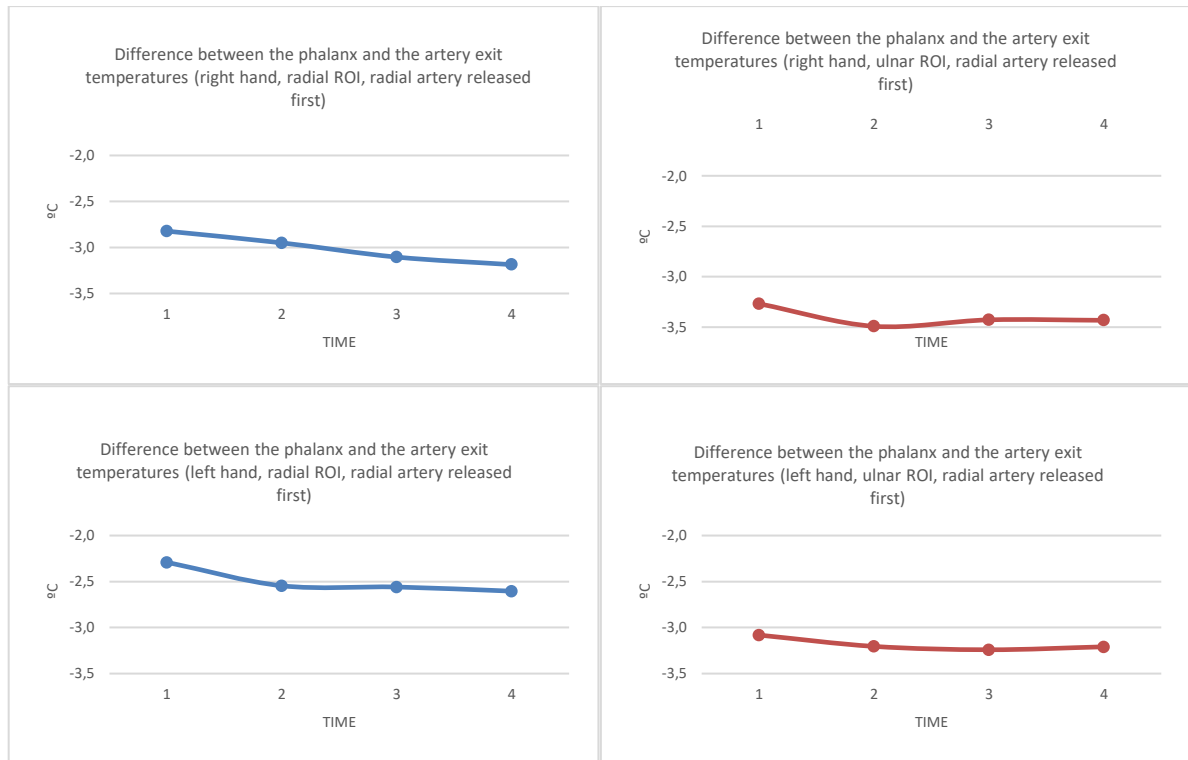
Figure 24 – Graphics representing the differences between the phalanges and the corresponding artery exit, over time (times 1, 2, 3 and 4 correspond to the situations 0, 1, 2 and 3, respectively), for both hands, when the radial artery is released first.

The statistical analysis for this methodology showed that the data distribution is normal, after Shapiro-Wilk and z-score tests. The Mauchly's Test of Sphericity was performed and the appropriate corrections were included whenever it was necessary. This way, it was possible to properly interpret the repeated measures ANOVA results. Tables 2 and 3 show the results of this statistic test for the ROIs temperature, regarding the between-subjects and within-subjects factors, respectively.

Table 2 — Result of the Repeated Measures ANOVA (ROIs temperature) – between-subjects factor.

Factor, ROI	$F(df_{time}, df_{error})$=F-value, p=p-value
Sex, middle area of the thumb	$F(1,20)=1.590$, $p=0.222$
Sex, middle phalanx of the little finger	$F(1,20)=1.777$, $p=0.198$

Table 3 — Result of the Repeated Measures ANOVA (ROIs temperature) – within-subjects factors.

Factor, ROI	$F(df_{time}, df_{error})$=F-value, p=p-value
Compression order, middle area of the thumb	$F(1,20)=1.430$, $p=0.246$
Compression order, middle phalanx of the little finger	$F(1,20)=0.254$, $p=0.620$
Hand, middle area of the thumb	$F(1,20)=0.476$, $p=0.498$
Hand, middle phalanx of the little finger	$F(1,20)=0.298$, $p=0.591$
Time, middle area of the thumb	$F(1.452,29.050)=20.343$, $p=0.000$
Time, middle phalanx of the little finger	$F(2.363,47.251)=17.129$, $p=0.000$

By analysing Table 2, it is possible to verify that sex does not have a statistically significant influence in the ROIs temperature (p>0.05).

According to the results described in Table 3, there is a statistically significant effect of time on the middle area of the thumb ROI and middle phalanx of the little finger ROI temperatures (p<0.05), but the effect of the analysed compression order or hand is not significant (p>0.05).

Table 4 shows the results of this statistic test for the gradient between phalanges ROIs temperatures.

Table 4 – Result of the Repeated Measures ANOVA (gradient between phalanges ROIs temperatures).

Factor, ROI	$F(df_{time}, df_{error})$=F-value, p=p-value
Compression order, Gradient between phalanges	$F(1,21)=3.923$, $p=0.061$
Hand, Gradient between phalanges	$F(1,21)=0.041$, $p=0.842$
Time, Gradient between phalanges	$F(2,42)=3.875$, $p=0.029$

The results described in Table 4 show that there is a statistically significant effect of time on the gradient between the phalanges temperatures (p=0.029), but the effect of the analysed compression order or hand is not significant (p>0.05).

Table 5 shows the results of this statistic test concerning the gradient between the phalanges and the corresponding artery exit temperatures. The factor hand is the only that does not have a statistically significant effect in the ulnar gradient (p=0.336).

Table 5 – Result of the Repeated Measures ANOVA (gradient between the phalanges and the corresponding artery exit temperatures).

Factor, ROI	$F(df_{time}, df_{error})$=F-value, p=p-value
Compression order, Gradient between the middle area of the thumb and radial artery exit	$F(1,21)=7.657$, $p=0.012$
Compression order, Gradient between the middle phalanx of the little finger and ulnar artery exit	$F(1,21)=7.854$, $p=0.011$
Hand, Gradient between the middle area of the thumb and radial artery exit	$F(1,21)=9.237$, $p=0.006$
Hand, Gradient between the middle phalanx of the little finger and ulnar artery exit	$F(1,20)=0.968$, $p=0.336$
Time, Gradient between the middle area of the thumb and radial artery exit	$F(1.794,37.681)=22.580$, $p=0.000$
Time, Gradient between the middle phalanx of the little finger and ulnar artery exit	$F(3,63)=9.452$, $p=0.000$

In what concerns the second methodology, Figures 25 and 26 show the average of the temperature difference between situation 1 and situation 0, for both hands, 7, 15 and 30 seconds after artery release, representing the thermic manifestation that happens in each ROI when the blood leaves the hand, in response to the occlusion of both arteries, when the ulnar artery is released first and when the radial artery is released first, respectively. In what concerns the situation where the ulnar artery is released first (Figure 25), all values are statistically significant (p<0.05) for both hands, except for

the effect on the radial ROI, immediately after occlusion in the right hand ($p>0.05$). When the radial artery is released first (Figure 26), all values are statistically significant ($p<0.05$), except for the effect on the ulnar ROI, immediately after occlusion, in both hands ($p>0.05$).
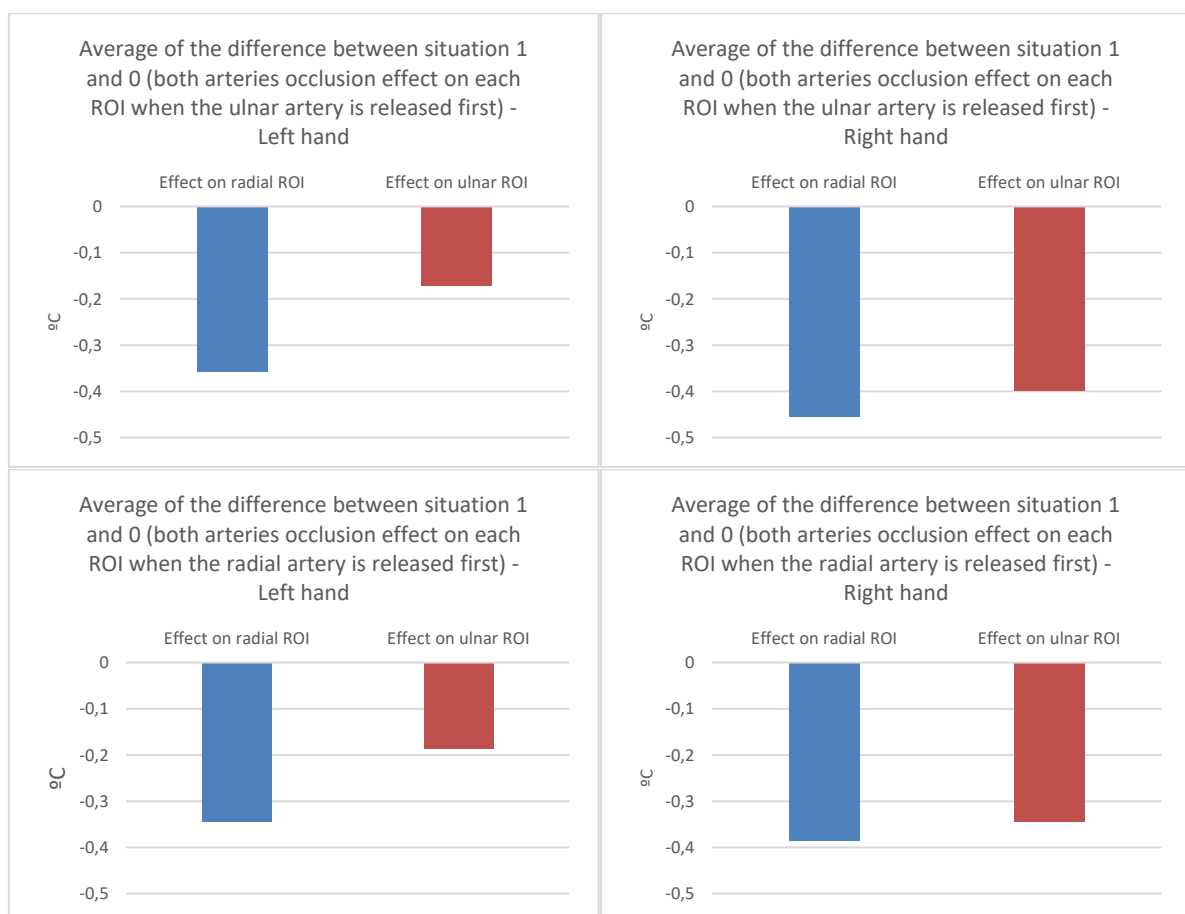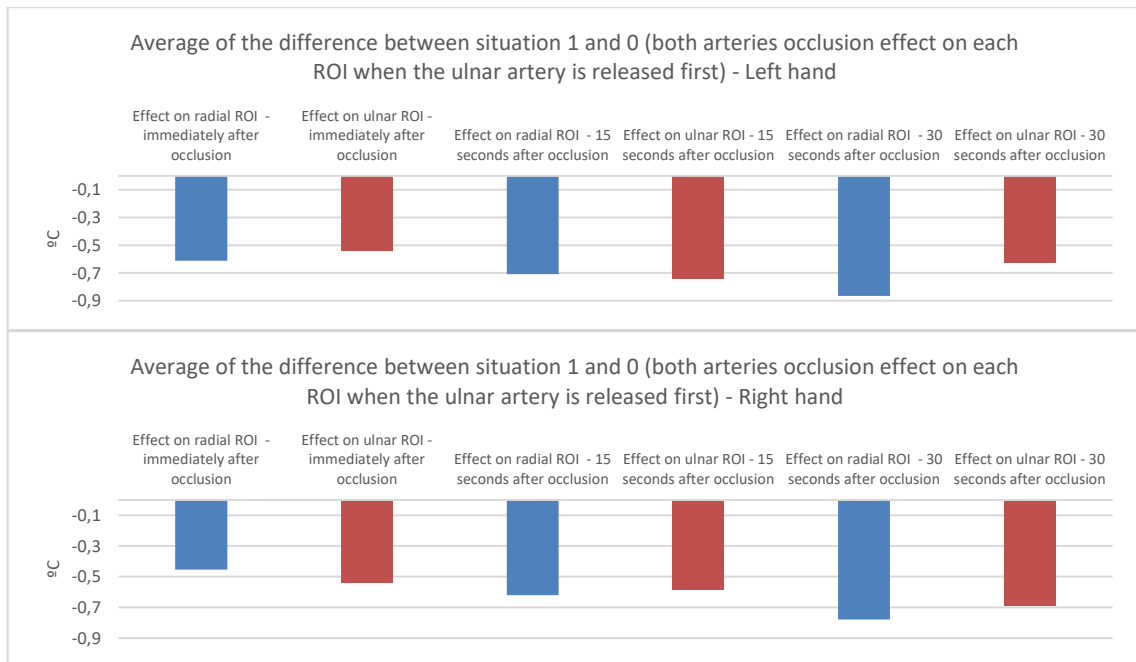

Figure 25 – Average of the temperature difference between the situation 1 and the situation 0, for the left (top) and right (bottom) hands, for 7, 15 and 30 seconds after artery release, when the ulnar artery is released first.
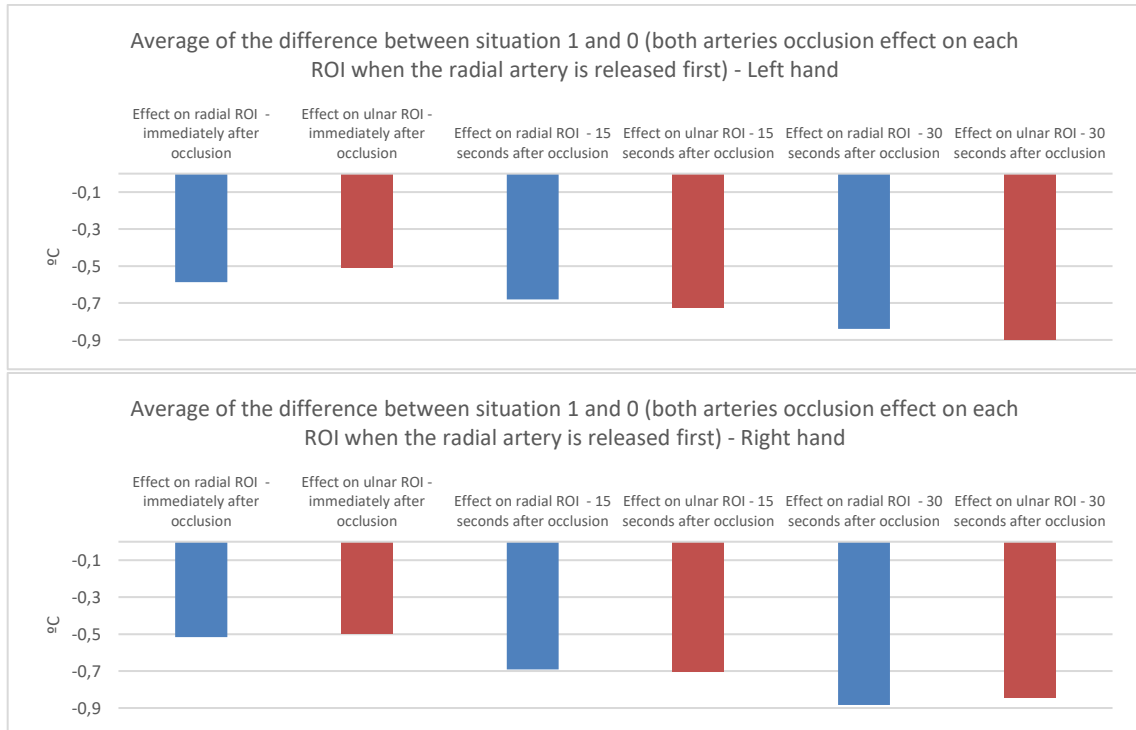
Figure 26 – Average of the temperature difference between the situation 1 and the situation 0, for the left (top) and right (bottom) hands, for 7, 15 and 30 seconds after artery release, when the radial artery is released first.

Figure 27 shows the average of the temperature difference between situation 2 and situation 1, for both hands, 7, 15 and 30 seconds after artery release, representing the thermic manifestation that happens in the blood reperfusion of the zone correspondent to the released artery. In the left hand, the only significant values are related with the 30 seconds cut-off (p=0.001 and p=0.000 for the ulnar and radial artery release, respectively). In the right hand, the only significant values are related with the 30 seconds cut-off (p=0.032 and p=0.000 for the ulnar and radial artery release, respectively) and the radial zone reperfusion 15 seconds after the radial artery release (p=0.032).
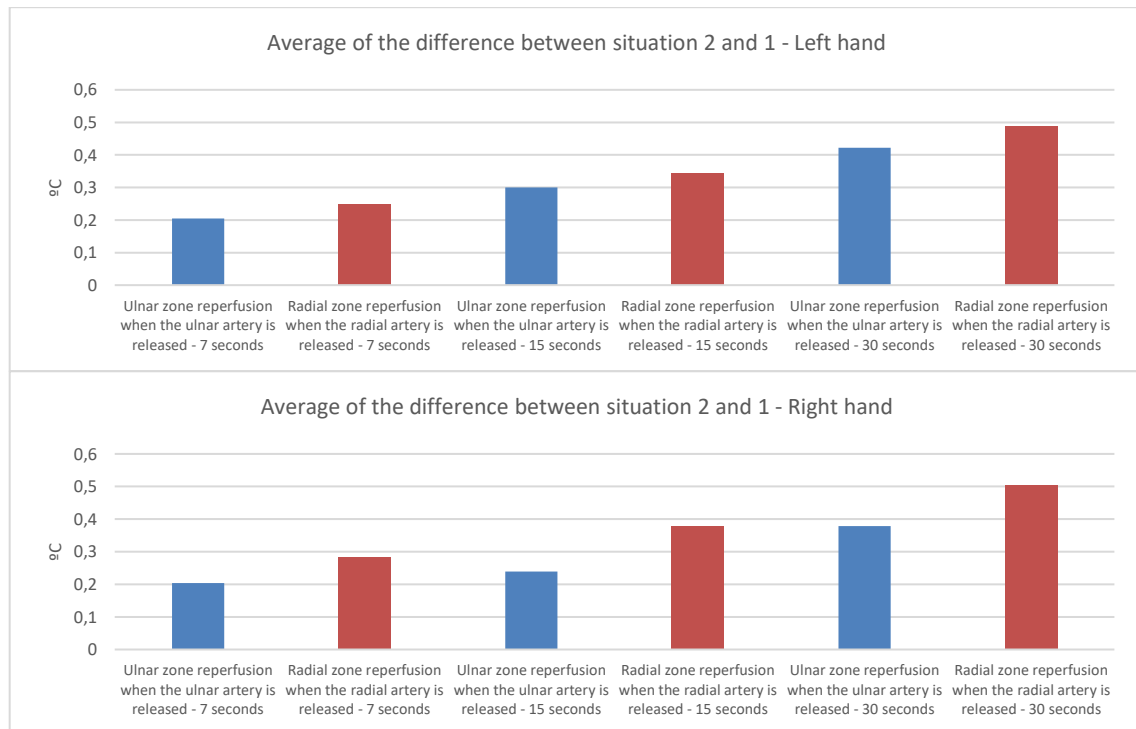
Figure 27 – Average of the temperature difference between situation 2 and situation 1, for the left (top) and right (bottom) hands, for 7, 15 and 30 seconds after artery release (reperfusion of the zone correspondent to the released artery).

Figure 28 shows the average of the temperature difference between situation 2 and situation 1, for both hands, 7, 15 and 30 seconds after artery release, representing the thermic manifestation that happens in the blood reperfusion of the opposite zone to the released artery. None of the values is statistically significant (p>0.05).

The temperature differences from each situation (both arteries compressed, one artery released and both arteries released) to the basal situation were calculated. Figures 29, 30 and 31 show the thermal indexes (gradients) Ti1, Ti2 and Ti3 that represent the differences between the ROIs corresponding to the artery released firstly and the artery released later, regarding the differences of situation 1, 2 and 3, respectively, to the basal situation. Figure 29 regards the thermograms taken immediately after occlusion and 7 seconds after arteries release. Figure 30 regards the thermograms taken 15 seconds after occlusion and 15 seconds after arteries release. Figure 31 regards the thermograms taken 30 seconds after occlusion and 30 seconds after arteries release.

Statistically, when the radial artery is released first, in the left hand, the difference between Ti2 and Ti1 is significant (p=0.007, p=0.001 and p=0.000 for 7, 15 and 30 seconds cut-off time, respectively). The difference between Ti3 and Ti2 is not statistically significant (p>0.05), in any cut-off time.
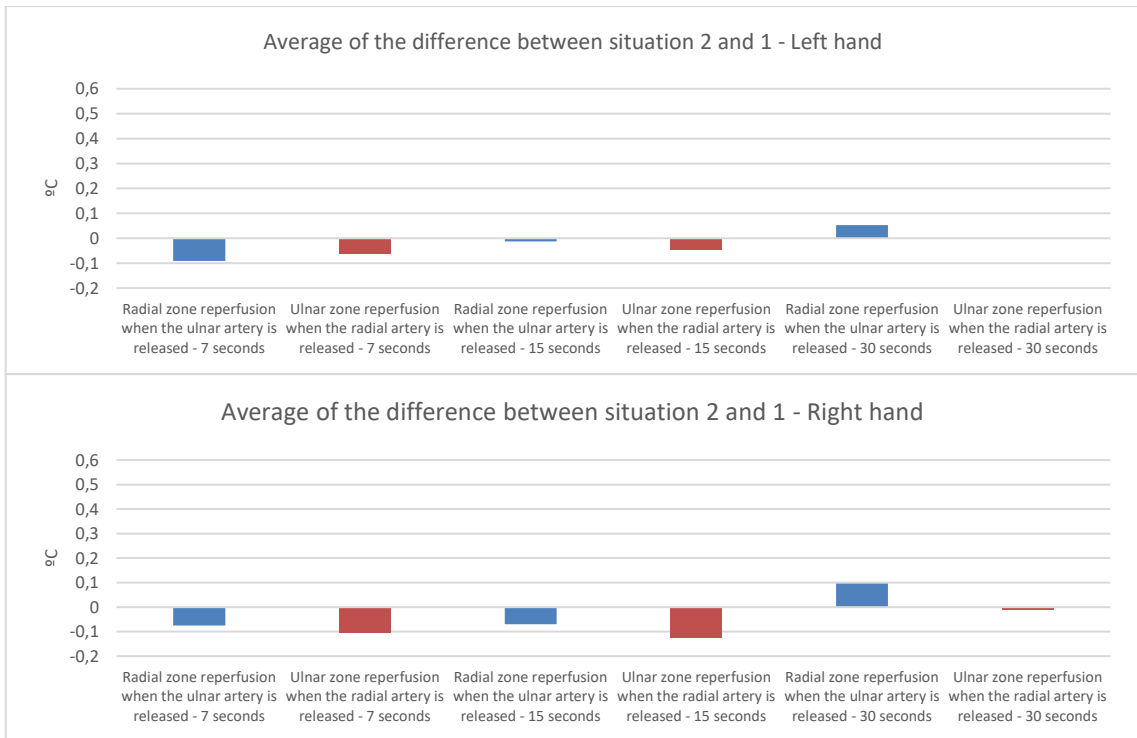
Figure 28 – Average of the temperature difference between situation 2 and situation 1, for the left (top) and right (bottom) hands, for 7, 15 and 30 seconds after artery release (reperfusion of the opposite zone to the released artery).
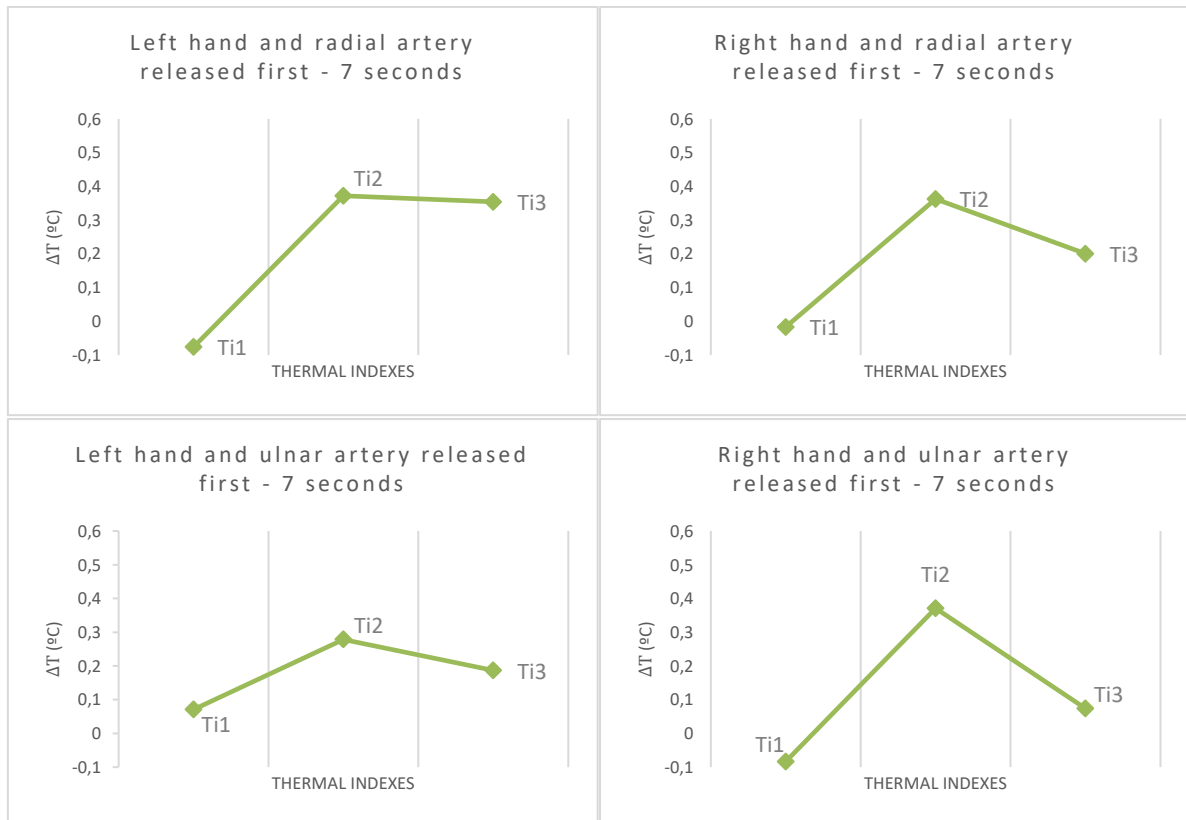
Figure 29 – Graphics representing the thermal indexes for both hands, when the ulnar artery or radial artery is released first, regarding the 7 seconds cut-off after artery release.
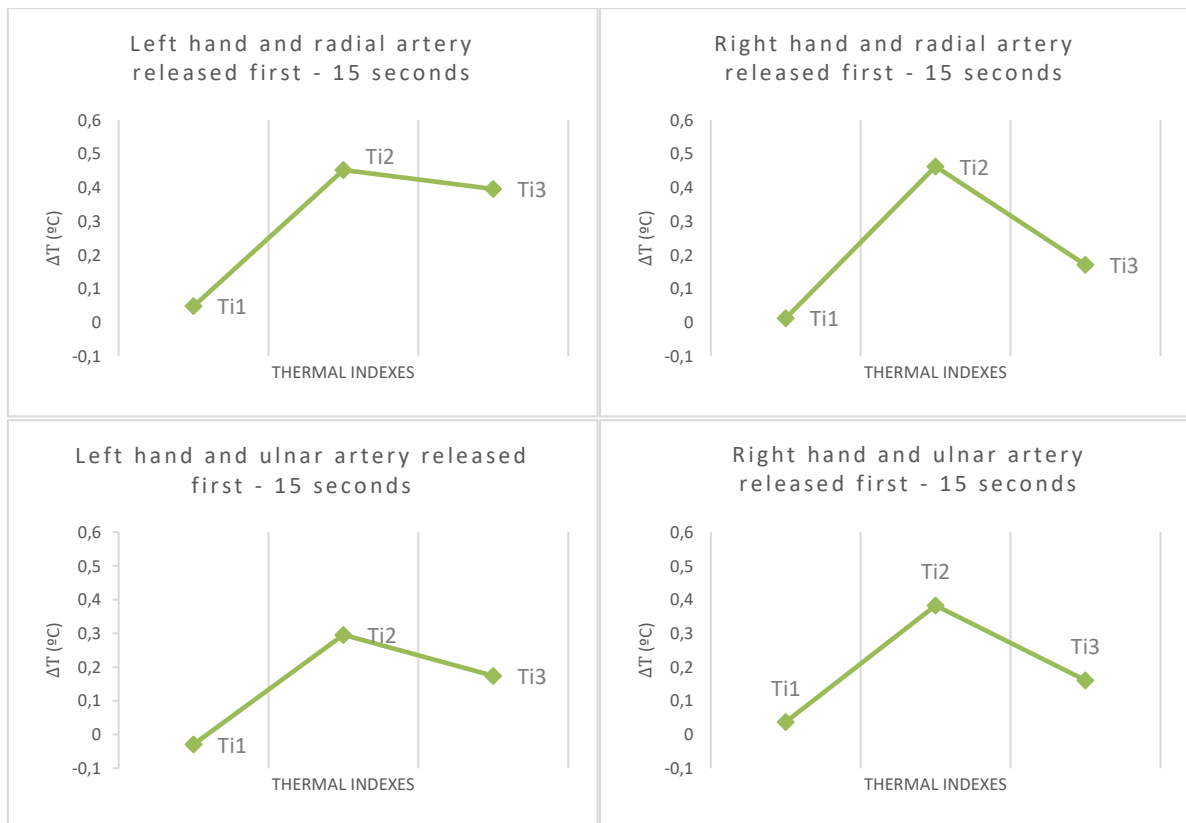
Figure 30 – Graphics representing the thermal indexes for both hands, when the ulnar artery or radial artery is released first, regarding the 15 seconds cut-off after artery release.
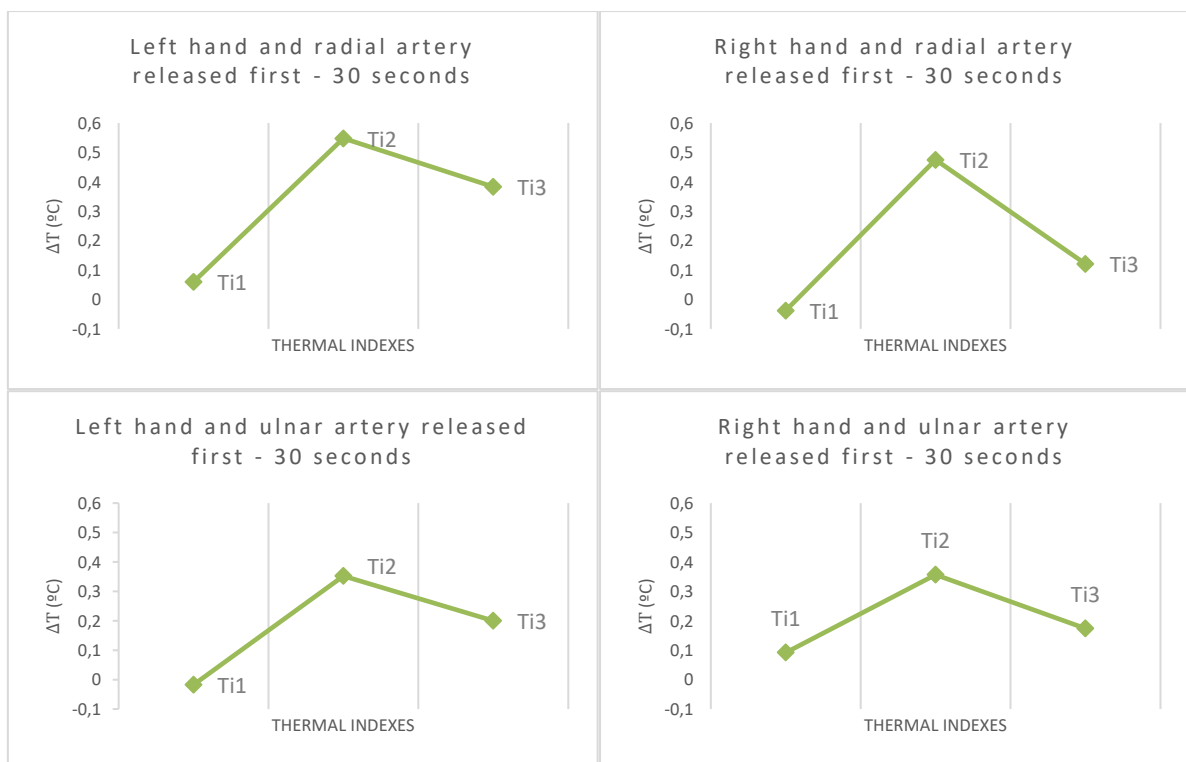
Figure 31 – Graphics representing the thermal indexes for both hands, when the ulnar artery or radial artery is released first, regarding the 30 seconds cut-off after artery release.

In the situation where the radial artery is released first, in the right hand, the difference between Ti3 and Ti2 is only statistically significant (p=0.029) in the 30 seconds cut-off, while the difference between Ti2 and Ti1 is only statistically significant in the 15 and 30 seconds cut-off (p=0.000).

When the ulnar artery is released first, in the left hand, the difference between Ti2 and Ti1 is only statistically significant (p=0.002) in the 30 seconds cut-off, while the difference between Ti3 and Ti2 is not statistically significant (p>0.05) in any cut-off time.

In the situation where the ulnar artery is released first, in the right hand, the only statistically significant (p=0.000) difference is between Ti2 and Ti1, in the 7 seconds cut-off.

Figures 32 and 33 show the temperature differences between the phalanges and the corresponding artery exit (for example, the middle phalanx of the little finger and the ulnar artery exit, which are the ulnar ROIs), over time, for both hands, when the ulnar artery is released first and when the radial artery is released first, respectively. Next, a statistical analysis of each graphic will tell which changes are significant.
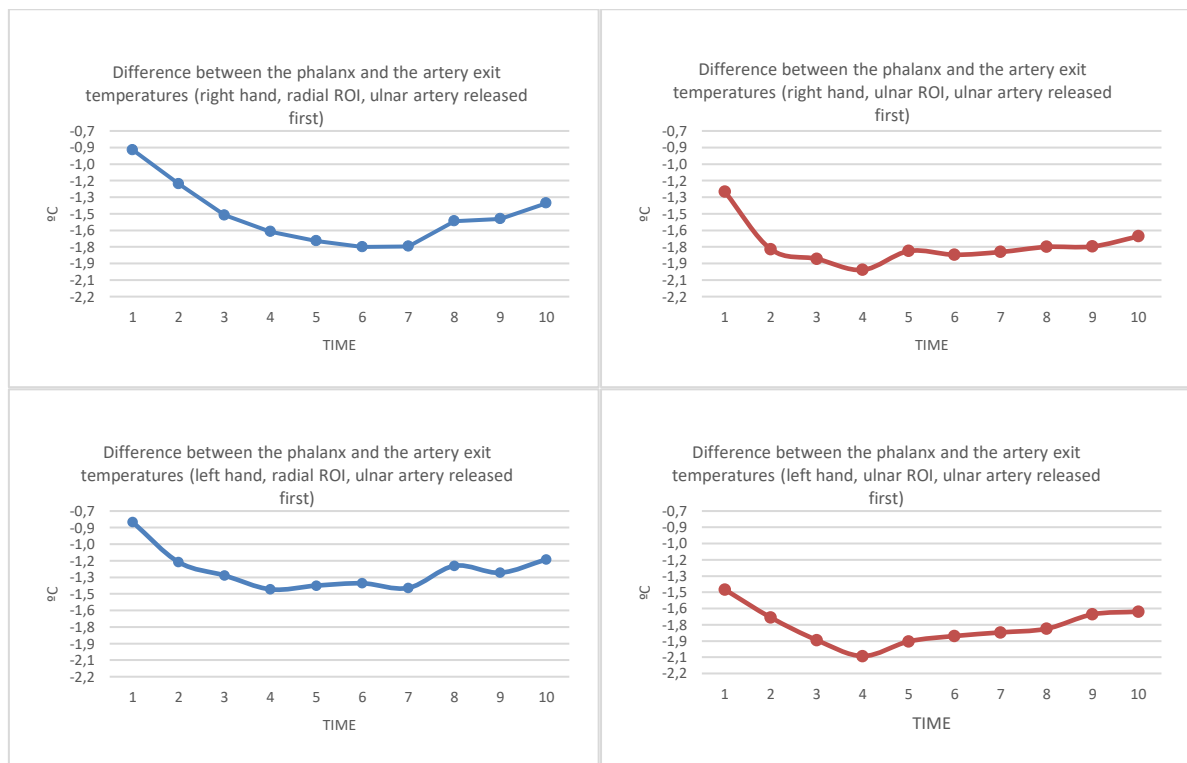
Figure 32 – Graphics representing the differences between the phalanges and the corresponding artery exit, over time (times 1, 2, 3, 4, 5, 6, 7, 8, 9 and 10 correspond to the situations 0, 1 where the thermogram was taken immediately, 15 and 30 seconds after arteries occlusion, 2 where the thermogram was taken 7, 15 and 30 seconds after artery release, and 3 where the thermogram was taken 7, 15 and 30 seconds after artery release, respectively), for both hands, when the ulnar artery is released first.
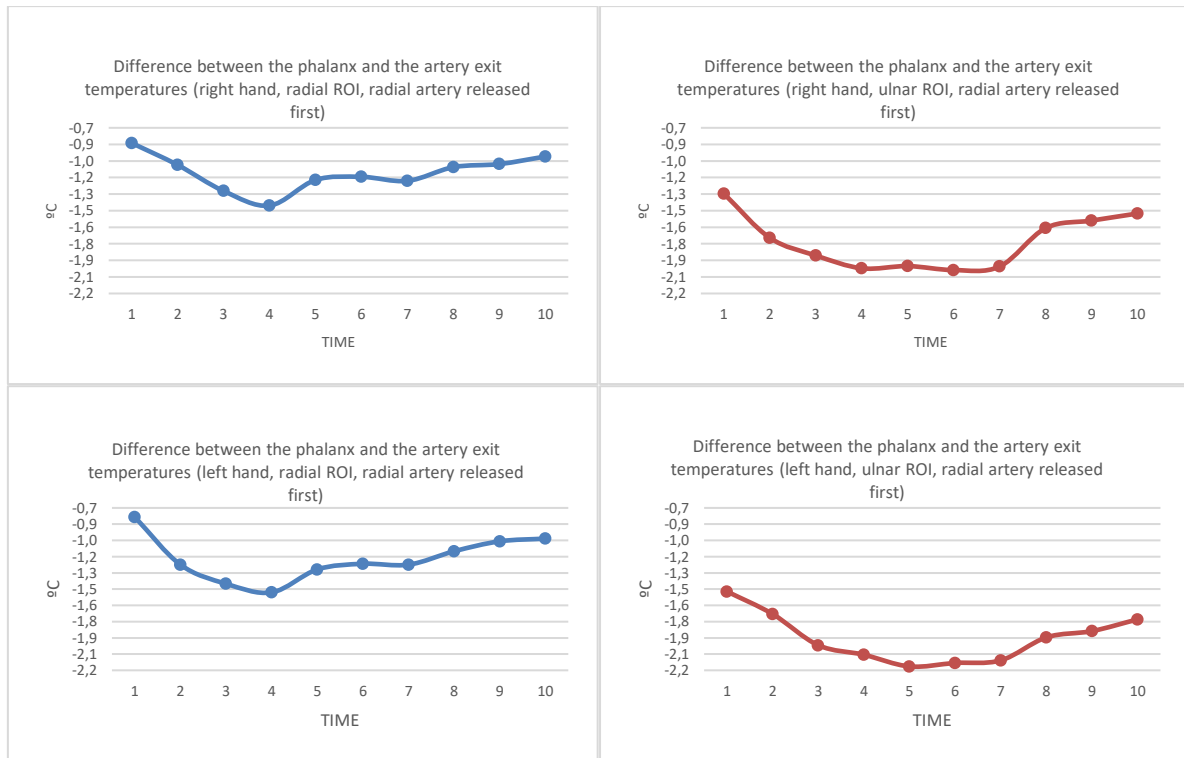
Figure 33 – Graphics representing the differences between the phalanges and the corresponding artery exit, over time (times 1, 2, 3, 4, 5, 6, 7, 8, 9 and 10 correspond to the situations 0, 1 where the thermogram was taken immediately, 15 and 30 seconds after arteries occlusion, 2 where the thermogram was taken 7, 15 and 30 seconds after artery release, and 3 where the thermogram was taken 7, 15 and 30 seconds after artery release, respectively), for both hands, when the radial artery is released first.

In Figure 32, in the top left graphic, the difference between gradients in time 3 and 1 is statistically significant (p=0.050), showing a radial gradient decrease 15 seconds after arteries occlusion. Also, the difference between gradients in time 10 and 7 is statistically significant (p=0.010), showing a radial gradient increase 30 seconds after radial artery is released. The difference between gradients in time 10 and 1 is not statistically significant (p>0.05), so the thermic pattern in time 10 is similar to the basal situation.

At the top right graphic, the difference between gradients in time 2 and 1 is statistically significant (p=0.001), showing an ulnar gradient decrease immediately after arteries occlusion. The difference between gradients in time 10 and 1 is not statistically significant (p>0.05), so the thermic pattern in time 10 is similar to the basal situation. The difference between gradients in time 5, 6 or 7 and 4 is not statistically significant (p>0.05).

In the bottom left graphic, the difference between gradients in time 4 and 1 is statistically significant (p=0.000), showing a radial gradient decrease 30 seconds after arteries occlusion. Also, the difference between gradients in time 10 and 7 is statistically significant (p=0.046), showing a radial gradient increase 30 seconds after radial artery is released. The difference between gradients in time 10 and 1 is not statistically significant (p>0.05), so the thermic pattern in time 10 is similar to the basal situation.

At the bottom right graphic, the difference between gradients in time 4 and 1 is statistically significant (p=0.008), showing an ulnar gradient decrease 30 seconds after arteries occlusion. Also, the only other statistically significant (p=0.027) difference is between times 10 and 4. The difference between gradients in time 5, 6 or 7 and 4 is not statistically significant (p>0.05).

In Figure 33, in the top left graphic, the difference between gradients in time 3 and 1 is statistically significant (p=0.000), showing a radial gradient decrease 15 seconds after arteries

occlusion. The difference between gradients in time 8 and 1 is not statistically significant (p>0.05), so the thermic pattern in time 8 is similar to the basal situation. The difference between gradients in time 5, 6 or 7 and 4 is not statistically significant (p>0.05).

At the top right graphic, the difference between gradients in time 3 and 1 is statistically significant (p=0.001), showing an ulnar gradient decrease 15 seconds after arteries occlusion. The difference between gradients in time 8 and 7 is statistically significant (p=0.010), so the thermic manifestation of the ulnar gradient recovery happens 7 seconds after the ulnar artery release (time 8).

In the bottom left graphic, the difference between gradients in time 2 and 1 is statistically significant (p=0.003), showing a radial gradient decrease immediately after arteries occlusion. The difference between gradients in time 8 and 1 is not statistically significant (p>0.05), so the thermic pattern in time 8 is similar to the basal situation. The difference between gradients in time 5, 6 or 7 and 4 is not statistically significant (p>0.05).

At the bottom right graphic, the difference between gradients in time 3 and 1 is statistically significant (p=0.003), showing an ulnar gradient decrease 15 seconds after arteries occlusion. Also, the difference between gradients in time 10 and 7 is statistically significant (p=0.012), showing an ulnar gradient increase 30 seconds after ulnar artery is released. The difference between gradients in time 9 and 1 is not statistically significant (p>0.05), so the thermic pattern in time 9 is similar to the basal situation.

The statistical analysis for this second methodology showed that the data distribution is not normal, after Shapiro-Wilk and z-score tests. Therefore, a non-parametric method was used (Friedman's two-way analysis of variance). Tables 6, 7 and 8 show the results of this test for ROIs temperature, gradient between phalanges ROIs temperature and gradient between the phalanges and the corresponding artery exit, respectively. When p-value is lower than 0.05, it means that there is at least one difference that is statistically significant, which was verified in all variables (and presented previously). Also, Mann-Whitney U test showed that only 2 out of the 196 variables significantly differ (p<0.05), based on sex.

Table 6 — Result of the Friedman's test (ROIs temperature).

Variables	$X^2(df)$=Chi-square, p=p-value
Temperature in the right hand, radial ROI, when the ulnar artery is released first	$X^2(9)$=105.892, p=0.000
Temperature in the right hand, ulnar ROI, when the ulnar artery is released first	$X^2(9)$=63.597, p=0.000
Temperature in the left hand, radial ROI, when the ulnar artery is released first	$X^2(9)$=104.516, p=0.000
Temperature in the left hand, ulnar ROI, when the ulnar artery is released first	$X^2(9)$=96.931, p=0.000
Temperature in the right hand, radial ROI, when the radial artery is released first	$X^2(9)$=96.126, p=0.000
Temperature in the right hand, ulnar ROI, when the radial artery is released first	$X^2(9)$=129.872, p=0.000
Temperature in the left hand, radial ROI, when the radial artery is released first	$X^2(9)$=118.917, p=0.000
Temperature in the left hand, ulnar ROI, when the radial artery is released first	$X^2(9)$=99.216, p=0.000

Table 7 — Result of the Friedman's test (gradient between phalanges ROIs temperature).

Variables	X^2(df)=Chi-square, p=p-value
Gradient in the left hand when the radial artery is released first	X^2(8)=70.821, p=0.000
Gradient in the right hand when the radial artery is released first	X^2(8)=62.957, p=0.000
Gradient in the left hand when the ulnar artery is released first	X^2(8)=32.469, p=0.000
Gradient in the right hand when the ulnar artery is released first	X^2(8)=42.585, p=0.000

Table 8 — Result of the Friedman's test (gradient between the phalanges and the corresponding artery exit temperatures).

Variables	X^2(df)=Chi-square, p=p-value
Gradient in the right hand, radial ROI, when the ulnar artery is released first	X^2(9)=99.964, p=0.000
Gradient in the right hand, ulnar ROI, when the ulnar artery is released first	X^2(9)=45.035, p=0.000
Gradient in the left hand, radial ROI, when the ulnar artery is released first	X^2(9)=70.170, p=0.000
Gradient in the left hand, ulnar ROI, when the ulnar artery is released first	X^2(9)=29.414, p=0.001
Gradient in the right hand, radial ROI, when the radial artery is released first	X^2(9)=57.110, p=0.000
Gradient in the right hand, ulnar ROI, when the radial artery is released first	X^2(9)=87.164, p=0.000
Gradient in the left hand, radial ROI, when the radial artery is released first	X^2(9)=83.660, p=0.000
Gradient in the left hand, ulnar ROI, when the radial artery is released first	X^2(9)=76.597, p=0.000

Chapter 5

Automatic detection of hand fingertips and phalanges in thermal images

Manual analysis of thermal images and definition of regions of interest (ROI), especially in hands, is a tedious and time-consuming task. A solution might be an algorithm that automatically detects ROIs. Concerning phalanges, few research has been done (Santos & Oliveira, 2015). In order to develop a fully automated solution for the standardisation of hand anatomical thermal ROIs, with automated discovery of control points, an algorithm to automatically detect fingertips and phalanges is proposed, using MATLAB®.

5.1   Methodology

The development of this algorithm was performed in a Sony Corporation VAIO, model SVF1421Z2EW, with Intel(R) Core(TM) i5-3337U CPU @ 1.80 GHz processor, with 6.00 GB of RAM and a 64 bits operating system, using MATLAB® R2015a.

The first step was the pre-processing, including: reading the image, converting it from RGB to gray, converting it to a binary image, based on a threshold (0.2), applying a binary dilation with a square structuring element (width of 2 pixels), filling the image holes and keeping the largest object (hand), deleting other objects, such as the temperature scale (result shown in Figure 36). Next, hand edge extraction was performed using the Roberts algorithm (Roberts, 1965; Russ, 2011a). The following step consisted in computing the convex hull of the hand object, returning a binary convex hull image. Roberts algorithm (Roberts, 1965; Russ, 2011a) was also used to extract the edges of this convex hull image. The results are presented in Figure 37. The following step consisted in finding the finger roots. In order to do that, firstly the pre-processed image was subtracted from the convex hull mask that was produced in the previous step. As a result, regions between fingers will be white. The next step was finding the connected regions (discarding the smallest regions), which allows the storage of all 6 white regions of interest in a cell structure (each cell element contains an array of points that belong to one region). The next operation consisted in computing the distance between each point of each white region and the hand centroid point using the Euclidean distance. The closest point (smallest Euclidean distance) is the finger root (Figure 38).

The following step consisted in finding the fingertips. This step was performed using two different approaches. The first analyses the lines of the previously detected convex hull shape through Hough transform (Russ, 2011b; VC, 1962), and finds the respective initial and end points (Figure 39). If 2 found points are too close (distance < 20), meaning that the found line does not begin exactly where the previous ends, the average/mid-point was calculated and will substitute those two points. Wrist tips were eliminated by excluding the points with a y coordinate higher than 220. In some cases (Figure 40), due to a not good convex hull shape detection, Hough transform is not able to properly detect its lines. Therefore, in order to try to correct some points misalignment, a search within a 10x10 pixel region around the detected fingertips is performed: if a white point is found with a lowest y coordinate, it becomes the new fingertip, in what concerns the little, ring, middle and index fingers. In what regards the thumb, if it is a left hand (thumb located at the left of the image), if a white point is found with a lowest x coordinate, it becomes the new thumb fingertip. If it is a right hand (thumb located at the right of the image), a similar reasoning is applied: if a white point is found with a highest x coordinate, it becomes the new thumb fingertip. The results are presented in Figure 40.

In what regards the second approach to detect the fingertips, firstly, the white regions contained in the previously described cell structure were organized so as to match the fingertips, such as depicted in Figure 34.
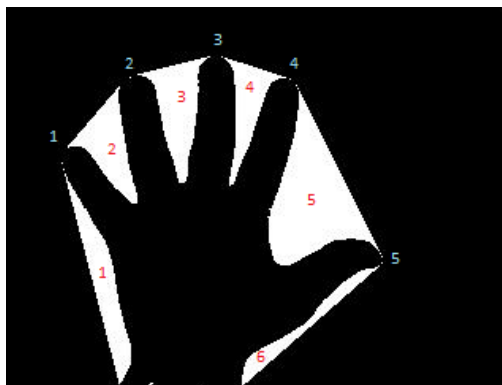
Figure 34 - Organization of white regions and fingertips.

Regions 1 and 6 contain points with the highest y coordinate. To differentiate between these two, x coordinate was evaluated: if a region contains low x coordinate points, it is set as Region 1; otherwise, it is set as Region 6. The other four regions were set evaluating the points with the lowest x coordinate belonging to each region, organizing them by that x coordinate. If it is a right hand, fingertip 1 is the point with the lowest x coordinate belonging to Region 1. Fingertips 5 and 4 are the points with the highest x coordinate belonging to Region 5 and 4, respectively. For fingertips 2 and 3, since the index and middle fingers are more vertically oriented, it is also necessary to evaluate the y coordinate, since the point with lowest or highest x coordinate might not correspond to the fingertip. In what concerns the left hand, a similar reasoning was used. The results are presented in Figure 41.

The next step consisted in finding the middle and distal phalanges separations inside the fingers. Firstly, the finger roots were organized by their x coordinate so as to make the correspondence between each finger root and each fingertip. Secondly, the midpoints between each two finger roots were calculated. However, by organizing finger roots by their x coordinate, some cases regarding the thumb do not work because the last finger root is sometimes to the left of the previous one (Figure 42a). So, if the distance between each fingertip and the corresponding midpoint is too large (>100), depending on whether it is the left or right hand (Figure 35), the order is switched. The result is shown in Figure 42b.
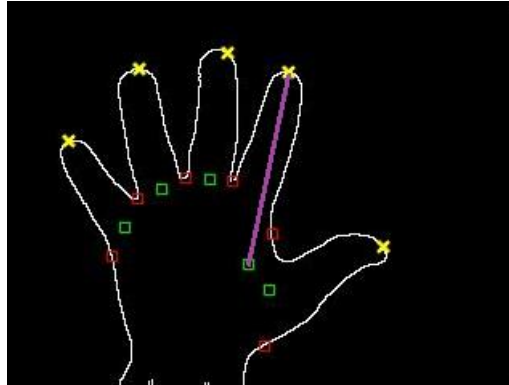
Figure 35 - Correction of the inadequate finger roots and midpoints (green points) x coordinate organization, by checking if the distance between each fingertip and mid-point (purple line) is too large (>100).

Finding middle and distal phalanges separations inside the fingers is done by computing the division by 3 of the distance between the tip and the midpoint and adding 1/3 and 2/3 of that distance (Figure 43). The middle phalanx center – midpoint between blue and magenta squares presented in Figure 43 – was calculated. Middle phalanx radius will be the distance between the center and the nearest white contour point (yellow squares in Figure 44). A circumference is drawn, with the respective center and radius. For signaling the middle divisions in the hand contour, it is necessary to find the nearest white point at left and right of the magenta points (cyan star points in Figure 45). In order to find the distal phalanges and divisions in the hand contour, a similar approach was followed.

The error depicted in Figure 46a was noticed, in some cases. The nearest white point at left of the blue point in the thumb (representing the distal phalanx), is not the desired one. Therefore, a test was performed: if the two divisions are too close (<12), it means that both are in the same finger side, which is not desirable. In that case, the approach changes: the algorithm will now work with the y coordinate (above/below) instead of the x coordinate (left/right). If both divisions are below the blue point, the furthest is substituted by the nearest white point above the blue point, with approximately the same x coordinate, and vice-versa. The results are shown in Figure 46b.

This algorithm was developed using a training set of 48 thermographic baseline images (320x240) collected from six participants, acquired with FLIR® E60sc thermal camera. In order to evaluate both approaches, a test set of 12 images was used. A metric including different parameters was calculated, so that the algorithms evaluation fits the purpose of the study (Table 9). This metric assesses the hand binarization and edge extraction (50% weight), the fingertips detection (20% weight) and the phalanges detection (30% weight). The evaluation of the fingertips and phalanges detections is performed based on the resultant location, i.e., if the detected fingertip/phalanx is exactly where it was supposed to be, or if it is slightly or very displaced, being given a score accordingly.

The relationship between the average temperature of the detected phalanges and of the manual marked phalanges, used as a reference, was evaluated. FLIR® Researcher Pro 2.10 software (a Windows-based infrared software package for capturing, recording, and analyzing thermal images) allows to export a MATLAB® file containing thermal image information, including the temperature values of each image pixel. Having the algorithms detected phalanges coordinates, it was possible to calculate the phalanges average temperature and study their correlation with the average temperature of the manual ROI marking retrieved from the FLIR® Researcher software, used as reference.

Table 9 — Parameters assessed in the evaluation metric and the corresponding weight percentage.

Parameter number	Parameter	Weight percentage (%)
1	Correct hand binarization and edge extraction	50
2	Correct thumb fingertip detection	4
3	Correct index fingertip detection	4
4	Correct middle fingertip detection	4
5	Correct ring fingertip detection	4
6	Correct little fingertip detection	4
7	Correct thumb distal phalanx detection	3
8	Correct index finger distal phalanx detection	3
9	Correct middle finger distal phalanx detection	3
10	Correct ring finger distal phalanx detection	3
11	Correct little finger distal phalanx detection	3
12	Correct thumb middle zone detection	3
13	Correct index finger middle phalanx detection	3
14	Correct middle finger middle phalanx detection	3
15	Correct ring finger middle phalanx detection	3
16	Correct little finger middle phalanx detection	3

5.2   Results

Figure 36 shows the pre-processing results and Figure 37 shows the edge extraction results. Finger roots detection results are presented in Figure 38. Figure 39 presents the initial and end points of the convex hull shape lines detected through Hough transform. Figures 40 and 41 show the fingertip detection results using the first approach (before and after a misalignment correction) and the second approach, respectively. Figures 42a and 42b show the results of the detection of the midpoints between each two finger roots, before and after the purposed correction (checking if the distance between each fingertip and midpoint is too large), respectively. The detection of the middle and distal phalanges separations inside the fingers is shown in Figure 43, while Figure 44 presents the middle phalanges detection results. Figure 45 shows the middle divisions in the hand contour. In Figure 46a, it is possible to see the inadequate distal thumb division in the hand contour, corrected by the purposed alteration (Figure 46b).
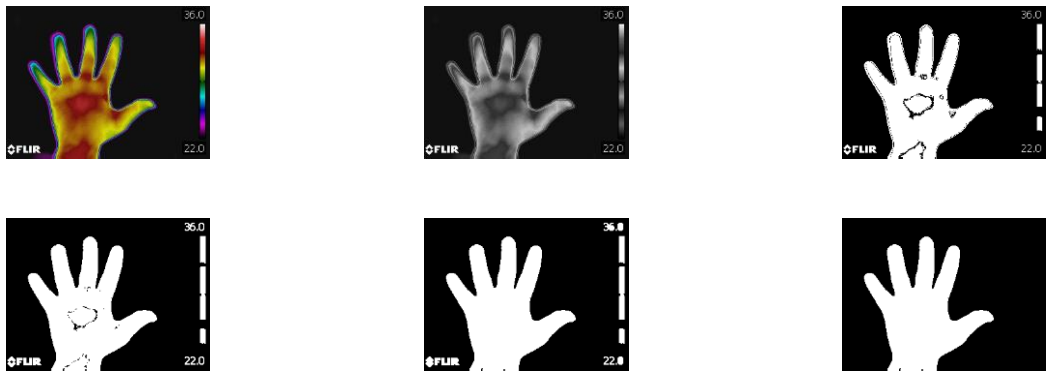
Figure 36 – Results of each pre-processing step.
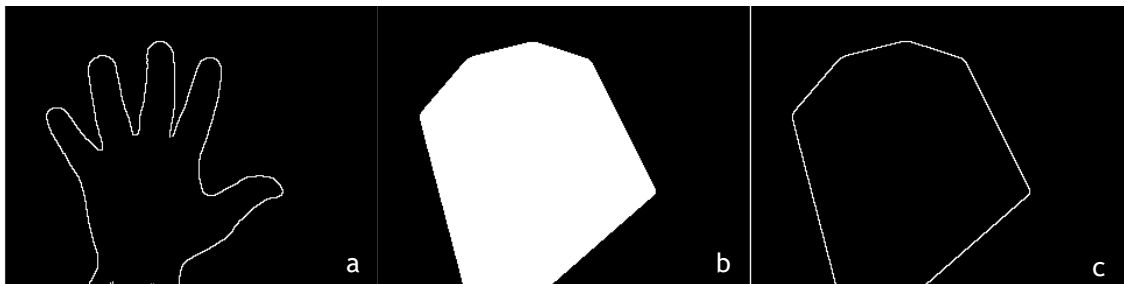
Figure 37 - Hand edge extraction (a), convex hull (b) and convex hull edge extraction (c).

Figure 38 - Finger roots (red squares) detection result and hand centroid (red circle).
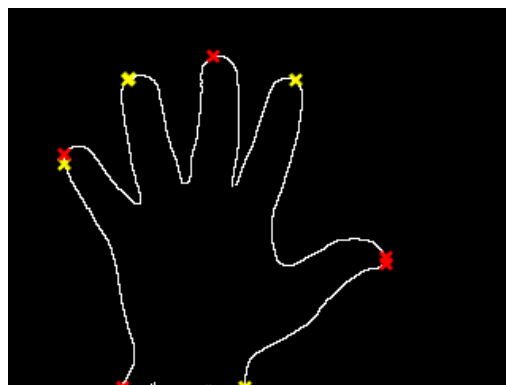
Figure 39 - Initial and end points of the Hough transform detected lines, in yellow and red, respectively.
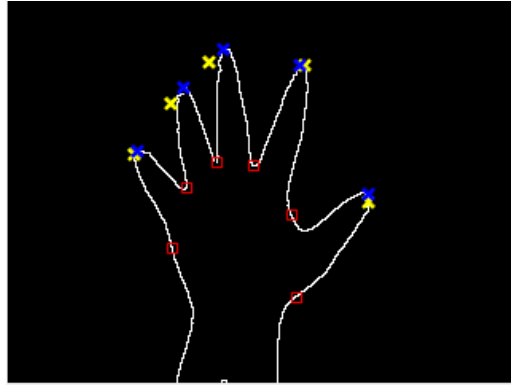
Figure 40 - Improper fingertip detection (yellow crosses), due to an inadequate Hough transform convex hull shape lines detection; correct fingertip detection (blue crosses), after a misalignment correction, using the first approach.
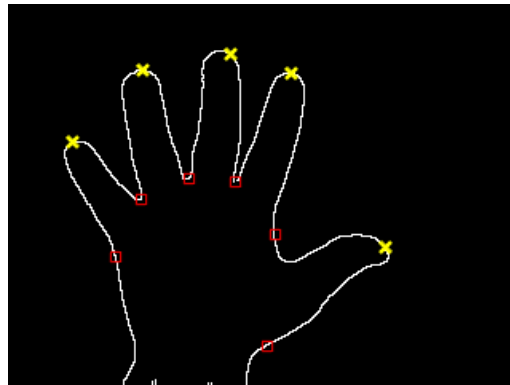
Figure 41 - Second approach final fingertip (yellow crosses) detection results.
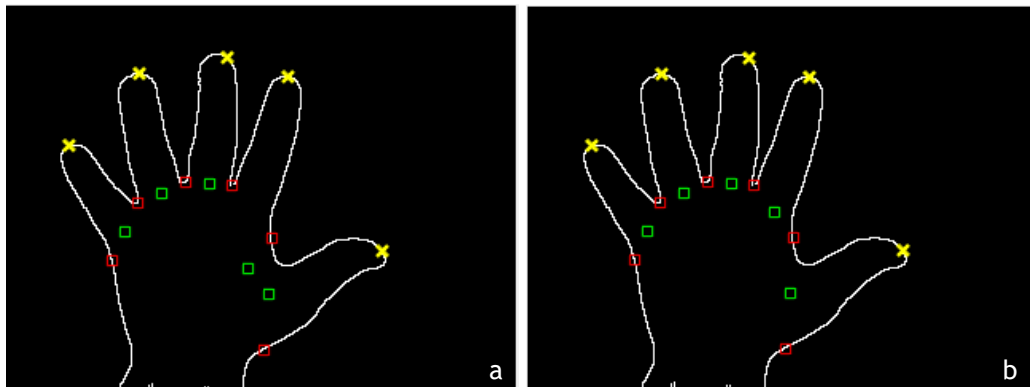
Figure 42 - Inadequate finger roots and midpoints (green squares) x coordinate organization (a) and adequate detection of midpoints between each two finger roots (b).
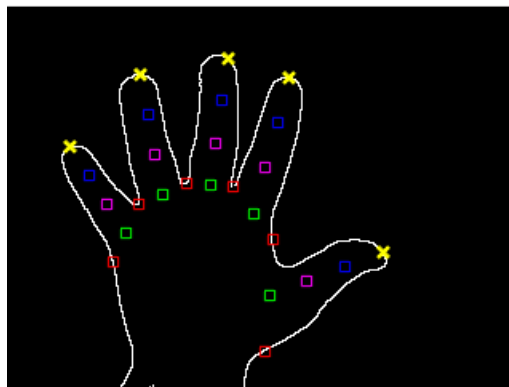
Figure 43 - Middle and distal phalanges separations inside the fingers (magenta and blue squares, respectively).
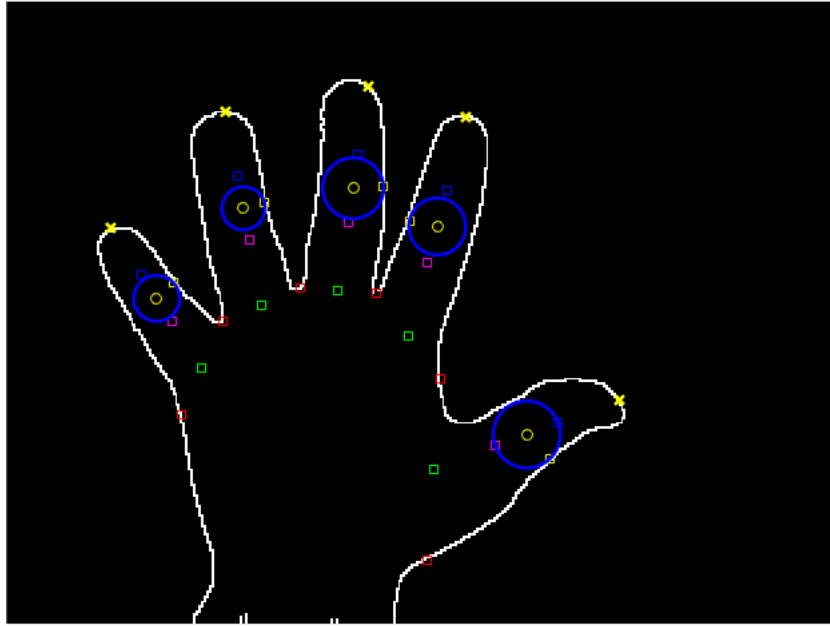
Figure 44 - Middle phalanges representation (blue circles), whose center is the midpoint between blue and magenta squares and whose radius is the distance between the center and the nearest white contour point (yellow squares).
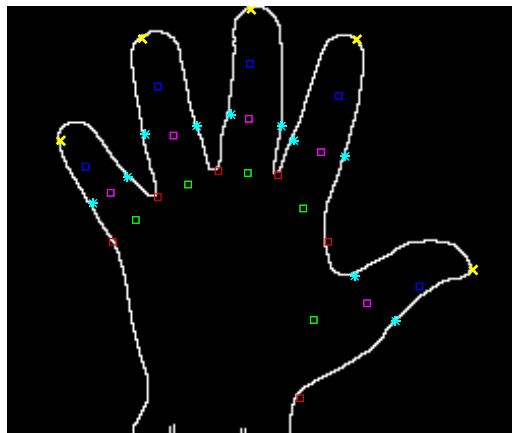
Figure 45 - Middle divisions in the hand contour representation (cyan star points).
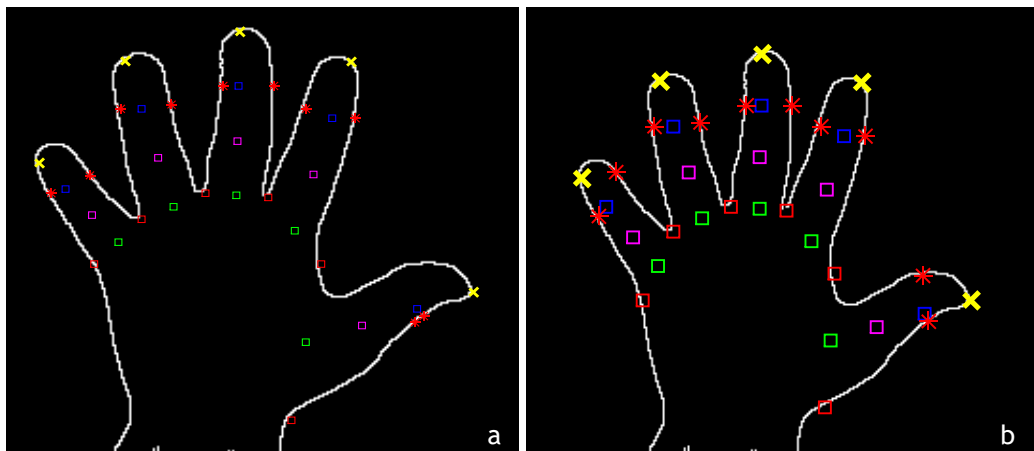
Figure 46 - Inadequate distal thumb division in the hand contour (a), corrected by working with y coordinate (b).

Inadequate segmentation/edge extraction occurred in 12 images, mainly due to little care during the image acquisition, which might have contributed to less quality hand images, such as depicted in Figure 47. This might be enhanced in the acquisition session. In what concerns the first approach to detect the fingertips, improper fingertip detection occurred in 24 images. For example, in one case, Hough transform did not recognize the two upper lines in the convex hull shape, as shown in Figure 48. In other cases, Hough transform detected extra undesired lines in the convex hull shape (Figure 49), because it has not the best quality.
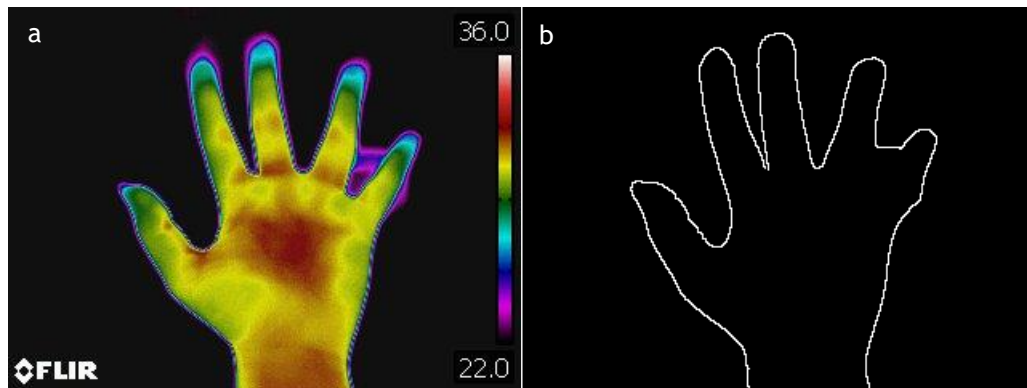
Figure 47 - Example of an inadequate segmentation/edge extraction (b) of a hand thermal image (a).
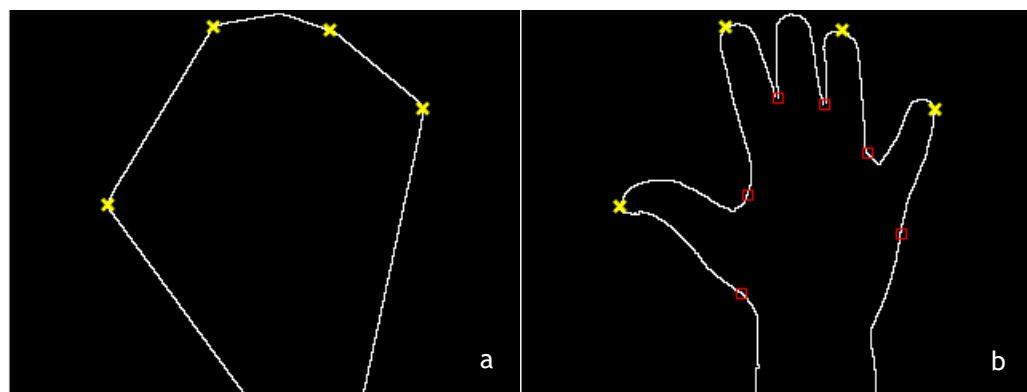
Figure 48 - Example of an inadequate fingertip detection (b) because Hough transform did not recognize the two upper lines in the convex hull shape (a).
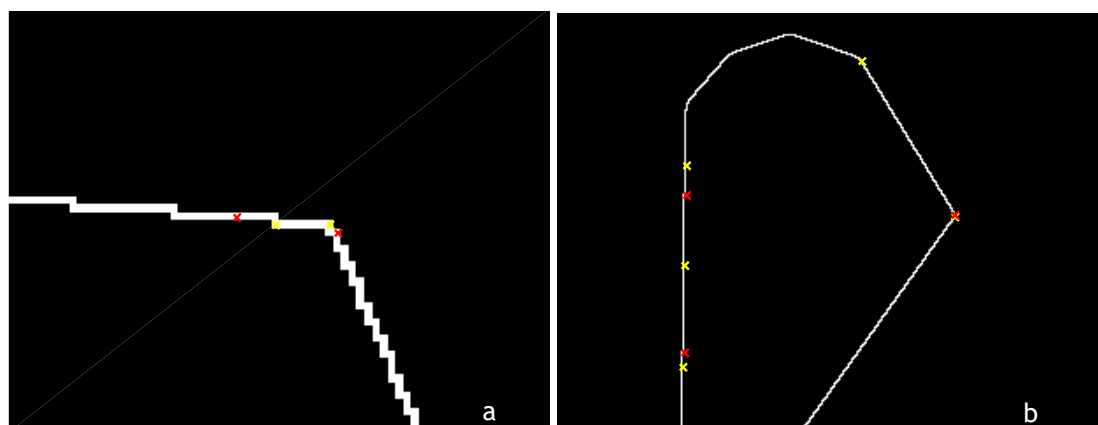
Figure 49 - Two examples (a) and (b) of extra undesired line detections using Hough transform.

These convex hull shapes might be enhanced in an acquisition session, by asking the participants to fully open their fingers and try to adopt a centered position. Good results were obtained for 12 images of the training set (25%). Since this is not a proper result, the second approach to detect the

fingertips was developed, showing a better performance, only failing if the fingers are not open/separated, or when the hand is in too much extension, in what regards the training set. Tables 10 and 11 show the hit scores for the first and second approaches, respectively, considering each parameter (described in Table 9), and each test set image (12 in total). A score is not attributed (0%) to a phalanx when it is not detected, or when it is but it is not even near the appropriate place. The first approach showed a performance of 70.2%, while the second approach had a better performance of 88.6%.

Figures 50 and 51 show the relationships between the average temperature of the detected phalanges by the first and second approaches, respectively, and of the manual marked phalanges, used as a reference, considering the test set images 10 and 12 for the first approach (because the algorithm failed to detect the phalanges in the others – see Table 10) and all the 12 test set images for the second approach.

Table 10 — First approach evaluation.

Test set Image/ Parameter Number	First Approach Score (%)																
	1	2	3	4	5	6	7	8	9	10	11	12	13	14	15	16	Total
1	50	4	4	4	4	4	---	---	---	---	---	---	---	---	---	---	70
2	50	4	4	4	4	4	---	---	---	---	---	---	---	---	---	---	70
3	50	0	4	4	4	4	---	---	---	---	---	---	---	---	---	---	66
4	50	4	0	4	4	4	---	---	---	---	---	---	---	---	---	---	66
5	50	0	0	0	4	4	---	---	---	---	---	---	---	---	---	---	58
6	50	4	0	4	4	4	---	---	---	---	---	---	---	---	---	---	66
7	50	4	4	4	4	0	---	---	---	---	---	---	---	---	---	---	66
8	50	4	4	4	0	4	---	---	---	---	---	---	---	---	---	---	66
9	50	0	4	0	4	4	---	---	---	---	---	---	---	---	---	---	62
10	50	4	4	4	4	4	3	3	3	2	1	3	3	3	2	2	95
11	50	0	4	4	4	4	---	---	---	---	---	---	---	---	---	---	66
12	50	4	4	4	4	4	2	3	2	1	1	2	3	3	2	2	91
Average score = 70.2%																	

Automatic detection of hand fingertips and phalanges in thermal images

Table 11 — Second approach evaluation.

Test set Image/ Parameter Number	Second Approach Score (%)																
	1	2	3	4	5	6	7	8	9	10	11	12	13	14	15	16	Total
1	50	0	4	4	4	4	0	3	2	3	2	3	1	2	3	1	86
2	50	0	4	4	4	4	0	3	2	3	1	3	1	2	3	1	85
3	50	4	4	4	4	4	2	2	2	2	3	2	3	2	2	3	93
4	50	0	4	4	4	4	1	2	2	2	3	3	2	2	2	3	88
5	50	4	4	4	4	4	2	3	2	3	3	2	2	3	3	2	95
6	50	4	4	4	4	0	3	3	2	3	0	2	2	3	3	2	89
7	50	0	4	4	0	4	0	3	1	0	3	3	2	2	0	3	79
8	50	0	4	4	4	4	1	2	2	3	2	2	2	2	3	2	87
9	50	4	4	4	4	4	2	3	2	2	2	2	3	3	3	2	94
10	50	0	4	4	4	4	0	2	1	3	2	3	3	2	3	2	87
11	50	4	4	4	4	4	2	3	1	3	3	2	3	2	3	3	95
12	50	4	4	0	4	4	0	3	0	3	3	2	2	0	3	3	85
Average score = 88.6%																	
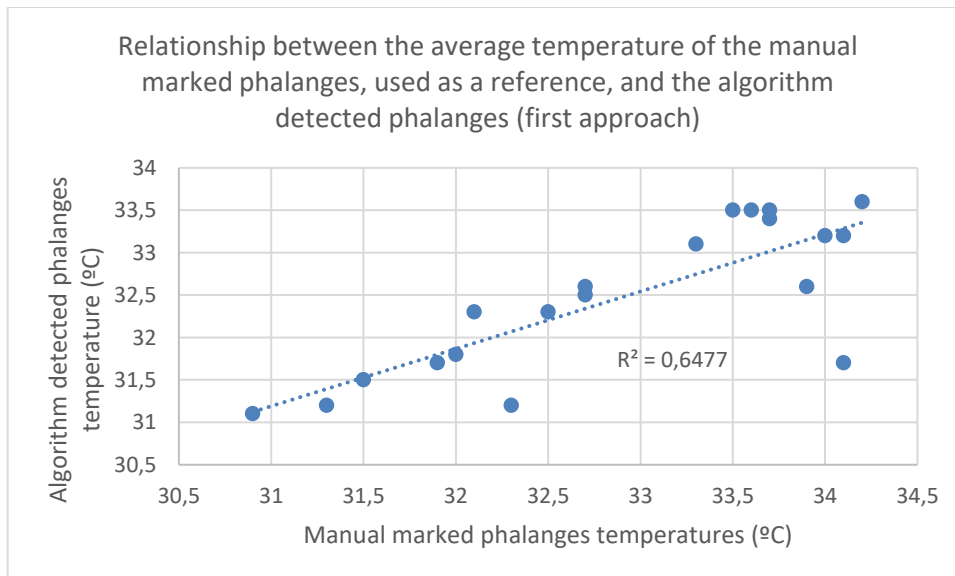
Figure 50 - Relationship between the average temperature of the manual marked phalanges, used as a reference, and the algorithm detected phalanges (first approach).
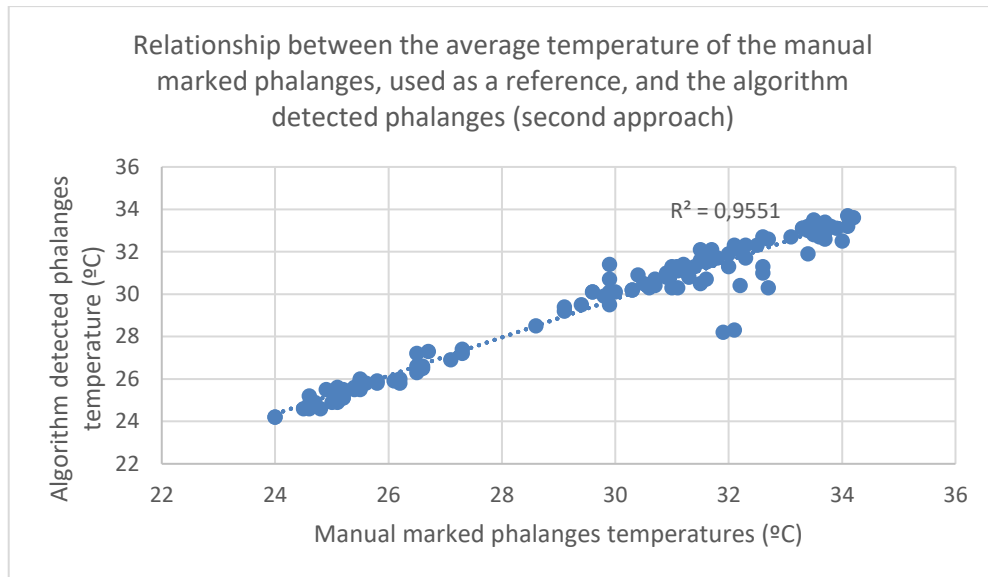
Figure 51 - Relationship between the average temperature of the manual marked phalanges, used as a reference, and the algorithm detected phalanges (second approach).

5.3 Discussion

The first approach low score is caused by the errors described in the final part of the Results section regarding the training set images, that were maintained in the test set images. Extra fingertips were found in 83% of the test set images, which prevented the detection of the phalanges. As explained before, this is caused by an inappropriate convex hull shape lines detection using Hough transform.

The performance of the second approach is better. By analyzing the results, the majority of the differences between average temperature of the detected phalanges and manual marked phalanges (used as a reference) might be due to the fact that small errors in the areas of interest definition can lead to significant differences in the measured temperatures. Also, many detected phalanges circle points were on the hand contour, which usually has a very different temperature, which caused the discrepancy between marked and detected phalanges average temperature. In some cases, numeric parameters that were used in methodology steps are not suitable (Figure 52). This means that a larger set of images should be part of the training set, in order to optimize and adjust some algorithm's numeric parameters. The slight rotation or over extension of some hand images also influenced the analysis of the white regions between the fingers, which led to improper detections of fingertips and hand contour phalanx separations (Figure 53). This should be considered, when improving the algorithm.

The first approach shows a reasonable linear correlation (Figure 50) between the average temperature of the detected phalanges and the manual marked phalanges (R^2=0.6477). The coefficient of determination in the second approach is close to 1 (R^2=0.9551), as shown in Figure 51. The variables are highly associated, meaning that the algorithm's prediction temperatures mirror the reference temperature tightly, which proves the efficiency of this approach.
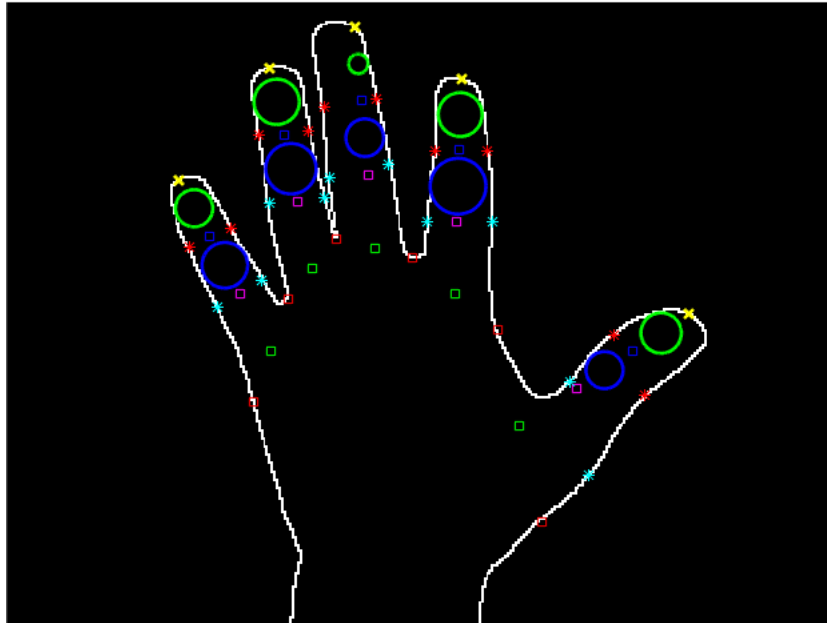
Figure 52 - Final result of test set image 11.
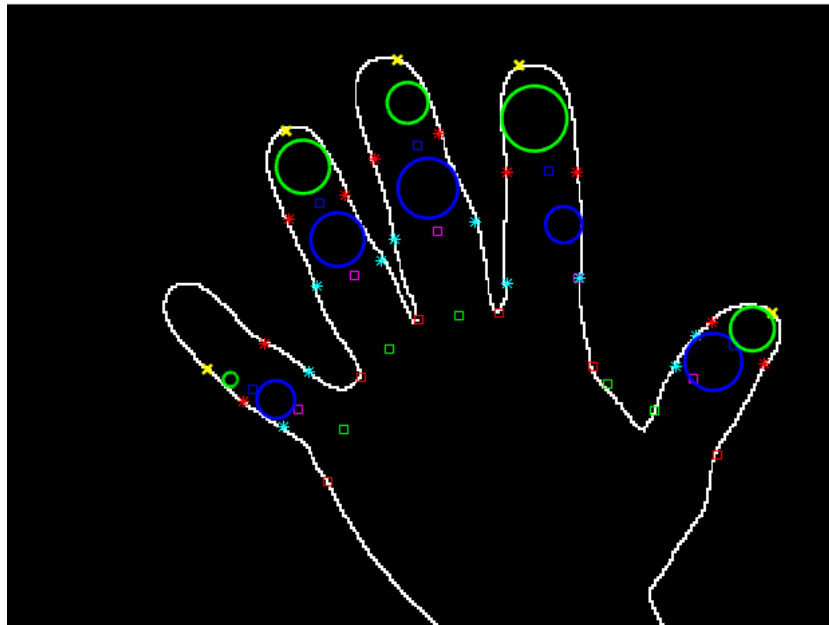
Figure 53 - Final result of test set image 6.

Chapter 6

Discussion

In this chapter, the results presented in Chapter 4 are discussed.

It was not possible to study the influence of age, handedness, smoking, hypertension, type II diabetes, autonomic dysfunction (health problems that possibly could influence hand blood circulation) and cholesterol level in this study, because the total sample is not representative nor distinctive enough.

Regarding the results of the first methodology, the ROIs temperature is the same irrespectively of the sex, the analysed compression order or hand, while time significantly influences the middle area of the thumb and middle phalanx of the little finger ROI temperatures.

The negative values observed in the graphics in Figure 19 suggest an effective occlusion of both arteries, which lead to the decrease of the ROIs temperatures. The differences are statistically significant. Although the radial artery mainly supplies the radial ROI and vice-versa, both arteries do supply both ROIs, so it is not possible to establish conclusions about which artery occlusion causes the higher temperature decrease.

Figure 20 shows a positive average temperature difference between situations 2 and 1, for both hands and both radial and ulnar ROIs (7 seconds after the corresponding artery is released). This temperature increase is consistent with the blood returning to the blood vessels. However, the values are low and statistically not significant.

The Figure 21 describes the thermic changes in the ROI opposite to the artery that was released. Since one ROI is mainly supplied by the corresponding artery (see Section 2.4), it is expected that this temperature manifestation is not so expressive as the previously described. This is verified, except the case where radial artery is released, in the right hand. Concerning the same hand, a negative temperature difference is verified in the radial ROI when the ulnar artery is released, suggesting that the reperfusion of the radial ROI caused by ulnar artery release does not cause a thermic manifestation. However, the values are very low and again not statistically significant, so these results are not meaningful.

Figure 22 shows the alteration of the thermal index (gradient between ROIs). The thermal index should firstly increase and secondly decrease. After compressing both arteries, one of them is released, therefore the corresponding ROI is more supplied with blood (see Chapter 2.4), comparing to the other ROI (proven by the previous discussion), which should increase the thermal index. Later, as both the arteries are released, the difference of temperatures between the two ROIs should be

attenuated, which should decrease the thermal index. This is verified, except for the right hand when the radial artery is released first. This fact also contributes to the result of the statistical analysis: the difference between Ti2 and Ti1 is not significant (p=0.135), while the difference between Ti3 and Ti2 is statistically significant (p=0.046). Therefore, it is clear that time has a significant influence in the gradient between the phalanges temperatures (p=0.029), but its variation is the same irrespectively of the analysed compression order or hand (p>0.05).

The artery exit ROI has a higher temperature than the corresponding phalanx ROI, since the blood reaches the fingers after reaching the arteries exits. Accordingly, Figures 23 and 24 show the negative values of temperature difference between these ROIs. Following the arteries occlusion (moment 2 in the graphics), this difference should be even lower, since this mechanical interference prevents the blood from reaching the fingers. After one artery release, the difference between ROIs corresponding to that artery should increase, because there was a thermal recovery, so the thermal pattern should be similar to the basal situation. Figures 23 and 24 show that firstly this gradient decreases and, accordingly to the statistical analysis, this decrease is generally significant (p=0.002) but, after that, the thermal recovery is not noticeable and it is not statistically significant from moment 2 to 3 (p=0.101), neither from moment 3 to 4 (p=1.000). The ulnar gradient is the same irrespectively of the analyzed hand. However, compression order statistically influences both ulnar and radial gradients and hand factor statistically influences the radial gradient. This might be caused by different types of forces applied by the physician when changing these factors during the modified Allen test, which might affect gradient values (visible when comparing the graphics).

A possible explanation for the non-significant results described so far relies on the fact that, although the physician can tell, by visual inspection (due to the color changes), that the arteries occlusion is effective and the blood reperfusion is successful 7 seconds after the arteries release, suggesting that the blood leaves and reaches the hand blood vessels, respectively, it may not have yet triggered a thermic reaction, so the thermal camera may not be able to properly detect the blood reperfusion, because it records the skin temperature. For this reason, a second methodology was followed (see Section 3.2.2), to check if it is possible to record a proper thermal response correlated to the blood reperfusion.

Sex does not have a statistically significant influence in the second methodology either.

The negative values observed in the graphics in Figures 25 and 26 suggest an effective occlusion of both arteries, which lead to the decrease of the ROIs temperatures. The increasing thermal manifestation immediately, 15 and 30 seconds after arteries occlusion validate the new methodology as well. The only exception is the case where the effect of both arteries occlusion on the radial ROI temperature is lower after the 30 seconds waiting period than in the 15 seconds, regarding the situation where the ulnar artery is going to be released first. One possible justification relies on the fact that the force applied to occlude the arteries might not have been the same throughout the entire occlusion process. The fact that some values related to the thermograms taken immediately after occlusion are not statistically significant (p>0.05), as described in the Results section, also validates the second methodology.

Figure 27 shows a positive average temperature difference between situations 2 and 1, for both hands and both radial and ulnar ROIs, 7, 15 and 30 seconds after the corresponding artery is released. Since the blood is returning to the hand blood vessels, this temperature increase was expected. These results also validate the change in methodology, since the thermic manifestation 15 seconds after artery release is higher than the 7 seconds cut-off and lower than the 30 seconds cut-off. Additionally, the significant values (p<0.05) are only related with the 15 and/or 30 seconds cut-off, as described

in the Results section. In both hands, the changes in temperature are higher in the radial ROI when the radial artery is released first, than in the ulnar ROI when the ulnar artery is released first.

Figure 28 describes the thermic changes in the ROI opposite to the artery that was released. As explained before, since one ROI is mainly supplied by the corresponding artery (see Section 2.4), it is expected that this temperature manifestation is not so expressive as the one verified in Figure 27. This is verified in all cases, for all cut-off times. In fact, negative and near zero temperature differences are verified, suggesting that the reperfusion of one ROI caused by the opposite artery release (collateral reperfusion) does not cause a thermic manifestation. Moreover, none of the values is statistically significant ($p > 0.05$).

Figures 29, 30 and 31 show the alteration of the thermal index (gradient between phalanges ROIs). As explained before, the thermal index should firstly increase and secondly decrease.

In the situation where the radial artery is released first, in the left hand, the statistical analysis suggests that there is a strongest thermic manifestation of the radial ROI reperfusion, comparing to the ulnar ROI, when the radial artery is released, as expected (see Chapter 2.4) and proved by previous results. They also suggest that the ulnar artery release (that causes the last reperfusion) does not cause such a significant thermal manifestation in the ulnar ROI.

When the radial artery is released first, in the right hand, the significant values ($p < 0.05$) are only related with the 15 and/or 30 seconds cut-off. This validates the new methodology, since the 7 seconds cut-off does not cause a significant thermic manifestation.

In the situation where the ulnar artery is released first, in the left hand, the statistical analysis suggests that the radial artery release (that causes the last reperfusion) does not cause such a significant thermal manifestation in the radial ROI as the ulnar artery release (that causes the first reperfusion) does in the ulnar ROI.

When the ulnar artery is released first, in the right hand, the only statistically significant ($p < 0.05$) difference is between Ti2 and Ti1, in the 7 seconds cut-off, which is not coherent with the results reported in Figure 27.

It is important to notice that the last reperfusion (corresponding to Ti3) might not be as effective as the first one (corresponding to Ti2), because the artery is being compressed for a long time and the physician might not be applying the same force as in the beginning, involuntarily, so the last artery release might cause a weaker thermic manifestation.

Figures 32 and 33 show the negative values of temperature gradient between the phalanx ROI and the corresponding artery exit ROI, which was expected, as explained previously. All the graphics show a decrease in this metric when the artery occlusion takes place and an increase in the time point where the corresponding artery is released, as expected. However, just some of these changes are statistically significant and are going to be discussed.

In Figure 32, the top left graphic shows a radial gradient decrease 15 seconds after arteries occlusion. It increases 30 seconds after radial artery is released, when a fully recovery of the thermic pattern occurs (it becomes similar to the basal situation), as expected.

In the top right graphic, the ulnar gradient decrease immediately after arteries occlusion. The thermic pattern only recovers in time 10, when it is similar to the basal situation. However, this recovery should have happened sooner, when the ulnar artery is released (time 5), but the difference between gradients in time 5, 6 or 7 and 4 is not statistically significant ($p > 0.05$), so the thermal effect of the ulnar artery release in the ulnar gradient increase is not meaningful.

According to the bottom left graphic, there is a radial gradient decrease 30 seconds after arteries occlusion. It increases 30 seconds after radial artery is released, when a fully recovery of the thermic pattern occurs (it becomes similar to the basal situation), as expected.

At the bottom right graphic, the ulnar gradient decrease in the 30 seconds after arteries occlusion. It increases 30 seconds after the radial artery is released. However, this gradient increase should have happened sooner, when the ulnar artery is released (time 5), but the difference between gradients in time 5, 6 or 7 and 4 is not statistically significant ($p>0.05$), so the thermal effect of the ulnar artery release in the ulnar gradient increase is not meaningful.

In Figure 33, the top left graphic shows a radial gradient decrease 15 seconds after arteries occlusion. The thermic pattern only recovers in time 8, when it is similar to the basal situation. However, this recovery should have happened sooner, when the radial artery is released (time 5), but the difference between gradients in time 5, 6 or 7 and 4 is not statistically significant ($p>0.05$), so the thermal effect of the radial artery release in the radial gradient increase is not relevant.

According to the top right graphic, there is an ulnar gradient decrease 15 seconds after arteries occlusion. It increases 7 seconds after ulnar artery is released, when a fully recovery of the thermic pattern occurs (it becomes similar to the basal situation), as expected.

At the bottom left graphic, the radial gradient decreases immediately after arteries occlusion. The thermic pattern only recovers in time 8, when it is similar to the basal situation. However, this recovery should have happened sooner, when the radial artery is released (time 5), but the difference between gradients in time 5, 6 or 7 and 4 is not statistically significant ($p>0.05$), so the thermal effect of the radial artery release in the radial gradient increase is not meaningful.

The bottom right graphic shows an ulnar gradient decrease 15 seconds after arteries occlusion. Although the gradient increase is only statistically significant 30 seconds after ulnar artery is released, a recovery of the thermic pattern occurs 15 seconds after (it becomes similar to the basal situation, as expected).

A possible reason for the non-significant thermal effects in the temperature gradient between the phalanx ROI and the corresponding artery exit ROI, when the first artery is released, relies on the fact that the artery exit might also receive some blood, which may cause the late gradient recovery.

It was confirmed that the thermic manifestation happens in a more significant way if the waiting time for taking the thermograms after each step of the test is higher, which validates the change to the second methodology.

It should be mentioned that there are uncontrollable factors that affect the blood flow (see Section 2.3). Moreover, the modified Allen test is not 100% reliable and it is a subjective measurement (see Section 3.2). Also, the temperature of the room was maintained at $23.8\pm1.4°C$, above the 22ºC recommended by the "Glamorgan protocol" (Ammer, 2008). All these factors might have influenced the results.

Chapter 7

Conclusion

In conclusion, medical thermography was able to objectively quantify the thermal effects of the modified Allen test. This technique showed that, in both hands, the changes in temperature are higher in the radial ROI when the radial artery is released first, than in the ulnar ROI when the ulnar artery is released first. Furthermore, collateral reperfusion by both arteries does not cause a strong thermal manifestation. There is not a clear conclusion on which artery contributes the most to the hand blood perfusion, because the efficiency of both collateral and non-collateral reperfusions need to be evaluated to clarify the vascular dominance.

A method that automatically detects the fingertips and phalanges in thermal images is also presented. The best approach presented a hit score of 88.6%. Future work includes improving the algorithm, using a larger training set, so as to fix some issues that lower the performance, by adjusting some numeric parameters and considering various hand postures (or, in alternative, use a mould in the thermography acquisition so that all hands are in similar positions). In the future, it could be applied as an automatic routine when physicians need to get information about the hand/fingers blood perfusion, or get objective measurements of the modified Allen's test effect. Having a thermal camera, physicians could acquire the thermograms and automatically get access to the phalanges temperatures.

Future work includes studying a larger and more representative and distinctive sample, so as to validate these results. Occluding and releasing the arteries could also be performed using a cuff (adapted to be able to release one artery at a time), as an alternative to the modified Allen test, to check whether its effect is similar or not. It is suggested to use a LDPI equipment that is appropriate to evaluate the hands' blood flow. Furthermore, future work includes PPG data acquisition with a less bulky recording equipment containing, for example, fingertip adhesive probes. It is also suggested to develop a motion artifact reduction algorithm to process the PPG pulse waveform, so that it is possible to monitor the fingers blood volume alterations while a modified Allen test is performed. Another suggestion for future work relies on the use of iPPG technique, also with the purpose of monitoring the microvascular perfusion.

References

Abramson, D. I. (1967). *Circulation in the Extremities*. Academic Press.

Allen, J. (2007). Photoplethysmography and its application in clinical physiological measurement. *Physiological Measurement*, *28*(3), R1–R39. https://doi.org/10.1088/0967-3334/28/3/R01

Allen, J., & Howell, K. (2014). Microvascular imaging: techniques and opportunities for clinical physiological measurements. *Physiological Measurement*, *35*(7), R91–R141. https://doi.org/10.1088/0967-3334/35/7/R91

Ammer, K. (2006). Influence of Imaging and Object Conditions on Temperature Readings from Medical Infrared Images, *15*(4), 2001–2003.

Ammer, K. (2008). The Glamorgan Protocol for recording and evaluation of thermal images of the human body. *Thermology International*, *18*(4), 136–144.

Ammer, K. (2016). Temperature measurements and thermography of the palmar surface of the human hand - An overview. *Thermology International*, *26*(4).

Briers, J. D. (2001). Laser Doppler, speckle and related techniques for blood perfusion mapping and imaging. *Physiological Measurement*, *22*(4), R35–R66. https://doi.org/10.1088/0967-3334/22/4/201

Charkoudian, N., & Rabbitts, J. A. (2009). Sympathetic neural mechanisms in human cardiovascular health and disease. *Mayo Clinic Proceedings*, *84*(9), 822–30. https://doi.org/10.1016/S0025-6196(11)60492-8

Chellappan, K., Zahedi, E., & Ali, M. A. M. (2007). Effects of physical exercise on the photoplethysmogram waveform. *2007 5th Student Conference on Research and Development, SCORED*, (December), 1–5. https://doi.org/10.1109/SCORED.2007.4451399

Coleman, S., & Anson, B. (1961). Arterial patterns in the hand based upon a study of 650 specimens. *Surgery, Gynecology & Obstetrics*, *113*, 409. Retrieved from http://www.ncbi.nlm.nih.gov/pubmed/13694610

DeBakey, M. E., & Simeone, F. a. (1946). Battle Injuries of the Arteries in World War II: an analysis of 2,471 cases. *Annals of Surgery*, *123*(4), 534–579. https://doi.org/10.1097/00000658-194604000-00005

Doscher, W., Viswanathan, B., & Stein, T. (1983). Hemodynamic assessment of the circulation in 200 normal hands. *Annals of Surgery*, *198*(6), 776. Retrieved from http://www.ncbi.nlm.nih.gov/pmc/articles/PMC1353229/

Drake, R. L., Vogl, Wayne, A., & Mitchell, A. W. M. (2014). Gray's Anatomy for Students. *Elsevier Health Sciences*, *53*, 810-818. https://doi.org/10.1017/CBO9781107415324.004

Dumanian, G., Segalman, K., & Buehner, J. (1998). Analysis of digital pulse-volume recordings with radial and ulnar artery compression. *Plastic and Reconstructive Surgery*, *102*(6), 1993–1998. Retrieved from http://journals.lww.com/plasreconsurg/Abstract/1998/11000/Analysis_of_Digital_Pulse_Volume_Recordings_with.28.aspx

Fullerton, a, Stücker, M., Wilhelm, K.-P., Wårdell, K., Anderson, C., Fischer, T., … Serup, J. (2002). Guidelines for visualization of cutaneous blood flow by laser Doppler perfusion imaging. *Contact Dermatitis*, *46*(3), 129-140. https://doi.org/10.1034/j.1600-0536.2002.460301.x

Greenfield, A. D. M. (1965). The effects of emotion on the peripheral circulation. *Journal of Psychosomatic Research*, *9*(1), 155–158. https://doi.org/10.1016/0022-3999(65)90024-3

Haerle, M., Haffner, H. M., Dietz, K., Schaller, H. E., & Brunelli, F. (2003). Vascular dominance in the forearm. *Plastic and Reconstructive Surgery*, *111*(6), 1891–1898. https://doi.org/Doi

10.1097/01.Prs.0000057529.76413.D7

Haerle, M., Häfner, H.-M., Schaller, H.-E., & Brunelli, F. (2002). Dominances in Finger Arteries. *The Journal of Hand Surgery: Journal of the British Society for Surgery of the Hand*, *27*(6), 526–529. https://doi.org/10.1054/jhsb.2002.0856

Healthwise. (2015). Nerves of the Arm. Retrieved January 12, 2017, from http://www.webmd.com/brain/nerves-of-the-arm

Holling, H. (1965). Effect of Embarrassment on Blood Flow to Skeletal Muscal. *Transactions of the American Clinical and Climatological Association*, *76*, 49. Retrieved from https://www.ncbi.nlm.nih.gov/pmc/articles/PMC2279463/

IBM Knowledge Center. (2015). One-Way ANOVA Post Hoc Tests. Retrieved June 5, 2017, from https://www.ibm.com/support/knowledgecenter/en/SSLVMB_24.0.0/spss/base/idh_onew_post.html

Iida, Y., Numata, T., Shiba, K., & Nagata, H. (2002). Hemodynamic changes of the hand after radial forearm flap harvesting. *Annals of Plastic Surgery, 49(2)*, *49*(2), 156–160. Retrieved from http://journals.lww.com/annalsplasticsurgery/Abstract/2002/08000/Hemodynamic_Changes_of_the_Hand_After_Radial.8.aspx

Izzati Zainal, N., & Azami Sidek, K. (2016). Real Time PPG Data Acquisition with GUI based Application for HRV Measurement. *Indian Journal of Science and Technology*, *9*(28). https://doi.org/10.17485/ijst/2016/v9i28/97730

Jarvis, M. A., Jarvis, C. L., Jones, P. R. ., & Spyt, T. J. (2000). Reliability of Allen's test in selection of patients for radial artery harvest. *The Annals of Thoracic Surgery*, *70*(4), 1362–1365. https://doi.org/10.1016/S0003-4975(00)01551-4

Jaworski, Ł., Siondalski, P., Jarmoszewicz, K., & Rogowski, J. (2007). Arm temperature distribution in thermographic pictures after radial artery harvesting for coronary bypass operation. *Interactive Cardiovascular and Thoracic Surgery, 6(5)*, *6*(5), 598–602. Retrieved from http://icvts.oxfordjournals.org/content/6/5/598.short

Jayasree, V. (2009). *Selected cardiovascular studies based on photoplethysmography technique*. Cochin University of Science and Technology. Retrieved from http://citeseerx.ist.psu.edu/viewdoc/download?doi=10.1.1.471.5324&rep=rep1&type=pdf

John, H. E., Niumsawatt, V., Rozen, W. M., & Whitaker, I. S. (2016). Clinical applications of dynamic infrared thermography in plastic surgery: a systematic review. *Gland Surgery*, *5*(2), 122–32. https://doi.org/10.3978/j.issn.2227-684X.2015.11.07

Jones, B. F. (1998). A reappraisal of the use of infrared thermal image analysis in medicine. *IEEE Transactions on Medical Imaging*, *17*(6), 1019–1027. https://doi.org/10.1109/42.746635

Jones, B. F., & Plassmann, P. (2002). Digital Infrared Thermal Imaging of Human Skin. *IEEE Engineering in Medicine and Biology Magazine*, *21*(6), 41–48. https://doi.org/10.1109/MEMB.2002.1175137

Just, M., Chalopin, C., Unger, M., Halama, D., Neumuth, T., Dietz, A., & Fischer, M. (2015). Monitoring of microvascular free flaps following oropharyngeal reconstruction using infrared thermography: first clinical experiences. *European Archives of Oto-Rhino-Laryngology*, *273*(9), 2659–2667. https://doi.org/10.1007/s00405-015-3780-9

Keys, A., Fidanza, F., Karvonen, M., & Kimura, N. (1972). Indices of relative weight and obesity. *Journal of Chronic Diseases*, *25*(6–7), 329–343. Retrieved from http://www.sciencedirect.com/science/article/pii/0021968172900276

Kim, H.-Y. (2013). Statistical notes for clinical researchers: assessing normal distribution (2) using skewness and kurtosis. *Restorative Dentistry & Endodontics*, *38*(1), 52–4. https://doi.org/10.5395/rde.2013.38.1.52

Kleinert, J. M., Fleming, S. G., Abel, C. S., & Firrell, J. (1989). Radial and ulnar artery dominance in normal digits. *The Journal of Hand Surgery*, *14*(3), 504–508. https://doi.org/10.1016/S0363-5023(89)80012-7

Koff, P. (2010). *Clinical Use of Pulse Oximetry Pocket Reference*. WONCA/ICC. Retrieved from http://www.copd-alert.com/OximetryPG.pdf

Kohonen, M., Teerenhovi, O., Terho, T., Laurikka, J., & Tarkka, M. (2007). Is the Allen test reliable enough? *European Journal of Cardio-Thoracic Surgery*, *32*(6), 902–905. Retrieved from http://ejcts.oxfordjournals.org/content/32/6/902.short

Laerd Statistics. (2013a). Friedman Test in SPSS Statistics - How to run the procedure, understand the output using a relevant example. Retrieved June 5, 2017, from https://statistics.laerd.com/spss-tutorials/friedman-test-using-spss-statistics.php

Laerd Statistics. (2013b). Mann-Whitney U Test in SPSS Statistics | Setup, Procedure &

Interpretation. Retrieved June 7, 2017, from https://statistics.laerd.com/spss-tutorials/mann-whitney-u-test-using-spss-statistics.php

Laerd Statistics. (2013c). Repeated Measures ANOVA - Understanding a Repeated Measures ANOVA. Retrieved June 5, 2017, from https://statistics.laerd.com/statistical-guides/repeated-measures-anova-statistical-guide.php

Laerd Statistics. (2013d). Understanding Sphericity - An introduction to, testing for, and interpreting sphericity. Retrieved June 5, 2017, from https://statistics.laerd.com/statistical-guides/sphericity-statistical-guide.php

Lenasi, H. (2011). Assessment of human skin microcirculation and its endothelial function using laser Doppler flowmetry. *INTECH Open Access Publisher*. Retrieved from http://cdn.intechopen.com/pdfs/25172/InTech-Assessment_of_human_skin_microcirculation_and_its_endothelial_function_using_laser_doppler_flowmetry.pdf

Lippincott Williams & Wilkins. (2007). *Best practices: evidence-based nursing procedures.* (2nd ed.). Lippincott Williams & Wilkins. Retrieved from https://books.google.pt/books?id=HXWmZ9cdBbsC&dq=oximetry&hl=pt-PT&source=gbs_navlinks_s

Little, J. M., Zylstra, P. L., West, J., & May, J. (1973). Circulatory patterns in the normal hand. *British Journal of Surgery*, *60*(8), 652–655. https://doi.org/10.1002/bjs.1800600819

Mabuchi, K., Genno, H., Matsumoto, K., Chinzei, T., Fujimasa, I., & Ring, E. (1995). Autonomic thermoregulation and skin temperature: the role of deep body temperature in the determination of skin temperature. *The Thermal Image in Medicine and Biology*, *121*(9).

Martins, R. (2010). *Desenvolvimento de um sensor de fotopletismografia para monitorização cardíaca para aplicação no pulso*. Retrieved from https://estudogeral.sib.uc.pt/handle/10316/14086

Merla, A., Romualdo, S. Di, Donato, L. Di, Proietti, M., Salsano, F., & Romani, G. . (2007). Combined thermal and laser Doppler imaging in the assessment of cutaneous tissue perfusion. *Engineering in Medicine and Biology Society, 2007. EMBS 2007. 29th Annual International Conference of the IEEE*, 2630–2633. Retrieved from http://ieeexplore.ieee.org/abstract/document/4352869/

Miller-Keane Encyclopedia and Dictionary of Medicine, Nursing, and Allied Health, S. E. (2003). Flap. Retrieved November 18, 2016, from http://medical-dictionary.thefreedictionary.com/flap

Moor Instruments. (2016). Tissue Blood Flow and Temperature Monitoring with MoorVMS-LDF. Retrieved February 11, 2016, from http://www.ntnu.edu/documents/221360533/1261827882/Moore+Tissue+blood+flow+and+temperature+monitoring.pdf/331aa2b0-dd7c-40c2-822d-bd0fca5f753a

NHLBI. (2005). High Blood Cholesterol: What You Need To Know. Retrieved June 3, 2017, from https://www.nhlbi.nih.gov/health/resources/heart/heart-cholesterol-hbc-what-html

Oerlemans, H., Graff, M., & Dijkstra-Hekkink, J. (1999). Reliability and normal values for measuring the skin temperature of the hand with an infrared tympanic thermometer: a pilot study. *Journal of Hand Therapy 12.4*, *12*(4), 284–290. Retrieved from http://www.sciencedirect.com/science/article/pii/S0894113099800659

Oettle, A., Niekerk, A. van, & Boon, J. (2006). Evaluation of Allen's test in both arms and arteries of left and right-handed people. *Surgical and Radiologic Anatomy*, *28*(1), 3–6. Retrieved from http://link.springer.com/article/10.1007/s00276-005-0039-y

OpenStax. (2016). *Anatomy & Physiology*. OpenStax CNX. Retrieved from http://cnx.org/contents/14fb4ad7-39a1-4eee-ab6e-3ef2482e3e22@8.25

Peterson, L., Khabiri, H., Litzendorf, M., & Stawicki, S. (2013). Hemodialysis Access: Initial Considerations and the Difficult Patient. In *Hemodialysis*. InTech. Retrieved from https://www.researchgate.net/profile/Stanislaw_Stawicki/publication/271839699_Hemodialysis_Access_Initial_Considerations_and_the_Difficult_Patient/links/54d3a1ee0cf28e069728880d.pdf

Pola, P., Serricchio, M., Flore, R., Manasse, E., Favuzzi, A., & Possati, G. F. (1996). Safe removal of the radial artery for myocardial revascularization: A doppler study to prevent ischemic complications to the hand. *The Journal of Thoracic and Cardiovascular Surgery*, *112*(3), 737–744. https://doi.org/10.1016/S0022-5223(96)70060-0

Rauh, R., & Posfay, A. (2003). Quantification of inspiratory-induced vasoconstrictive episodes: a comparison of laser Doppler fluxmetry and photoplethysmography. *Clinical Physiology and Functional Imaging*, *23*(6), 344-348. Retrieved from http://onlinelibrary.wiley.com/doi/10.1046/j.1475-0961.2003.00516.x/full

Ring, E. F. J., Thomas, R. A., & Howell, K. J. (2010). Sensors for Medical Thermography and Infrared Radiation Measurements. In *Biomedical Sensors* (p. 417).

Ring, E. F. J., & Ammer, K. (2012). Infrared thermal imaging in medicine. *Physiological Measurement, 33*(3), R33. https://doi.org/10.1088/0967-3334/33/3/R33

Roberts, L. (1965). Machine Perception of Three-Dimensional Solids. *Optical and Electro-Optical Information Processing (J. Tippett, Ed.), * 159–197.

Russ, J. (2011a). *The image processing handbook - 6th edition*. CRC press, 296-319. Retrieved from https://www.google.com/books?hl=pt-PT&lr=&id=ROSYCgAAQBAJ&oi=fnd&pg=PP1&dq=The+Image+Processing+Handbook,+Seventh+Edition&tots=daQKY3DC7a&sig=R9Dy2T23-CpP15OQoDS7mbbXcJ8

Russ, J. (2011b). *The image processing handbook - 6th edition*. CRC press, 567-574. Retrieved from http://journals.lww.com/jcat/Citation/1995/11000/The_Image_Processing_Handbook,_2nd_Ed.26.aspx

Ryan, J. F., Raines, J., Dalton, B. C., & Mathieu, A. (1973). Arterial dynamics of radial artery cannulation. *Anesthesia & Analgesia, 52*(6), 1017–1023. Retrieved from http://journals.lww.com/anesthesia-analgesia/Citation/1973/11000/Arterial_Dynamics_of_Radial_Artery_Cannulation.49.aspx

Santos, T., & Oliveira, L. (2015). Finger phalanx detection and tracking by contour analysis on RGB-D images. *Conference on Graphics, Patterns and Images, 28*. Retrieved from http://ivisionlab.dcc.ufba.br/doc/publication/2015/Finger_phalanx_detection_and_tracking_by_contour_analysis_on_RGB-D_images.pdf

Seeley, R. R., VanPutte, C. L., Regan, J., & Russo, A. (2011). *Seeley's Anatomy & Physiology*.

Seifalian, A. M., Stansby, G., Jackson, A., Howell, K., & Hamilton, G. (1994). Comparison of laser doppler perfusion imaging, laser doppler flowmetry, and thermographic imaging for assessment of blood flow in human skin. *European Journal of Vascular Surgery, 8*(1), 65–69. https://doi.org/10.1016/S0950-821X(05)80123-9

Shafique, M., Kyriacou, P., & Pal, S. (2012). Investigation of photoplethysmographic signals and blood oxygen saturation values on healthy volunteers during cuff-induced hypoperfusion using a multimode PPG/SpO2 sensor. *Medical & Biological Engineering & Computing, 50*(6), 575–583. Retrieved from http://link.springer.com/article/10.1007/s11517-012-0910-z

Shamir, M., Eidelman, L. A., Floman, Y., Kaplan, L., & Pizov, R. (1999). Pulse oximetry plethysmographic waveform during changes in blood volume. *British Journal of Anaesthesia Br J Anaesth, 82*(82), 178–81. Retrieved from https://oup.silverchair-cdn.com/oup/backfile/Content_public/Journal/bja/82/2/10.1093_bja_82.2.178/1/178.pdf?Expires=1496137465&Signature=CIoz9J8WdgCzPOpkSMh2EYpyQLO5mlQXY-jMpawPGFmk5RqAfqvFIcq7zftu6V4psj0813AVkGIBb2xGJrvY5RB5ZlAlA2v9cEYUQkouGr-NTB6MJ3F0Tz

Shepherd, A. (1990). History of laser-Doppler blood flowmetry. In *Laser-Doppler blood flowmetry*.

Sieg, P., & Bierwolf, S. (2001). Ulnar versus radial forearm flap in head and neck reconstruction: An experimental and clinical study. *Head and Neck-Journal for the Sciences and Specialties of the Head and Neck, 23*(11), 967–971.

Sieg, P., Jacobsen, H. C., Hakim, S. G., & Hermes, D. (2006). Superficial ulnar artery: Curse or blessing in harvesting fasciocutaneous forearm flaps. *Head and Neck*. https://doi.org/10.1002/hed.20367

Suichies, H., Aarnoudse, J., Wouda, A., & Jentink, H. (1992). Digital blood flow in cooled and contralateral finger in patients with Raynaud's phenomenon. Comparative measurements between photoelectrical plethysmography. *Angiology*. Retrieved from http://ang.sagepub.com/content/43/2/134.short

Sun, Y., Hu, S., Azorin-Peris, V., Greenwald, S., Chambers, J., & Zhu, Y. (2011). Motion-compensated noncontact imaging photoplethysmography to monitor cardiorespiratory status during exercise. *Journal of Biomedical Optics, 16*(7), 77010. https://doi.org/10.1117/1.3602852

Suominen, S., & Asko-Seljavaara, S. (1996). Thermography of Hands after a Radial Forearm Flap has Been Raised. *Scandinavian Journal of Plastic and Reconstructive Surgery and Hand Surgery, 30*(4), 307–314. https://doi.org/10.3109/02844319609056409

Tonks, A., Lawrence, J., & Lovie, M. (1995). Comparison of ulnar and radial arterial blood-flow at the wrist. *The Journal of Hand Surgery: British & European Volume, 20*(2), 240-242. Retrieved from http://www.sciencedirect.com/science/article/pii/S0266768105800609

Tortora, G. J., & Grabowski, S. R. (2003). *Principles of anatomy and physiology* (10th ed.). John Wiley

& Sons. Retrieved from https://books.google.pt/books?id=UXzDQgAACAAJ&hl=pt-PT&source=gbs_book_other_versions

Tse, J., Rand, C., Carroll, M., Charnay, A., Gordon, S., Morales, B., … Weese-Mayer, D. (2016). Determining peripheral skin temperature : subjective versus objective measurements. *Acta Paediatrica*, *105*(3), e126–e131. https://doi.org/10.1111/apa.13283

Tur, E., Tur, M., Maibach, H., & Guy, R. (1983). Basal perfusion of the cutaneous microcirculation: measurements as a function of anatomic position. *Journal of Investigative Dermatology*, *81*(5), 442–446. Retrieved from
http://www.sciencedirect.com/science/article/pii/S0022202X15432312

Ubbink, D. (2004). Toe blood pressure measurements in patients suspected of leg ischaemia: a new laser Doppler device compared with photoplethysmography. *European Journal of Vascular and Endovascular Surgery*, *27*(6), 629–634. Retrieved from
http://www.sciencedirect.com/science/article/pii/S1078588404000590

VanPutte, C., Regan, J., & Russo, A. (2015). *Seeley's Essentials of Anatomy and Physiology. McGraw-Hill*. Retrieved from http://www.google.com/patents/US420171

Vardasca, R., & Simoes, R. (2013). Current Issues in Medical Thermography. *Topics in Medical Image Processing and Computational Vision*, 223–237. https://doi.org/10.1007/978-94-007-0726-9

VC, H. P. (1962). Method and means for recognizing complex patterns. *US Patent 3,069,654*. Retrieved from https://www.google.com/patents/US3069654

Winkler, J., Lohr, J., Bukhari, R. H., Hearn, A., Goller, R., Parlato, D., … Smith, M. J. (1998). Evaluation of the Radial Artery for Use in Coronary Artery Bypass Grafting. *Journal of Vascular Technology*, *22*(1), 23–29.

Young, B., Woodford, P., & O'Dowd, G. (2013). *Wheater's functional histology: a text and colour atlas*. Elsevier Health Sciences. Retrieved from https://www.google.com/books?hl=pt-PT&lr=&id=HUlYAQAAQBAJ&oi=fnd&pg=PP1&dq=wheater%2527s+histology+young+et+al&ots=F6F23WvSBB&sig=MnIsN1nGMP14lkqEOWwQiV0sFFk

Yu, P., Chang, E. I., Selber, J. C., & Hanasono, M. M. (2012). Perforator Patterns of the Ulnar Artery Perforator Flap. *Plastic and Reconstructive Surgery*, *129*(1), 213–220. https://doi.org/10.1097/PRS.0b013e3182362a9c

Appendix

A. Ethical approval from Centro Hospitalar de S. João health ethical committee and Board of administration
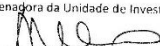
Assunto: Pedido de autorização para realização de estudo/projecto de investigação

Nome do Investigador Principal: Elsa Filipa Quadrado de Sousa

Título do projecto de investigação: Estudo da dominância vascular do pulso

Pretendendo realizar no(s) Serviço(s) de Cirurgia Plástica, Reconstrutiva e Unidade de Queimados do Centro Hospitalar de S. João – EPE o estudo/projecto de investigação em epígrafe, solicito a V. Exa., na qualidade de Investigador/Promotor, autorização para a sua efectivação.

Para o efeito, anexa toda a documentação referida no dossier da Comissão de Ética do Centro Hospitalar de S. João respeitante a estudos/projectos de investigação, à qual endereçou pedido de apreciação e parecer.

Com os melhores cumprimentos.

Porto, Janeiro de 2017

O INVESTIGADOR/PROMOTOR

Elsa Filipa Sousa

Comissão de Ética para a Saúde do Centro Hospitalar de S. João/Faculdade de Medicina da Universidade do Porto
Modelo CrS 01

67
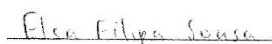
Comissão de Ética para a Saúde do HSJ
Parecer

Projecto de investigação: "Estudo da dominância vascular do pulso".

Nome da Investigadora Principal: Elsa Filipa Quadrado de Sousa

Promotor: Faculdade de Engenharia da Universidade do Porto (FEUP).

Concepção e pertinência do estudo

Trata-se de um estudo que se insere no âmbito do Mestrado Integrado em Engenharia Biomecânica da FEUP, a defender pela Investigadora Principal, Elsa Filipa Quadrado de Sousa, sob orientação do Prof. Doutor Ricardo Ângelo Rosa Verdasca, que tem como objetivo investigar a dominância vascular do pulso, utilizando a termografia médica (infravermelha), como método de avaliação (pretendem os Investigadores esclarecer a dominância da artéria radial e cubital ao nível do antebraço, e possível influência da preferência bilateral, e de que modo estas contribuem para a perfusão sanguínea da mão).

O protocolo do estudo é baseado no "Glamorgan Protocol", uma referência para os procedimentos padrão recomendados para a recolha e avaliação das imagens térmicas em aplicações médicas.

A termografia médica é um método complementar de diagnóstico, não-invasivo, inofensivo e indolor.

Todos os procedimentos investigacionais estão bem descritos (sala de exames; ambiente controlado; equipamento necessário; cuidados para o equipamento termográfico; informações para o participante; preparação pré-recolha; posições para a recolha das imagens; campo de visão; captura de imagens).

É referido no protocolo/formulário da CES que vão ser estudados voluntários sãos avaliados no Serviço de Cirurgia Plástica, Reconstrutiva e Unidade de Queimados do Centro Hospitalar de S. João (CHSJ); *no entanto, não estão referenciados o tamanho da amostra, o método de recrutamento, possíveis ressarcimentos pelas despesas de deslocação e tempo perdido (por exemplo)*.

O estudo terminará em junho de 2017.

O estudo é importante, pertinente e bem fundamentado.

A Investigadora Principal, Elsa Filipa Quadrado de Sousa, estudante de Engenharia Biomédica (tendo como elo de ligação ao CHSJ, o Professor António Ferreira, docente da FMUP e Médico especialista de Cirurgia Plástica do Centro Hospitalar de S. João EPE, e orientador da Tese o Professor Ricardo Ângelo Rosa Verdasca), dispõe das competências técnicas e científicas para a realização do estudo.

O estudo será realizado no Serviço de Cirurgia Plástica, Reconstrutiva e Unidade de Queimados do Centro Hospitalar de S. João (CHSJ), que dispõe das condições necessárias para a realização do estudo. O estudo está autorizado pelo Diretor de Serviço, Dr. Álvaro Silva.

– Benefício/Risco
Dada a natureza do estudo, não haverá riscos, incómodos ou benefícios para os participantes.

– Respeito pela liberdade e autonomia do sujeito do ensaio
A folha de informação submetida à CES contém a informação relevante relacionada com o tipo de estudo proposto.

Estão consignados os direitos e referenciadas as (não) consequências para o sujeito do estudo em não participar e, uma vez dado o seu consentimento, ter a possibilidade de exercer o direito de não continuar no estudo sem que daí resulte qualquer modificação dos cuidados médicos a prestar.

– Confidencialidade dos dados
A confidencialidade dos dados está garantida globalmente.

– Indemnização por danos: Não aplicável.
– Continuação do tratamento: Não aplicável.
- Propriedade dos dados: Do Promotor.

Conclusão
Em face da análise do protocolo do estudo "Estudo da dominância vascular do pulso", proponho a sua aprovação pela CES do HSJ/FMUP, depois de obtida a resposta à questão formulada em itálico e em sublinhado.

Porto, 24 de Março de 2017

O Relator
Prof. Manuel Vaz Silva

RESPOSTAS ADEQUADAS ÀS QUESTÕES FORMULADAS
21/4/2017

CES

COMISSÃO DE ÉTICA PARA A SAÚDE

7. SEGURO

a. *Este estudo/projecto de investigação prevê intervenção clínica que implique a existência de um seguro para os participantes?*

SIM ☐ (Se sim, junte, por favor, cópia da Apólice de Seguro respectiva)

NÃO ☐

NÃO APLICÁVEL ■

8. TERMO DE RESPONSABILIDADE

Eu, Elsa Filipa Quadrado de Sousa, abaixo-assinado, na qualidade de Investigador Principal, declaro por minha honra que as informações prestadas neste questionário são verdadeiras. Mais declaro que, durante o estudo, serão respeitadas as recomendações constantes da Declaração de Helsínquia (com as emendas de Tóquio 1975, Veneza 1983, Hong-Kong 1989, Somerset West 1996 e Edimburgo 2000) e da Organização Mundial da Saúde, no que se refere à experimentação que envolve seres humanos. Aceito, também, a recomendação da CES de que o recrutamento para este estudo se fará junto de doentes que não tenham participado em outro estudo no decurso do actual internamento ou da mesma consulta.

Porto, Janeiro de 2017

24/03/17

Elsa Filipa Sousa

O Investigador Principal

[stamp:] Comissão de Ética para a Saúde tendo aprovado o parecer do Relator, aguarda o Investigador/Promotor esclareça as que nele enunciadas para que possa parecer definitivo.

PARECER DA COMISSÃO DE ÉTICA PARA A SAÚDE DO CENTRO HOSPITALAR DE S. JOÃO/FACULDADE DE MEDICINA DA UNIVERSIDADE DO PORTO

emitido na reunião plenária da CES de / /
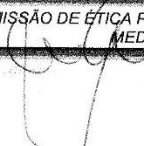
Centro Hospitalar **São João**

CONSIDERADOS QUE FORAM COMO SATISFATÓRIOS OS ESCLARECIMENTOS PRESTADOS PELO(A) INVESTIGADOR(A), A CES APROVA POR UNANIMIDADE O PARECER DO RELATOR, PELO QUE NADA TEM A OPOR À REALIZAÇÃO DESTE PROJETO DE INVESTIGAÇÃO.

20/04/17

VI

B. Thermography Protocol

ESTUDO DA DOMINÂNCIA VASCULAR DO PULSO

PROTOCOLO DE TERMOGRAFIA

Este protocolo é baseado no "*Glamorgan Protocol*", uma referência para os procedimentos padrão recomendados para a recolha e avaliação de imagens térmicas em aplicações médicas.

1. **Localização para a recolha de imagens térmicas**

Sala de exames
- Deve ser mantida uma distância mínima entre a câmara térmica e o indivíduo, normalmente 1 metro. A sala deve ter, no mínimo, 2x3 metros.
- A sala deve conter apenas o material necessário para a recolha de imagens, de forma a evitar reflexões térmicas e criar artefactos nas imagens.

Ambiente controlado
- A sala deve ser mantida num ambiente controlado com uma temperatura entre 18-24°C, normalmente 22±1°C, humidade inferior a 50%, circulação de ar inferior a 2 m/s e ausência de iluminação incidente. Será necessário que antes de iniciar a captura das imagens, que o indivíduo permaneça na sala durante 10 minutos para que o seu corpo se mantenha em equilíbrio com a temperatura da sala.
- Radiação ultravioleta deve ser evitada. Todas as janelas e portas devem ser devidamente fechadas.
- A sala deve conter um equipamento de ar condicionado, de forma a manter a temperatura recomendada constante. O fluxo de ar proveniente do equipamento não deve ser orientado para o indivíduo.
- O equipamento deve ser mantido fora da zona do indivíduo, de modo a evitar perturbações.
- Deve existir um cubículo mínimo na sala de exame, com as mesmas condições ambientais, para que o indivíduo possa retirar/vestir as roupas com privacidade e descansar durante o período de aclimatização.
- Não deve haver luz diretamente incidida no indivíduo, para evitar reflexões térmicas.

2. **Equipamento necessário**

O equipamento necessário para a recolha de dados será:
- Câmara térmica *FLIR E60sc*, para a captura das imagens de termografia. Este equipamento tem uma resolução de 320x240 *pixéis*, podendo medir valores de temperatura dos -20°C aos +120°C. Apresenta uma precisão de <50mK e possui exatidão de ±2% da gama definida de leitura;
- *FLIR Researcher Pro 2.10*, software de análise de imagens infravermelhos;

- Tripé;
- Sensor *Testo 175 H1*, para medir a humidade e temperatura da sala;
- IBM® SPSS® v24.0.0.1 (*Statistical Package for the Social Sciences*), *software* de análise estatística.

3. Cuidados para o equipamento termográfico

- A câmara térmica deve ser ligada 10 minutos antes da captura de imagens.
- O equipamento deve garantir um foco automático ou manual.
- É recomendado o uso da temperatura externa como referência para a calibração, de modo a garantir a qualidade da imagem e sensibilidade da câmara.
- O tipo de lentes da câmara deve ser considerado. Lentes com ângulos mais abertos reduzem a distância entre a câmara e o sujeito, mas ao mesmo tempo aumentam a distorção periférica da imagem.
- Cada imagem, ou conjunto de imagens deve indicar a gama de temperatura usada e o respetivo código de cor / escala de temperaturas. A escala e gama de cores, comummente utilizado em aplicações médicas, varia entre 21°C e 37°C e usa-se a palete *Rainbow*.
- As temperaturas do fundo que podem diminuir a intensidade da imagem devem ser evitadas. As respetivas cores devem ser substituídas por branco, preto ou cinzento, de forma a conseguir uma melhor apresentação visual.

4. Indivíduo

Informação para o indivíduo

O indivíduo deve ser informado para:
- Evitar o uso de aplicações tópicas: como o uso de ornamentos e maquilhagem no dia do exame.
- Evitar grandes refeições e ingestão de café ou chá duas horas anteriores ao exame.
- Não fumar durante duas horas anteriores ao exame.
- Evitar o uso de roupas justas e apertadas ao corpo.
- Evitar a prática de exercício físico incluindo métodos de fisioterapia, como: eletroterapia, ultrassons, tratamento com calor, crioterapia, massagens e hidroterapia, nas últimas 6 horas anteriores ao exame.
- Evitar a ingestão de medicamentos, nomeadamente: esteróides, bloqueadores do sistema nervoso autónomo e medicações vasoativas, opiáceos e autocolantes dérmicos, pelo menos 24 horas anteriores ao exame. Exceções devem ser anotadas.

Preparação pré-recolha

- O indivíduo deve ser informado sobre os procedimentos do exame, antes do seu início.
- O indivíduo deve ser instruído para retirar a roupa e os ornamentos.
- O indivíduo deve ser informado para sentar-se ou descansar na sala de exames no período de aclimatização. O período mínimo é de 10 minutos.

- O indivíduo deve evitar contacto entre as partes do corpo, como dobrar ou cruzar braços e pernas.

Posições para a recolha das imagens

- O indivíduo deve assumir posições corretas, de forma a serem adquiridas vistas padrão de regiões do corpo.
- Alguma comparação/conclusão obtida em diferentes condições deve ser evitada.

Campo de visão

- O indivíduo deve conservar a distância mínima à câmara estabelecida (0.7 a 1.2m), para que o campo de visão varie o mínimo possível e a região de interesse ocupe 2/3 da imagem. O tamanho da imagem está dependente desta distância e da distância focal da lente da câmara.

5. Captura de imagens

A captura das imagens térmicas será efetuada nos seguintes passos:

Figura 1 – Esquema representando os momentos de captura das imagens termográficas aquando da execução do teste modificado de Allen.

A sequência descrita na Figura 1 é repetida para o outro braço e para a outra artéria. Primeiramente, a mão direita é testada com a oclusão da artéria radial, seguindo-se o teste à mão esquerda. Esta sequência é repetida, com a oclusão da artéria ulnar. A primeira imagem será tirada após o período de aclimatização. Depois, a captura é feita imediatamente, 15 e 30 segundos após a oclusão, e 7, 15 e 30 segundos após a libertação de uma artéria e a libertação de ambas as artérias, com o antebraço apoiado numa superfície, enquanto o teste modificado de Allen está a ser executado. A câmara termográfica é colocada num tripé, a uma distância de 50 cm do participante, em média, para a captação de toda a mão. É pedido ao participante a abertura total dos dedos da mão.

C. Information to the participants

INFORMAÇÃO AOS PARTICIPANTES

Projeto de investigação: **Estudo da Dominância Vascular do Pulso**

Faculdade de Engenharia da Universidade do Porto

Faculdade de Medicina da Universidade do Porto / Centro Hospitalar S. João, EPE

1. O porquê deste projeto de investigação?

Este projeto pretende investigar a dominância vascular do pulso, utilizando a termografia infravermelha como métodos de avaliação. Pretende-se esclarecer a dominância da artéria radial e cubital ao nível do antebraço e de que modo estas contribuem para a perfusão sanguínea da mão e assim permitir aos médicos fazer uma escolha mais consciente e acertada em processos cirúrgicos.

O que é um termograma?

Um termograma é uma imagem da distribuição da temperatura à superfície da pele. Tal pode ser observado nas seguintes figura:

A termografia médica é um método complementar de diagnóstico e terapêutica por imagem simples, rápido, não-ionizante, não-invasivo, inofensivo e indolor, portanto livre de riscos para os utentes. As imagens recolhidas vão ser usadas para fins clínicos e académicos, sendo que os dados de cada utente irão ser preservados e mantidos confidenciais, assim como toda a informação irá ser guardada de forma segura.

2. O que necessito que faça para participar neste projeto?

É necessário antes da captura dos termogramas que o indivíduo permaneça numa sala aclimatizada expondo a área de interesse por um período de 10 minutos. Enquanto isso, o individuo deverá

preencher e tomar conhecimento de alguns formulários. Entre estes incluem-se, o consentimento informado e o questionário.

No dia da recolha algumas precauções deverão ser tomadas antes do período de recolha, tais como:

- Evitar ingerir uma refeição pesada e ingestão de café ou chá até 2h antes;
- Evitar participar em atividades desportivas ou de fisioterapia nas últimas 6 horas anteriores ao exame;
- Não ingerir bebidas alcoólicas e fumar, num período até 2h antes;
- Evitar a ingestão de medicamentos, nomeadamente: esteróides, bloqueadores do sistema nervoso autónomo e medicações vasoativas, opiáceos e autocolantes dérmicos, pelo menos 24 horas anteriores ao exame.
- Remover todo o tipo de bijuteria presente e evitar o uso de roupas justas e apertadas ao corpo, próximo da área de interesse durante o período de captura;
- Não aplicar qualquer tipo de óleos ou cremes na superfície da pele;
- Por fim, permanecer estático durante 10 minutos, sem cruzar pernas ou braços, ou entrar em contacto entre partes do corpo nas zonas de interesse para o exame.

3. Quanto tempo vai durar?

A participação de cada indivíduo neste projeto irá demorar aproximadamente 15 minutos (incluindo o tempo de aclimatização).

4. Vou ser pago pela minha participação?

Infelizmente, este projeto não possuí financiamento, pelo que não poderá receber qualquer pagamento pela sua participação neste estudo. Contudo, irá contribuir significativamente para desenvolvimentos únicos e importantes na área da utilização da termografia médica na avaliação da dominância vascular do pulso. Após a participação, as imagens recolhidas poderão também ser enviadas via email caso sejam solicitadas pelo participante.

5. Contacto

Nome: Elsa Filipa Quadrado de Sousa
Instituição: Faculdade de Engenharia da Universidade do Porto
email: bio12047@fe.up.pt

D. Biometric data questionnaire

Participante: _____   Idade: ____ anos

Género: F__   (dias desde a última menstruação: ____) M __

Peso _____ kg   Altura _____ m

Fumador(a)? Sim _____   Não _____   Dominância? Destro _____ Esquerdino _____

Tem algum problema de saúde? Não _____ Sim _____, qual?_____

Teve algum trauma nos membros superiores? Não _____ Sim _____,
qual?_____

Toma alguma medicação? Não _____ Sim _____, qual?_____

Tem conhecimento acerca do seu nível de colesterol? Não _____ Sim _____ (Nível: _____)

E. Informed Consent

CONSENTIMENTO INFORMADO, ESCLARECIDO E LIVRE

para participação em projeto de investigação

Estudo da Dominância Vascular do Pulso

Considerando a "Declaração de Helsínquia" da Associação Médica Mundial (Helsínquia 1964; Tóquio 1975; Veneza 1983; Hong Kong 1989; Somerset West 1996, Edimburgo 2000, Seoul 2008, Fortaleza 2013).

Nome do participante: _____

Participante/ Representante legal

· Compreendi a explicação que me foi facultada acerca do estudo que se tenciona realizar: os objetivos, os métodos, os benefícios previstos, os riscos potenciais e o eventual desconforto.

· Solicitei todas as informações de que necessitei, sabendo que o esclarecimento é fundamental para uma boa decisão.

· Fui informado da possibilidade de livremente recusar ou abandonar a todo o tempo a participação no estudo, sem que isso possa ter como efeito qualquer prejuízo na assistência que é prestada.

Concordo com a participação neste estudo, de acordo com os esclarecimentos que me foram prestados, como consta neste documento, do qual me foi entregue uma cópia.

Data: ___/___/_____

Assinatura do participante/Representante Legal: _____

Assinatura do Investigador Responsável: _____